

Green Solvents for Polymer Applications

Anna Sergeevna Zhenova

Doctor of Philosophy

Chemistry
University of York
June 2019

ABSTRACT

Discovery and development of green solvents for large-scale industrial applications is critical to the bioeconomy transition, yet academic solvent research focuses on use of solvents for organic synthesis, creating a knowledge gap in other areas. Polymer dissolution comprises at least 72% of solvent use in the EU, but is largely ignored in academic literature. This thesis addresses this disparity by uncovering new polymer-related applications for existing green solvents and identifying new green solvent candidates.

Dihydrolevoglucosenone, or CyreneTM, is a green solvent currently manufactured at commercial scale. Its abilities in promoting organic reactions are already well-known, but it is unexplored in polymer dissolution. This work investigates the potential of Cyrene and other solvents in dissolution of synthetic and natural polymers. In dissolution of PVDF, Cyrene was compared with conventional solvent NMP and greener alternatives DMSO, GVL, and CP. While DMSO and NMP slowly dissolved 10% w/v PVDF regardless of temperature, the ketone solvents (GVL, Cyrene, and CP) could achieve dissolution in under two hours at 60–90°C. This was attributed to the superior PVDF dispersion ability of the ketone solvents. Physical differences between solvent systems, including viscosity, gelation, and membrane formation were explored with a variety of analytical techniques.

Cyrene was also explored in biopolymer dissolution, tackling the challenging and poorly understood phenomenon of cellulose solvation. A wide range of additives were tested in combination with Cyrene, eventually leading to a combination of tetrabutylammonium chloride (TBAC) and Cyrene that could dissolve 0.4% w/v cellulose. This avenue is novel, but requires a great deal of further development to become industrially relevant, as commercial cellulose solvent systems can dissolve up to 20% w/v.

Cyrene is reported here for the first time in blends with its more stable ketal derivative, Cygnet 0.0. The solvatochromic parameters were measured for a range of blends of Cyrene and Cygnet, showing non-linear behaviour that may indicate preferential solvation. 50% Cygnet in Cyrene was tested in membrane formation, where it was found to moderately alter the morphologies of PI, PSU, and PES polymer systems.

Finally, a mixture of renewably-sourced ether oligomers (OMEs) was investigated as an alternative to conventional ether solvents. The mixture was found to work in Suzuki-Miyaura coupling, biocatalytic polymerisation, and dissolution of some polymers, but requires further safety testing before conclusions about its green status can be reached.

CONTENTS

ABSTRACT	3
CONTENTS	5
LIST OF FIGURES	9
LIST OF TABLES	13
ACKNOWLEDGMENTS	17
ABBREVIATIONS	19
1 INTRODUCTION AND BACKGROUND	21
1.1 Green Chemistry	21
1.1.1 History	21
1.1.2 Principles	22
1.1.3 Metrics	25
1.2 Solvation Theory and Practice	29
1.2.1 Enthalpy of Solvation	29
1.2.2 Entropy of Solvation	30
1.2.3 Kinetics of Solvation	30
1.2.4 Solubility Limits	31
1.2.5 Predicting Solvation Capability	31
1.3 Green Solvents	37
1.3.1 Legislative Drivers	38
1.3.2 Solvent Use	39
1.4 Polymer Dissolution	40
1.4.1 Membrane and Film Formation	42
1.5 Dihydrolevoglucosenone (Cyrene) as a Green Solvent	45
2 GREEN SOLVENTS FOR DISSOLUTION OF POLYVINYLIDENE DIFLUORIDE	49
2.1 Background	49
2.2 Modelling PVDF Dissolution	51
2.2.1 Solubility Prediction	51
2.3 Properties of PVDF Solutions	55

2.3.1	Final Candidates	55
2.3.2	Dissolution Differences Between Solvents	58
2.3.3	Gel Behaviour	59
2.3.4	Rheometry of Gels and Solutions	60
2.4	Practical Applications	63
2.4.1	Membrane Casting	63
2.5	Summary and Future Work	69
3	CELLULOSE DISSOLUTION IN CELLULOSE-BASED SOLVENT	73
3.1	Background	73
3.1.1	Solvent Systems	74
3.1.2	Swelling and Dispersion	77
3.1.3	General Principles of Dissolution	78
3.1.4	Potential of Cyrene for Cellulose Dissolution	80
3.2	Methodology	82
3.3	Results and Discussion	85
3.3.1	Design of Dissolution Systems	85
3.3.2	Cellulose Dissolution Trials	88
3.3.3	Improving Cellulose Dissolution	91
3.4	Summary and Future Work	93
4	BLENDING SOLVENTS FOR NOVEL PROPERTIES	95
4.1	Background	95
4.2	Greening of Cygnet Synthesis	98
4.3	Predicting Solubility Behaviour	99
4.3.1	HSP Predictions	99
4.3.2	KAT Measurements	100
4.4	Applications in Membrane Casting	102
4.4.1	Membrane Casting	102
4.5	Summary and Future Work	107
5	APPLICATIONS OF OXYMETHYLENE DIMETHYL ETHERS AS NOVEL SOLVENTS	111
5.1	Background	111
5.2	Predicting Solubility Behaviour	114
5.3	Use as Organic Reaction Medium	116
5.3.1	Suzuki-Miyaura Coupling	116
5.3.2	Enzymatic Polymerisation	118
5.3.3	Solvent Miscibility	122
5.4	Dissolution of Polymers and Coatings	122
5.5	Safety and Stability	127

5.5.1	Mutagenicity and Genotoxicity	128
5.5.2	Peroxide Formation Potential	129
5.5.3	Acid Stability	130
5.6	Summary and Future Work	131
6	CONCLUSION	133
6.1	Summary of Research	133
6.1.1	Green Solvents for Dissolution of Polyvinylidene Difluoride	133
6.1.2	Cellulose Dissolution in Cellulose-Based Solvent	134
6.1.3	Blending Solvents for Novel Properties	134
6.1.4	Applications of Oxymethylene Dimethyl Ethers as Novel Solvents	135
6.2	Solubility Parameters	135
6.3	Green Solvent Outlook	137
7	EXPERIMENTAL	139
7.1	Instrumentation and Analysis	139
7.2	Green Solvents for Dissolution of Polyvinylidene Difluoride	141
7.2.1	Materials	141
7.2.2	Experimental	142
7.3	Cellulose Dissolution in Cellulose-Based Solvent	144
7.3.1	Materials	144
7.3.2	Experimental	145
7.4	Blending Solvents for Novel Properties	147
7.4.1	Materials	147
7.4.2	Experimental	147
7.5	Applications of Oxymethylene Dimethyl Ethers as Novel Solvents	148
7.5.1	Materials	148
7.5.2	Experimental	149
APPENDIX A	SUPPLEMENTARY DATA	155
A.1	Green Solvents for Dissolution of Polyvinylidene Difluoride	155
A.2	Cellulose Dissolution in Cellulose-Based Solvent	159
A.3	Applications of Oxymethylene Dimethyl Ethers as Novel Solvents	160
ABBREVIATIONS	163
REFERENCES	184

LIST OF FIGURES

1.1	Green chemistry publications by year	22
1.2	Principles of green chemistry	23
1.3	Enthalpy changes during solution formation	30
1.4	Generation of solubility spheres with HSPiP software	34
1.5	Solvatochromic dyes for KAT parameter measurement	36
1.6	Examples of traditional dipolar aprotic solvents	39
1.7	Solvent use by industrial sector	40
1.8	Stages of polymer dissolution	41
1.9	NIPS method for membrane casting	42
1.10	NIPS membrane cross-sections showing macrovoid and bicontinuous morphologies	43
1.11	Synthesis of Cyrene from cellulose	46
1.12	HSP and KAT parameters of Cyrene and conventional solvents	46
1.13	Structure and properties of Cyrene	47
2.1	Electric vehicle use by year and region	50
2.2	PVDF structure and location in cathode	50
2.3	Predictive HSP modelling of PVDF dissolution	51
2.4	Comparison of PVDF HSP sphere with literature	53
2.5	Final solvent candidates for PVDF dissolution	57
2.6	PVDF dispersions and solutions	58

2.7	Gels made with 10% w/v PVDF	60
2.8	Viscosity of PVDF in various solvents at 100°C	61
2.9	Viscosity of PVDF in various solvents at 25°C	62
2.10	PVDF membranes prepared in green solvent candidates	64
2.11	SEM micrographs of 10% w/v PVDF in NMP and DMSO	65
2.12	SEM micrographs of 10% w/v PVDF in GVL	65
2.13	SEM micrographs of 10% w/v PVDF in Cyrene and CP	66
2.14	FT-IR spectra of PVDF films cast from various solvents	68
3.1	Origin of cellulose in plant biomass	74
3.2	Common solvents for cellulose dissolution	75
3.3	Swelling and dissolution modes of cellulose fibres	77
3.4	Structure of cellulose polymer chain	78
3.5	Structure of cellulose microfibrils	79
3.6	Formation of geminal diol from Cyrene and water	81
3.7	Cellulose pretreatment	83
3.8	General procedure for cellulose dissolution experiments	83
3.9	Cellulose crystalline phases by XRD and IR	84
3.10	Dissolution of additives in Cyrene	86
3.11	XRD of dissolved and dispersed cellulose	90
3.12	Attempts at improving cellulose dissolution	92
4.1	Structures of known Cygnets	96
4.2	Improved synthesis for Cygnet 0.0.	98
4.3	Predicted HSP for mixtures of Cygnet and Cyrene	99
4.4	Measured KAT parameters for mixtures of Cygnet and Cyrene	101

4.5	PI membranes cast in Cyrene and Cygnet	104
4.6	PSU membranes cast in Cyrene and Cygnet	106
4.7	PES membranes cast in Cyrene and Cygnet	107
5.1	Structures of traditional and neoteric ether solvents	112
5.2	OME synthesis from CO ₂ and H ₂	113
5.3	Structure of OMEs and their derivatives	114
5.4	Suzuki-Miyaura coupling yields	117
5.5	Suzuki-Miyaura coupling byproducts	118
5.6	Enzymatic polycondensation reaction figure	119
5.7	Enzymatic polycondensation results	120
5.8	Structures of polymers tested with OME ₃₋₅	123
5.9	Polymer dissolution in OME ₃₋₅	123
5.10	Paint removal with OME ₃₋₅	126
5.11	Acid stability of OME ₃₋₅	131
A.1	Amplitude sweep of PVDF in GVL	155
A.2	Amplitude sweep of PVDF in Cyrene	155
A.3	Amplitude sweep of PVDF in CP	156
A.4	Viscosity of PVDF in NMP at 25°C	156
A.5	Viscosity of PVDF in DMSO at 25°C	156
A.6	Viscosity of PVDF in NMP at 100°C	157
A.7	Viscosity of PVDF in DMSO at 100°C	157
A.8	Viscosity of PVDF in GVL at 100°C	157
A.9	Viscosity of PVDF in Cyrene at 100°C	158
A.10	SEM micrographs of room-temperature PVDF films	158

A.11 $^1\text{H-NMR}$ of OME_{3-5} polycondensation product 162

LIST OF TABLES

1.1	Hazard-related properties required in REACH registration	27
1.2	HSP RED for common solvents and membrane polymers	45
2.1	Results of single-solvent dissolution trials for PVDF	54
2.2	Results of blended solvent dissolution trials for PVDF	54
2.3	Solvent candidates for PVDF dissolution	56
2.4	Minimum gelator concentrations for PVDF solvents	60
2.5	Hansen distances (R_a) between solvent candidates and PVDF/water	67
2.6	Crystallinity of PVDF films and HSP of solvents	69
2.7	Summary of PVDF solvent candidate properties	70
3.1	Solubility parameters for traditional dipolar aprotics and Cyrene	81
3.2	Solubility of dissolution additives in Cyrene	85
3.3	Dispersion quality in cellulose dissolution trials	89
4.1	HSP for Cygnet 0.0 and related solvents	97
4.2	HSP RED for common membrane polymers	103
4.3	HSP and KAT parameters for Cyrene and 50% Cygnet blend	105
5.1	Physical properties of ether solvents	112
5.2	Physical properties of OMEs	113
5.3	Solubility parameters for OME mixture and other ethers	115

5.4	Comparison of enzymatic polycondensation conditions	121
5.5	Hansen Solubility Parameters of tested polymers	124
5.6	Polymers predicted to dissolve in OME ₃₋₅	125
5.7	Polymers used in paint formulations	126
5.8	Peroxide formation test results	130
A.1	Additive concentrations used in trials of cellulose dissolution systems . .	159
A.2	GC-MS Analysis of OME ₃₋₅	160
A.3	Solvent Miscibility of OME ₃₋₅	161
A.4	Suzuki Couplings in OME ₃₋₅	162

For Bobby, who made the whole thing possible.

ACKNOWLEDGEMENTS

My Ph.D. began with a brief conversation with Professor James Clark at a conference in Boston. Three months later, I started packing my things to move to England. I will always be thankful to James for inviting me to do a Ph.D. here, and for ensuring I had the funding and support necessary to complete my work. Professor Seishi Shimizu has been a steady wellspring of support and encouragement, always there to act as a sounding board when I got stuck. Dr. James Sherwood was instrumental to my solvent education, and Dr. Rob McElroy introduced me to new projects and helped me solidify my ideas. Dr. Noriyuki Isobe from the Japan Agency for Marine-Earth Science and Technology was extremely kind in hosting me for four weeks and teaching me about methods in cellulose dissolution science, and Dr. Helen Sneddon at GSK invited me to visit for a hectic week and take advantage of their excellent robots.

I want to extend a big thank you to everyone else who helped make my time at the Green Chemistry Centre easier. Alison Edmonds, Sophie Palmer, and Katy Brooke were the most helpful admin team I've ever worked with, and saved me a great deal of stress when dealing with travel, funding, and paperwork. Our technical team, led by Paul Elliott, kept the lab running and fought the forces of scientific chaos every day, and always found me a hotplate when I needed one. Roxana Milescu, Alessandro Pellis, and Tom Nicol worked closely with me on several projects and were delightfully reliable and supportive collaborators.

This research would not have been possible without funding from many generous benefactors. I am very thankful to GlaxoSmithkline and the RenewChem program, the Wild Scholarship Fund, the SCI Scholar program, and Circa and Fraunhofer for supplementary project funding.

AUTHOR'S DECLARATION

I declare that this thesis is a presentation of original work and I am the sole author. This work has not previously been presented for an award at this, or any other, university. All sources are acknowledged as references. Collaborative efforts are acknowledged below and in the relevant chapter sections.

Section	Collaborator	Contribution	Institution
5.3.2	Alessandro Pellis	Enzymatic polymerisation	University of York
4.3.2		Melting point measurement	
2.4.1	Roxana A. Milescu	Film casting/SEM assistance	University of York
4.4.2		Membrane casting, SEM	
5.4		Polymer dissolution/removal	
4.4	Noriyuki Isobe	Cellulose dissolution methods XRD measurements	JAMSTEC, Japan

Parts of this work have been published or submitted for publication as detailed below:

Chapter 3 – A. Alves Costa Pacheco, J. Sherwood, A. Zhenova, C. R. McElroy, A. J. Hunt, H. L. Parker, T. J. Farmer, A. Constantinou, M. De bruyn, A. C. Whitwood, W. Raverty and J. H. Clark, *ChemSusChem*, 2016, **9**, 3503–3512.

Chapter 5 – A. Zhenova, A. Pellis, R. A. Milescu, C. R. McElroy, R. J. White, J. H. Clark, *ACS Sustain. Chem. Eng.*, 2019, **7**, 14834-14840.

CHAPTER 1

INTRODUCTION AND BACKGROUND

The sustainability of human life on Earth is the fundamental challenge of the 21st century. Perhaps for this reason, it has sparked an abundance of controversy. There is debate about whether it is best to have a circular economy, a bioeconomy, or a precision economy;¹ how to achieve a just transition for all;² which crops should be used as industrial feedstocks;³ and even who is to blame for climate change.⁴ Amongst all this debate, the field of chemistry finds itself in a position both precarious and powerful.

The modern-day practice of chemistry is rooted in clever utilisation of petroleum, focusing more on efficiency than human or environmental health. While this has led to numerous scientific discoveries and beneficial advancements in chemical technology, unfortunately the field of chemistry has gained an unenviable reputation with the general public. *Chemical* has become synonymous with *poison*,^{5,6} and chemistry is now vulnerable to attacks by fearmongers across such diverse fields as food science,⁷ medicine,⁸ and skin care.⁹ Even chemists are now calling their research “chemical-free” as short-hand for clean or sustainable.^{10,11} The public, it would seem, is tired of traditional chemistry and hungry for new solutions.

There is enormous power in this hunger. The world is on the brink of transitioning away from fossil fuel dependence. Chemistry will, by necessity, play a pivotal role in that transition. Chemists have an opportunity to redefine the practice of chemistry itself, to stop playing by petrochemical rules and usher in an era of thoughtfully designed chemicals that cultivate safety, sustainability, and trust: the era of green chemistry.

1.1 Green Chemistry

1.1.1 History

Green chemistry is a young field, but growing rapidly. The seminal work, *Green Chemistry: Theory and Practice*, was published in 1998, after which the number of scientific publications incorporating green chemistry soared (Fig. 1.1). By 2016 (when this Ph.D. work was started), over 1,000 papers per year were being published in the field of green chemistry. Green chemistry has taken root around the world, with academic research

centres and networks devoted to the topic in the UK, the US, Canada, Australia, China, Japan, India, Brazil, and many European countries.

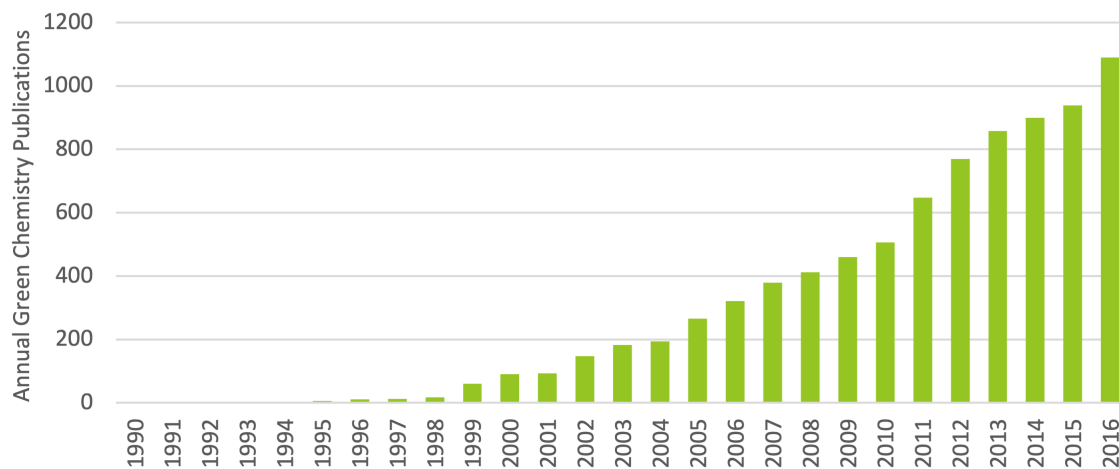


Figure 1.1: Annual green chemistry publications by year. *Data from Web of Science Online Database*

This surge of academic interest has been mirrored by legislative and industrial movement towards safer chemistry. In the EU, Registration, Evaluation, Authorisation and Restriction of Chemicals (REACH) has set an example for comprehensive chemical legislation that is inspiring similar statutes around the world.¹² In the US, the non-profit Green Chemistry & Commerce Council (GC3) has dozens of member companies working towards implementing green chemistry practices, including giants such as BASF, MilliporeSigma, and Wal-Mart.¹³ Retailers, manufacturers, and brands are acknowledging the business value of green chemistry.¹⁴ In short, green chemistry is catching.

1.1.2 Principles

Green chemistry is founded on twelve principles that were laid out by Anastas and Warner in 1998.¹⁵ These serve to guide the practice of green chemistry, and are primarily implemented at the design stage of a project, seeking to prevent waste, reduce hazards, and stop accidents before they happen. These twelve principles can be more simply viewed as three fundamental pillars: efficiency, safety, and circularity (Fig. 1.2). For each pillar, metrics have been introduced that make it possible to compare the relative sustainability of two chemical products or processes. These are described in more detail in the next section.

Efficiency is concerned with preventing waste of both energy and materials. Chemical reactions should be designed for minimal waste, ideally at the outset of a research project.



Figure 1.2: The twelve principles of green chemistry, rearranged into three fundamental pillars

More commonly, this is addressed at the scale-up stage, where the cost of waste becomes a significant concern. Common practices to achieve this include minimising synthetic steps, choosing solvent-free reactions, and preferring catalytic techniques to stoichiometric ones. These techniques are slowly gaining traction; importantly, they are being embedded in chemistry curricula around the world.¹⁶ In order to compare efficiency across reactions, many metrics can be used, ranging from traditional yield measurements to complex consideration of reaction mass efficiency and waste treatment energy requirements. Some of the more useful green chemistry efficiency metrics include:^{17–19}

- Atom economy
- Reaction mass efficiency
- E Factor
- Mass intensity
- Energy intensity

Safety calls for proactive analysis and reduction of hazards in chemical processes and products. Replacing hazardous solvents and reagents with safer options can reduce risk to workers and the environment. Real-time monitoring of chemical processes can detect accidents in the making, allowing system shut-off before the situation becomes truly dangerous. Furthermore, with careful molecular design and the use of predictive tools, inherent chemical hazards can be reduced or avoided altogether. This science is still relatively new, but computational tools are enabling leaps in understanding of structure-activity prediction.^{20–22}

Chemical hazards fall into two main categories: physical hazards, including flamma-

bility, oxidising potential, radioactivity, and so on, and environmental/health hazards, including toxicity, mutagenicity, aquatic toxicity, and other endpoints. While physical hazards are fairly simple to measure, environmental/health hazards typically require toxicological studies assessing multiple criteria and using a variety of tests, making the results difficult for non-specialists to interpret. For most chemicals, both types of hazard are summed up in classifications from the Globally Harmonized System of Classification and Labelling of Chemicals (GHS) system, allowing chemists to compare levels of a specific hazard across reagents. Holistic comparison of all hazards is more challenging, and by nature is semi-quantitative at best, as qualitative judgements must be made about the relative importance of hazards in a specific application. Ideally, all chemicals used or produced in a process would be hazard-free, but realistically, the hazards must be weighed against the risk of exposure—for example, a non-volatile solid with oral toxicity may be considered safer than a non-toxic liquid with flammable vapours. Software or tools such as solvent selection guides can assist in the decision-making process, but ultimately choices about chemical safety require human judgement.

Circularity is the most complex of the three pillars. In short, renewable feedstocks must be used for chemistry, and chemicals should be designed for recycling or biodegradation after use. This presents a major challenge. Petroleum-based chemistry gradually replaced traditional bio-based products over the last century, yet the reverse transition must be done in a few decades, without losing the functions society has grown to depend on.²³ The fundamental differences between petroleum- and bio-based chemistries complicate this further. While petroleum feedstocks consist primarily of hydrocarbons, bio-feedstocks tend to be highly oxygenated, changing their reactivity and often making traditional chemical processes untenable.^{24,25} Furthermore, a full circular economy incorporates cycles for technical nutrients—recycling of chemicals (such as durable plastics) may in some cases be more desirable than biodegradation, and metallic components must be reused or recycled.^{26,27} Incorporating such end-of-life considerations into chemical product design is a formidable problem. Metrics for this area are still in development, but include:

- Life cycle assessment
- Renewables percentage
- Renewables intensity
- Bio-based carbon content

- Biodegradability screening

The science and practice of green chemistry has advanced in the last two decades, and is branching out in directions that are not explicitly included in the original twelve principles. New metrics have arisen, including life-cycle assessment, various ecological footprints, and economic viability assessment.²⁸ Biotechnologies, including enzymatic catalysis and use of microorganisms, are gaining traction in industry.^{29,30} Nanotechnology is opening new frontiers in catalysis, medicine, and advanced manufacturing.³¹ New methods such as microwave chemistry³² and mechanochemistry³³ have expanded the palette of green processing options. In the future, new research will doubtless open even more avenues that are currently unknown.

1.1.3 Metrics

Efficiency The efficiency of a chemical reaction or process can be measured in a number of ways. Conventional chemistry metrics for this include yield, conversion, and selectivity, which focus on formation of the desired product or disappearance of a reagent. In green chemistry, it is valuable to look directly at the waste being generated, examining the impact of solvent, catalyst, and other auxiliary process components. This can be done on a basic level with metrics such as atom economy (Eq. 1.1), introduced by Trost in 1991, and the E Factor (Eq. 1.3), introduced by Roger Sheldon in 1992.³⁴

$$\text{Atom Economy} = \frac{\text{product MW}}{\text{total reagent MW}} \times 100 \quad (1.1)$$

Atom economy is very simple to use and can be calculated at the design stage to assess how efficiently a reaction uses reagents. Its simplicity means it discards considerations such as yield, stoichiometry, solvents, work-up additives, or other auxiliaries that are not directly involved in the reaction. Nevertheless, it is a useful tool for reaction design when combined with others. A modified version of atom economy is known as reaction mass efficiency (RME) (Eq. 1.2). While similar in principle, RME takes both yield and stoichiometry into account by looking at the total mass of product and reagents, making it a more realistic metric.¹⁸

$$\text{RME} = \frac{\text{product mass}}{\text{total reactant mass}} \times 100 \quad (1.2)$$

The E Factor, on the other hand, is easy to measure in a real industrial process, but requires definition of system boundaries, which can be challenging at the planning phase.

The related mass intensity (MI) metric compares the total mass of materials going into a reaction to the mass of product coming out (Eq. 1.4).¹⁷ Both of these metrics incorporate solvents and other auxiliaries, and can be used in their simplest forms or made more complex if needed. E Factor and MI do not take recycling of materials into account, and therefore may not fully represent the process efficiency.

$$\text{E Factor} = \frac{\text{input mass} - \text{product mass}}{\text{product mass}} = \frac{\text{waste mass}}{\text{product mass}} \quad (1.3)$$

$$\text{MI} = \frac{\text{input mass}}{\text{product mass}} = \text{E Factor} + 1 \quad (1.4)$$

Finally, energy efficiency of chemical processes can be compared with the simple metric of energy intensity (Eq. 1.5).¹⁹ This can be further divided into energy required for waste treatment, solvent recovery, or other considerations as needed.

$$\text{Energy Intensity} = \frac{\text{process energy}}{\text{product mass}} \quad (1.5)$$

These quantitative tools do not cover the full spectrum of decisions to be made in reaction design. Choices such as use of catalysts, batch vs. flow processes, work-up methods, can strongly impact efficiency, yet are usually made on a qualitative basis. A number of toolkits have been developed to aid in this process, with additional proprietary versions doubtless being used in industry.^{18,35,36} The right toolkit depends largely on the type of process being assessed—efficiency considerations in the pharmaceutical industry may be quite different from those in polymer processing, for example. Therefore, it is up to the individual chemist to decide which green chemistry toolkit or set of metrics is most practical for a specific project.

Safety Comparison of chemical hazards is fundamentally difficult, due to the varied nature of hazards and numerous gaps in available data. When available, data from REACH registrations and GHS hazard statements can be used to make decisions about chemical safety based on relative hazard levels in a category. Table 1.1 shows all hazard-related physical and chemical properties required under REACH legislation, though for lower production volumes not all of these are assessed. Depending on the application and likely exposure routes, some of these hazards will prove more important than others.

For more holistic comparison of hazards in process development, tools such as the environmental quotient, Environmental Assessment Tool for Organic Synthesis (EATOS),

Table 1.1: Hazard-related properties required in REACH registration

Physical	Chemical
vapour pressure	skin/eye irritation/corrosion
water solubility	skin sensitisation
octanol/water partition coefficient	mutagenicity
flash point	acute toxicity
flammability	chronic toxicity
explosive properties	reprotoxicity
auto-ignition temperature	toxicokinetics
oxidising properties	carcinogenicity
	aquatic toxicity
	terrestrial/avian toxicity
	environmental fate/degradation

and even full life cycle assessment (LCA) can be used.²⁸ Capello et al. developed a comprehensive framework incorporating LCA methods into green solvent assessment.³⁷ This provides a useful tool for comparing well-established solvents, but may be difficult to apply to newer technologies due to the required data on industrial production, recycling, and disposal processes. Additionally, the hazard assessment portion of the framework has not been updated to use GHS classifications.³⁸

In green solvent research, it is common to use solvent selection guides to simplify the process of hazard comparison. A number of these have been developed in the pharmaceutical industry and published over the last decade, including versions from AstraZeneca, GSK, Sanofi, and others.^{39,40} These guides provide a simplified solvent ranking based on safety metrics deemed important by the authoring company. The collaborative CHEM21 public-private research consortium published a version that uses GHS codes and includes a freely available tool to extend the ranking to new solvents.⁴¹ This guide is used in this work to give simplified solvent comparisons when needed. In the CHEM21 system, physical properties and GHS hazards are used to assign a color-coded ranking based on the solvent's worst safety/environmental characteristic, with four scores ranging from 'recommended' to 'highly hazardous'. While it is simple to use and understand, the CHEM21 guide is in some cases misleading. Data gaps automatically result in a 'problematic' score, as do high boiling points—a characteristic which is only truly problematic if distillation is intended as part of the process.³⁸ Nevertheless, it is a

helpful tool when used with care.

Circularity The complexity of the circularity pillar defies the use of simple, holistic metrics. Assessments of feedstock renewability or end-of-life degradation tend to be either quick or thorough, and the choice of metric depends largely on the overall focus of the study.

LCA is perhaps the best-developed method for complete assessment of chemical circularity. This iterative process quantifies the environmental impact of production, use, and disposal of a product, and has been recently applied in combination with green chemistry principles.^{28,42} LCA has been standardised by the ISO, making it possible to compare results across studies. However, the scope and complexity of an LCA study makes it difficult for most chemists to use this assessment method—indeed, LCA could be considered its own discipline, with an abundance of methodologies, tools, and software requiring expert knowledge to use properly.²⁸

To quickly quantify the renewable origin of a chemical, a few metrics are available. The renewables intensity (Eq. 1.6) measures the ratio of renewable mass to total product mass, while the renewables percentage (Eq. 1.7) combines renewables intensity with mass intensity to account for reaction efficiency.^{18,43} Similar metrics can be adopted for recycled material content and recyclability of a product.⁴⁴

$$\text{Renewables Intensity} = \frac{\text{mass of renewable materials used}}{\text{product mass}} \quad (1.6)$$

$$\text{Renewables Percentage} = \frac{\text{renewables intensity}}{\text{mass intensity}} \times 100 \quad (1.7)$$

These metrics are quite rudimentary, as not all renewable feedstocks are equal. For example, land use issues, competition with food supply, and efficiency of using a feedstock are not accounted for here. Likewise, the concept of recycling requires much more depth to assess fully. However, quick calculations such as these are straightforward and easy to implement, making their adoption more likely.

A simple measurement of bio-based content in a chemical can be made via radiocarbon content determination. Fossil fuels are free of ¹⁴C; therefore, presence of this isotope in a chemical product must be due to bio-based materials.⁴⁵ This measurement has been standardised for biofuels and is being expanded to bio-based plastics and solvents.⁴¹

In addition to feedstock origin, end-of-life options are also a concern for circularity. One of the most common end-of-life assessments performed for chemicals is ready biodegradability screening. This is required under REACH to rule out environmental persistence, and typically gives a simple yes/no answer based on amount of degradation under specific conditions within 14 days. This is useful to some extent, but can be too simplistic, and does not necessarily predict behaviour in real-world conditions.⁴⁶ However, the ready biodegradability test strikes a balance between accuracy and expense, and the data is available for all REACH-registered chemicals, making it easy to compare across substances.

1.2 Solvation Theory and Practice

While the word *solvent* is frequently used across many industries, definitions can vary depending on the user. IUPAC defines a solvent as simply one component of a solution.⁴⁷ In this work, a solvent is defined as a substance used to dissolve another substance, which is called the solute.

Solvation, or the formation of a solution from solute and solvent, is a physical process governed by both enthalpy (H) and entropy (S). In order for solvation to be thermodynamically favoured and occur spontaneously, the Gibbs energy (G , Eq. 1.8) of the solution must be lower than the Gibbs energy of the separate solute and solvent.⁴⁸

$$\Delta G = \Delta H - T\Delta S \quad (1.8)$$

1.2.1 Enthalpy of Solvation

Solvation can be endothermic ($\Delta H > 0$) or exothermic ($\Delta H < 0$) depending on the energy of the interactions involved. The overall enthalpy of solvation can be expressed as the sum of three steps:

$$\Delta H_{soln} = \Delta H_1 + \Delta H_2 + \Delta H_3 \quad (1.9)$$

The first two steps, ΔH_1 and ΔH_2 , refer to the breaking of intermolecular interactions in the solvent and solute, respectively. Solvent molecules must be separated to form a cavity for insertion of the solute, while the solute interactions (typically lattice energy, in a solid) must be overcome to place it in solution. The final step, ΔH_3 , refers to the introduction of new intermolecular interactions between solute and solvent in solution.

Figure 1.3 shows both the endothermic and exothermic cases.⁴⁹

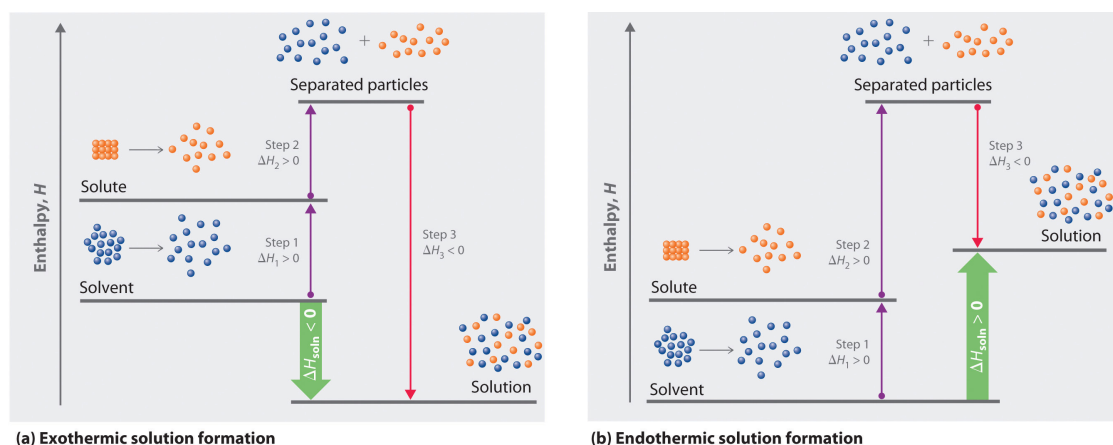


Figure 1.3: Changes in enthalpy accompanying formation of a solution. Image from LibreTexts licensed under CC BY-NC-SA 4.0

As both ΔH_1 and ΔH_2 are positive, exothermic solvation (Fig. 1.3a) requires ΔH_3 to be sufficiently negative to overcome the sum of these terms. In the endothermic case (Fig. 1.3b), the solvation process requires energy input, as the solvent-solute interactions are not sufficiently favourable to overcome the energy of separating the solute and solvent. However, endothermic dissolution can still proceed spontaneously if assisted by entropy or temperature.

1.2.2 Entropy of Solvation

The change in disorder, or entropy, during solvation is also important to its spontaneity. Formation of a solution increases the entropy of the system ($\Delta S > 0$), as ordered packing is disrupted and solute molecules are scattered in a disordered way throughout the solvent. This increase in disorder can drive solvation forward, and is particularly important in cases where ΔH_{soln} is positive. When the increase in entropy is small, heating the solute-solvent system can encourage spontaneous dissolution by increasing the $T\Delta S$ term of Gibbs energy.⁴⁸

1.2.3 Kinetics of Solvation

A negative Gibbs energy indicates that solvation will be spontaneous, but reveals nothing about the kinetics, or rate at which dissolution will occur. A process that is thermodynamically favoured could nonetheless proceed very slowly, with no observable dissolution on a timescale of days or weeks.⁵⁰ Solvation can be accelerated by increasing the rate at

which molecules of solute and solvent encounter each other. This is usually achieved by physically mixing the sample through stirring, shaking, or ultrasonication, or by simply heating the sample to increase the molecular kinetic energy.

1.2.4 Solubility Limits

Regardless of spontaneity, there is a limit to the amount of solute that can be dissolved in a given solvent. When the maximum amount of solid solute has been dissolved, the solution is said to be *saturated*, and excess solute will crystallise as quickly as it dissolves.⁴⁹ The ideal solubility of a crystalline solute—that is, its solubility in an ideal solvent that gives an activity coefficient of one—depends on its melting point, heat of fusion, and the change in heat capacity as it transforms from solid to liquid form.⁵¹ This can be important in planning formulations, as a formulation requiring a concentration above ideal solubility is fundamentally impossible.

1.2.5 Predicting Solvation Capability

Solvation capability, or the ability of a solvent to dissolve a target solute, is of great interest in chemistry. Solvents can strongly affect the rate of a reaction, the success of a purification, and the properties of a product formulation. Most commonly, the term used to predict a solvent's dissolution behaviour is *polarity*, which is not very well-defined. According to the IUPAC Gold Book, "When applied to solvents, this rather ill-defined term covers their overall solvation capability (solvation power) for solutes, which in turn depends on the action of all possible, nonspecific and specific, intermolecular interactions between solute ions or molecules and solvent molecules, excluding such interactions leading to definite chemical alterations of the ions or molecules of the solute."⁴⁷ In short, polarity is understood to be a metric for the solvation capability of a specific solvent, and solvents with similar polarities should have affinity for similar solutes.

There are a number of different single-component scales used to express polarity, with the most common being the electromagnetic parameter relative permittivity (ϵ_r). This simply measures the ability of a solvent to separate electrical charges and orient its dipolar molecules, accounting only for the behaviour of the bulk mixture and failing to consider specific intermolecular interactions.⁵² Similarly, the popular Hildebrand parameter (δ), defined as the square root of the cohesive energy density (Eq. 1.10), is limited in its usefulness. δ measures the interruption of solvent-solvent interactions that

occurs when solvent molecules are separated to make room for the solute, but fails to account for important interactions such as dipolarity or electron donation.⁵⁰

$$\delta = \sqrt{\frac{\Delta H_v - RT}{V_m}} \quad (1.10)$$

Indeed, the complexity of solvation interactions cannot be encompassed in one simple term, and a variety of multi-component solubility parameter systems have been developed to predict solvation capability with more accuracy. Two of the most popular, Hansen Solubility Parameters (HSP) and Kamlet-Abboud-Taft (KAT) parameters, use three parameters each and have been chosen in this work. While more complex systems exist, some with up to five parameters, three parameters have been found to provide sufficient accuracy in most cases, and allow easy visualisation in the form of three-dimensional plots. Additionally, HSP are accompanied by a software package and extensive database of values that allows rapid screening of thousands of solvents, as well as easy prediction of unknown values.⁵⁰ KAT parameters are quick and easy to measure empirically, and their popularity in the literature provides a sizeable basis for comparison with known values.^{53,54}

Hansen Solubility Parameters (HSP)

Hansen solubility parameters, or HSP, have been used for over fifty years and remain a popular method of assessing solvent behaviour today. They have enough depth to provide accurate predictions, while retaining enough simplicity to be easily understood and compared. HSP can enable rapid-throughput solvent screening through a combination of a database of empirically measured parameters and algorithmic prediction of unknown parameters.

HSP are derived from the historic Hildebrand solubility parameter (δ , Eq. 1.10).⁵⁰ The physical basis of these parameters is the cohesive energy density, or the energy required to transform a solvent to its ideal gas form, as these same intermolecular interactions must be overcome to separate solvent molecules and enable dissolution. Hildebrand parameters can be used in the Hildebrand-Scatchard equation to approximate the enthalpy of mixing, with V representing the volume of mixture, ϕ the solute volume fraction, and δ_S and δ_N the Hildebrand parameters of solvent and solute, respectively (Eq. 1.11).⁵⁵

$$\left(\frac{\Delta H}{V}\right) = \phi(1 - \phi)(\delta_S - \delta_N)^2 \quad (1.11)$$

In this relation, the enthalpy of mixing is at a minimum when the solubility parameters of the solute and solvent are as similar as possible, suggesting that this condition is best for successful solvation. Thus, the similarity of Hildebrand parameters has been used to predict compatible solvent and solute combinations for decades, becoming especially popular in the polymer industry. Empirically, this method often works well, but it crucially fails to account for non-dispersion interactions, such as hydrogen bonding and dipolar interactions.⁵⁵

Hansen solubility parameters address this issue by splitting the Hildebrand parameter into multiple independent components. Logically, the total cohesive energy density is the sum of its parts, and so the Hildebrand parameter can be divided into three HSP, each representing a type of intermolecular interaction:

$$\delta^2 = \delta_D^2 + \delta_P^2 + \delta_H^2 \quad (1.12)$$

This expression describes solvent behaviour in terms of three values: dispersion force (δ_D), polarity arising from dipole moments (δ_P), and hydrogen bonding capacity (δ_H). These parameters have units of $\text{MPa}^{1/2}$, and can be used similarly to the Hildebrand parameter—that is, when two compounds have similar HSP, their enthalpy of mixing will be minimised, predicting favourable solvation. However, the similarity of HSP are not calculated via a simple distance formula, but expressed as the HSP distance (R_a). This value is calculated with an unusual scaling factor of 4 for the dispersion parameter:

$$R_a^2 = 4(\delta_{D1} - \delta_{D2})^2 + (\delta_{P1} - \delta_{P2})^2 + (\delta_{H1} - \delta_{H2})^2 \quad (1.13)$$

This scaling factor is controversial, as there has been no theoretical validation for why it should exist.⁵⁰ It is entirely empirically based, yet used in all HSP calculations. There has been some work showing general asymmetry between the dispersive and dipolar terms, yet this need not necessarily be a constant.^{55,56} It continues to be included for lack of a better option.

Obviously, HSP do not present a complete picture of solvation. They can be improved upon in several ways that are theoretically sound, such as including solvent radii and splitting hydrogen bond donor/acceptor interactions.⁵⁶ There exist more com-

plex and complete predictors of solvation, such as the quantum-mechanically based COSMOTherm.^{57,58} However, their simplicity, relative accuracy, and ease of use for rapid screening have sustained their popularity for five decades, and they are used in this work for these reasons.

The HSP of a solute can be determined by measuring its solubility in a set of test solvents at a given concentration, as shown in Figure 1.4. A range of solvents with known HSP values are selected to cover a wide range of the solubility space (Fig. 1.4a), then tested for their ability to successfully dissolve the solute at a given concentration and temperature. Successful solvents are marked as blue spheres, while unsuccessful solvents are indicated as red cubes (Fig. 1.4b). Using this data, a Hansen solubility sphere is constructed, comprising a central set of three HSP values, and a fourth parameter, the sphere radius R_0 . This sphere is depicted in green (Fig. 1.4c), and solvents that fall within its radius are likely to dissolve the solute.

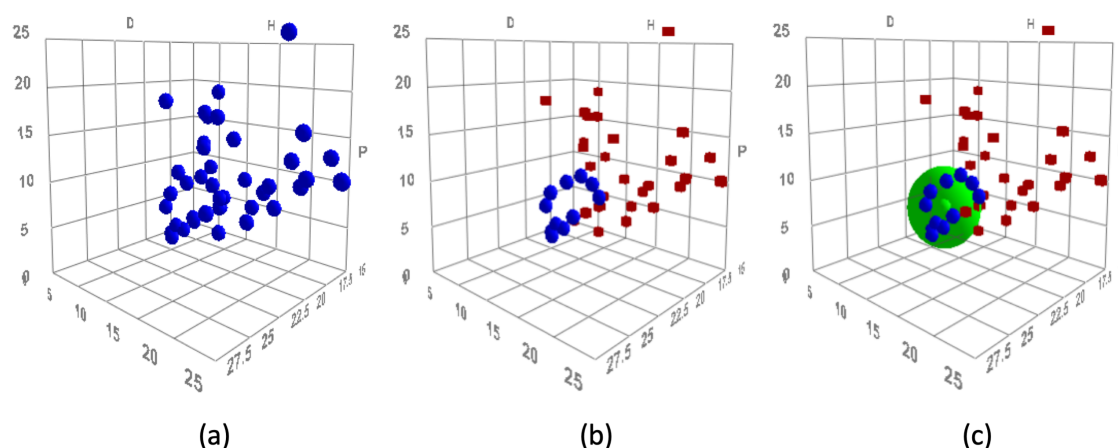


Figure 1.4: Stages of measuring HSP values of a solute. a) Test solvents with known HSP are selected and their values plotted in three-dimensional space; b) Solvents are tested for their ability to dissolve solute, with successful solvents marked in blue and unsuccessful in red; c) Solubility sphere is calculated and shown in green.

Plotting the solubility sphere in three-dimensional Hansen space alongside untested solvent candidates allows rapid prediction of which solvents are likely to dissolve the target—solvents that fall within the sphere will probably work, while those outside the sphere typically will not. This prediction can be simplified to a value known as the relative energy difference (RED), allowing quick calculation of whether a solvent candidate is likely to work:

$$\text{RED} = \frac{R_a}{R_0} \quad (1.14)$$

In this equation, R_a is the Hansen distance from the centre of the solubility sphere to the target solvent. If a solvent falls within the sphere, its R_a will be smaller than R_0 , and the RED will be less than 1, indicating that dissolution will likely occur. Conversely, an RED value above 1 indicates that the solvent falls outside the solubility sphere of the target solute, and is not likely to dissolve it.

HSP of mixtures or solvent blends can be predicted by simply using a linear combination of each individual solvent parameter, with components weighted by their proportion in the blend. This allows rapid assessment of a wider library of potential solvent candidates, but is not always accurate, as real-world systems do not behave as predictably as linear combinations.

While historically, HSP have been calculated from empirically-determined physical values, they can also be predicted from a molecular structure using various group contribution methods.⁵⁰ An algorithm (Yamamoto Molecular Break, or Y-MB) is built into the HSP software (Hansen Solubility Parameters in Practice, or HSPiP) and uses an automated group contribution method to allow fairly accurate HSP predictions based on molecular structure of a compound. While it is good enough for many purposes, Y-MB is deliberately kept simple to speed calculations. More involved group contribution calculations, such as the S-P (Stefanis-Panayiotou), may provide more accurate results.⁵⁹ In this work, HSP were drawn from the empirical HSPiP database if possible, or predicted via Y-MB if not.

Kamlet-Abboud-Taft (KAT) Parameters

Kamlet-Abboud-Taft (KAT) solvatochromic parameters are experimentally determined solvent polarity scales. Like HSP, KAT parameters separate solvent polarity into three separate components, offering a more complete picture than a single-parameter scale. Unlike HSP, they are based on intermolecular solvent-solute interactions, which are probed using an assortment of dyes added directly to the solvent.⁵³ KAT parameters are slower to assess than HSP, as three new experiments must be performed to fully assess each unknown solvent. However, because they are empirically measured, they can detect properties that may not be predictable from the molecular structure of a solvent. The molecules of solvatochromic dye interact with the layer of solvent directly surrounding them (the *cybotactic region*). In the case of blends, this layer may be composed primarily of one solvent component, and the KAT parameters may preferentially reflect the properties

of that single solvent.^{60,61} Thus, KAT parameters work well as a complement to HSP, which look at the bulk of the solvent.

KAT parameters use three scales to characterize a solvent: hydrogen bond donating ability (α), hydrogen bond accepting ability (β), and dipolarity/polarisability (π^*).^{53,62} Unlike earlier solvent scales, however, KAT parameters do not use a single indicator dye for each parameter; instead, a number of different dyes are used in combination to calculate normalised solvent parameters.⁵³ For high-polarity solvents, common choices of solvatochromic dyes include Reichardt's dye for α , N,N-diethyl-4-nitroaniline, (DEN) for π^* , and 4-nitroaniline (4-NA) for β (Fig. 1.5).⁵⁴

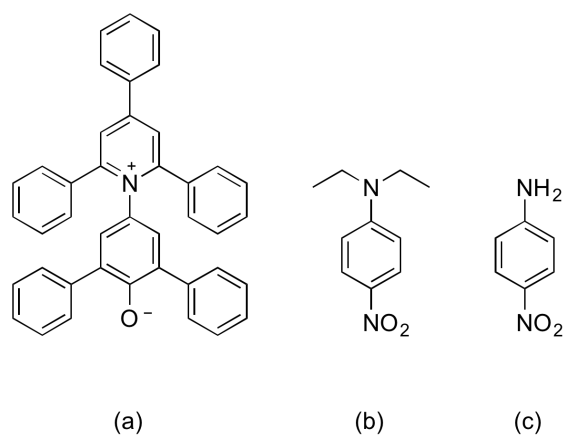


Figure 1.5: Solvatochromic dyes used to measure KAT parameters: a) Reichardt's dye, b) N,N-diethyl-4-nitroaniline, and c) 4-nitroaniline.

Each of these solvatochromic dyes has a ground state and excited state stabilised by certain solvent characteristics. The energy of transition between these states can be measured with UV-Vis spectroscopy, with each dye presenting an absorbance wavelength that is either *hypsochromic* (decreasing) or *bathochromic* (increasing) with increasing solvent characteristic. For example, the ground state of Reichardt's dye (Fig. 1.5a) involves a localised negative charge on the phenoxide oxygen, while the excited state spreads the charge over the conjugated system. The more polar ground state is stabilised by dipolar solvents, while the excited state is more stable in non-polar solvents, leading to a measurable energy gap affected by the dipolarity of the surrounding solvent. Reichardt's dye is therefore hypsochromic, as an increase in solvent dipolarity will increase the energy gap and decrease the wavelength of maximum absorbance. By combining three dyes that have varying responses to solvent characteristics, a full set of KAT parameters can be calculated.⁶³⁻⁶⁵

Each KAT parameter is scaled to reference solvents in order to normalise its values. For example, π^* is typically referenced to cyclohexane for a zero value, as cyclohexane has effectively zero polarity. Dimethylsulfoxide (DMSO) can be used as the high-polarity reference solvent with a value of one. For α and β , measurements from several solvents without hydrogen bonding capabilities are extrapolated to find a zero value. After scaling, most solvents measured will have KAT parameter values that fall between zero and one.⁵⁴ These can then be compared with known KAT values for common solvents to predict how similarly two solvents will behave. Finding similar solvents in the KAT space can suggest potential applications for a novel solvent, enhancing the predictions made with computed HSP values.

1.3 Green Solvents

Within green chemistry, solvents are a major challenge.⁶⁶ Though there has been a great deal of research in this area, there are still entire classes of solvents that lack safe replacements. Much of the research conducted in green solvents focuses on what the researchers find most interesting, not the areas of highest industrial need. Notable examples include the overwhelming academic interest in ionic liquids, though these are frequently not practical as solvent replacements, and a majority of solvent publications focusing on reaction media for organic synthesis, when the greatest proportion of volatile organic compounds (VOC) emissions are from outside the chemical industry.⁶⁷ This work will highlight areas of greatest need for solvent replacement, and focus on practical alternatives in these areas.

In order to avoid regrettable substitutions and accelerate the transition to a bioeconomy, a systematic and intelligent approach for solvent substitution is required. Safer and more sustainable solvents must:

- retain the functionality of the conventional solvent,
- avoid toxic and hazardous properties,
- use sustainable feedstocks, and
- be cost-effective.

Meeting these criteria can be challenging, as can comparing the relative sustainability of each solvent candidate. As discussed in Section 1.1.3, several solvent selection guides have been published to assist researchers in choosing safer or greener solvents. The

most broadly applicable guide to date is the CHEM21 selection guide, which weighs a number of different hazard criteria in order to assign one of four simplified rankings (from *recommended* to *highly hazardous*) to each solvent.⁴¹ The range of criteria included and the simplicity of the final ranking make this method quite useful, though researchers must use care when relying on these rankings as they are not absolute. The CHEM21 guide attempts to quantify three pillars of solvent safety based on measurable quantities related to each pillar:

- flammability (flash point, auto-ignition temperature, resistivity, peroxide formation)
- health (GHS hazards, volatility)
- environmental (boiling point, GHS hazards)

This method does not account for environmental partitioning, renewable origins, biodegradability, environmental impact of manufacturing, or many other green solvent requirements which are difficult to measure. Therefore, the CHEM21 guide can only serve as a starting point for solvent assessment, and other criteria must be taken into account by the researcher. In this work, hazards are assessed via CHEM21 when possible, with other green metrics being taken into account as needed.

1.3.1 Legislative Drivers

In the EU, much of the recent motivation behind solvent replacement is due to legislative drivers. While Europe has had chemical legislation for decades, the adoption of the REACH regulation in 2006 signaled a paradigm shift.⁶⁸ REACH not only shifted the burden of proving safety to chemical manufacturers and distributors, but also greatly broadened the impact of chemical regulation, affecting nearly every chemical product in the EU. Suddenly, every hazardous solvent in use was at risk of being restricted or banned outright. In particular, dipolar aprotic solvents like dichloromethane (DCM), *N*-methyl-2-pyrrolidinone (NMP) and dimethylformamide (DMF), which tend to have severe toxicity or mutagenicity issues, were designated candidates for future restriction (Fig. 1.6).⁶⁹ As there are very few options for safer dipolar aprotic solvents, this has caused considerable difficulty for industry, and safer replacements are in demand.⁶⁷

In addition to REACH, local legislation can act as a driver for solvent substitution. For example, there are pollution prevention and solvent emissions regulations in England and Wales that impose additional restrictions on industrial solvent users.^{70,71} Require-

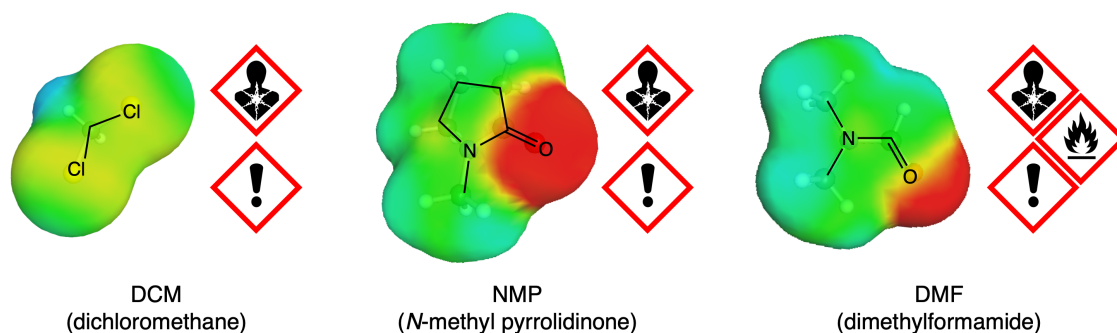


Figure 1.6: Traditional dipolar aprotic solvents DCM, NMP, and DMF with their associated hazard symbols.

ments from this legislation can generally be met with abatement equipment, reducing solvent emissions into the environment, but this can be expensive to install and operate. Replacing the restricted pollutants with green, biodegradable solvents could reduce long-term costs to manufacturers and users.

Finally, REACH is only the tip of the chemical legislation iceberg. Countries around the world, including major manufacturers like China, Korea, and Japan, have adopted their own versions of REACH, some with even higher safety requirements.¹² Future chemical legislation is likely to require stricter risk assessment, fewer hazards, and possibly even recycling and circular economy considerations.^{72,73} To guarantee long-term process viability, industry must proactively stay ahead of legislation, rapidly developing and adopting safer and greener chemical technologies.

1.3.2 Solvent Use

While most academic research in green solvents focuses on reaction media for organic synthesis, particularly for use in pharmaceutical or fine chemical manufacturing, this is not where the majority of solvents are used.⁶⁷ The biggest user of solvents by far is the paints and coatings sector (Fig. 1.7), which accounts for 46% of solvent use in the EU.⁶⁹

In paints and coatings, the role of a solvent is to dissolve and suspend the paint components, then evaporate once applied.⁷⁴ A large portion of the paint formulation is polymer binder, therefore, polymer solvents are crucial to the paints and coatings sector. Other sectors which require polymer dissolution include:

- adhesives, in which solvents dissolve the adhesive polymers to allow spreading onto a surface;⁷⁵
- cosmetics, in which polymers are used as stiffeners and gelling agents;⁷⁶

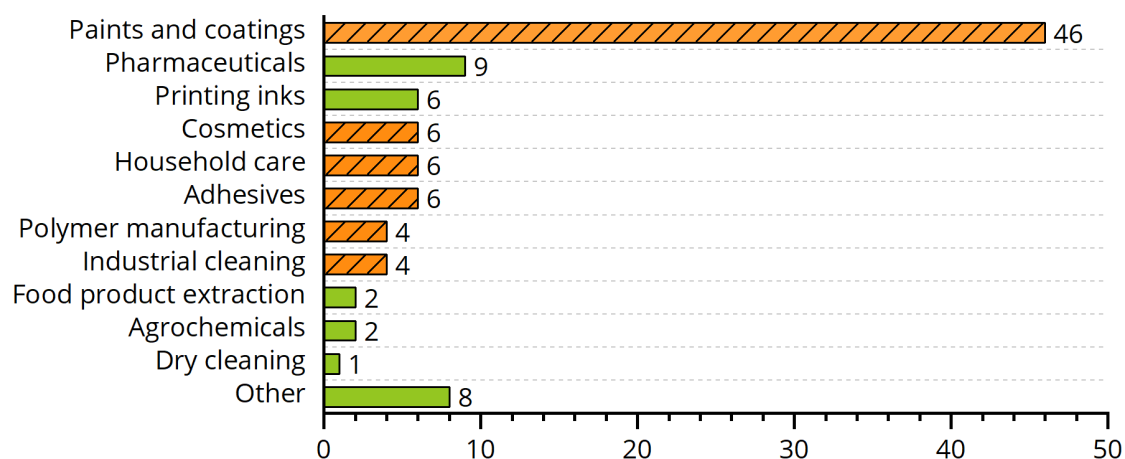


Figure 1.7: Solvent use by industrial sector. Sectors that require solvents for polymer dissolution are marked in striped orange.

- household care, in which polymers are used in laundry detergent formulations;⁷⁷
- polymer manufacturing, in which the polymer product must be dissolved during processing; and
- industrial cleaning, in which polymer coatings must be removed from surfaces.

After summing all of the above, it is apparent that sectors requiring solvents for polymer dissolution comprise at least 72% of solvent use in the EU, yet there are hardly any academic papers being published on green solvents for this application.⁶⁷ Furthermore, other applications such as membrane manufacturing, plastics recycling, electronics, and medicine require advanced knowledge of polymer dissolution.⁷⁸ It is clear that in order to make a meaningful difference in solvent use, research in green solvents for polymer applications is sorely needed.

1.4 Polymer Dissolution

As above, the dissolution of polymers depends on both enthalpy and entropy of mixing. While enthalpy can be treated the same way for monomeric and polymeric solutes, the entropy of mixing tends to be less favourable in polymers. Because the segments of a polymer are linked together in a chain, they cannot take full advantage of the volume increase available through mixing. Longer polymers are more affected by this phenomenon, while shorter chain lengths allow greater entropy change. This can be mathematically modelled with Flory-Huggins theory, which gives an adapted Gibbs energy equation for polymer-solvent interactions.⁷⁹

$$\Delta G = RT[n_1 \ln \phi_1 + n_2 \ln \phi_2 + n_1 \phi_2 \chi_{12}] \quad (1.15)$$

In Equation 1.15, the number of moles (n_1) and volume fraction of solvent (ϕ_1) as well as the number of moles (n_2) and volume fraction of polymer (ϕ_2) are combined with χ , a mixing parameter which describes specific solvent-polymer interactions. While simplified, this theory is useful in many cases, and gives an idea of the difference between monomeric and polymeric solvation energy. Added complexity can be found in the conformational entropy, which accounts for the change in a polymer's folding as it enters solution, and makes flexible polymers more soluble than rigid ones.⁸⁰

Kinetic considerations are particularly important in polymer dissolution. Monomeric compounds tend to disperse easily in a solvent, speeding molecular diffusion. Polymers, on the other hand, tend to undergo slow molecular diffusion, hampered by entanglement of their chains.⁸⁰ In practical terms, this results in a dissolution process distinct from that of monomeric materials, involving stages intermediate between undissolved and dissolved. The long chains that comprise a polymeric material are involved in complex intermolecular interactions that bind the material together and give it its unique properties. In order to dissolve a polymer, the solvent must diffuse into the polymer and disentangle its chains (Fig. 1.8). In the process, several layers are formed, each with a different level of solvent-solute interaction.⁷⁸

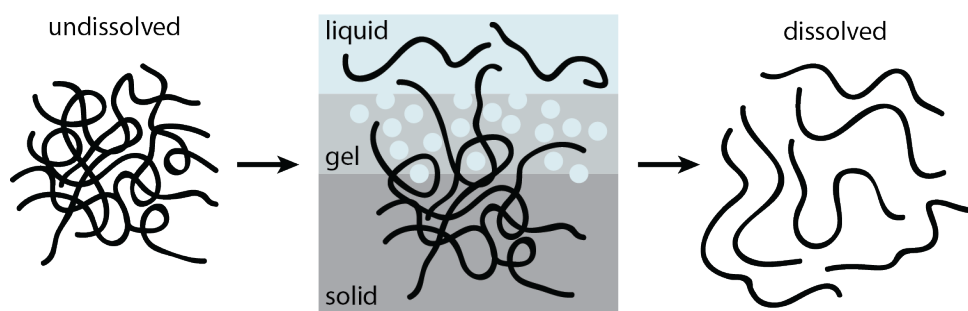


Figure 1.8: Stages of polymer dissolution. As the solvent penetrates the polymer, a gel layer forms between the bulk solid and dissolved liquid.

Depending on the polymer, solvent, and rate of diffusion, two general cases are possible: swelling, and cracking. In the swelling case, solvent slowly diffuses into the polymer, plasticising it and forming a swollen gel-like layer. Diffusion then continues at both the solvent-gel and gel-polymer interfaces, forming a gradient of semi-dissolved layers ranging from liquid to solid. These layers change in thickness throughout the

dissolution process, until eventually all polymer has completely dissolved. Polymer cracking is less common, and occurs when rapid diffusion of solvent into polymer forms stress cracks in the polymer matrix, breaking up the bulk of the polymer rather than forming a gel layer.⁷⁸

This complexity makes polymer dissolution considerably more challenging and difficult to predict than simple small molecule dissolution. The dissolution process can be controlled either by disentanglement of the polymer chains, or diffusion into the gel boundary layer. The strength of each of these effects depends on the polymer and solvent properties, both chemical and physical. Successful solvent selection for polymers therefore take into account the properties of individual polymers, and cannot be performed on a general basis.

1.4.1 Membrane and Film Formation

A key application for polymer solvents is the production of membranes for various applications. Membranes for water filtration are of increasing importance as water use grows and freshwater availability drops.⁸¹ Water filtration membranes are made using polymers with good thermal and chemical stability, such as polyvinylidene difluoride (PVDF), polyimide (PI), polysulfone (PSU) and polyethersulfone (PES).^{81,82} Membranes made from these polymers can also be used for other applications, including distillation, gas separation, and battery applications.⁸³ The most common method of membrane preparation is phase inversion, particularly non-solvent induced phase inversion (NIPS), in which the polymer of choice is dissolved in a suitable solvent, cast onto an inert substrate, and immersed in a non-solvent bath to force precipitation of the polymer (Fig. 1.9).^{84,85}

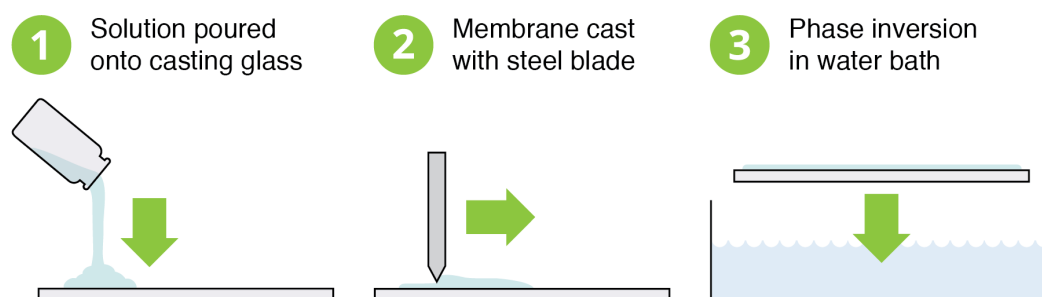


Figure 1.9: NIPS casting method for forming water filtration membranes from polymers

In this process, the choice of solvent is critically important in determining the properties of the membrane. Properties such as solvent/polymer interaction, solvent/non-solvent interaction, viscosity, and diffusivity can significantly alter the morphology of the membrane, and therefore its filtration properties and potential applications.^{86–88} The best-known solvent-related difference in NIPS membrane formation is the internal pore structure, which can change from an inhomogeneous series of finger-like macrovoids to a homogeneous, spongy, *bicontinuous* pore structure. These morphological differences are caused by two types of phase separation, which can be influenced by the rate of mutual diffusion between the polymer solution and non-solvent bath (Fig. 1.10).^{82,84}

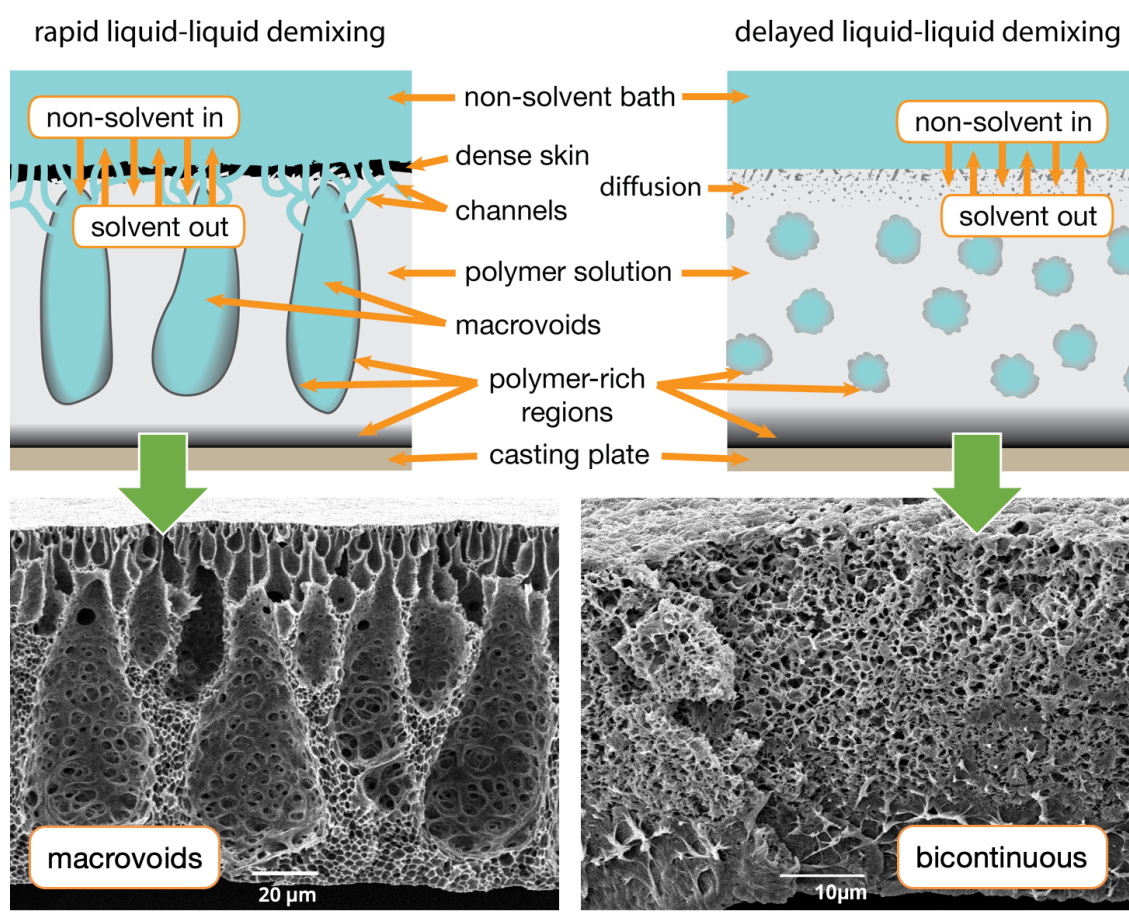


Figure 1.10: NIPS membrane cross-sections showing formation of macrovoid (left) and bicontinuous (right) morphologies

Macrovoid formation occurs when the diffusion between solvent and non-solvent is very rapid (Fig. 1.10, rapid liquid-liquid demixing). This results in immediate precipitation of the polymer at the solvent/non-solvent interface, forming a dense skin layer at the top of the membrane. Numerous pores in the skin layer allow channels of non-solvent to penetrate into the bulk of the polymer solution, pushing polymer aside

and concentrating it in regions that precipitate to shape finger-shaped voids. Typically, this morphology has a region of smaller voids at the top that result from the diffusion channels, irregular macrovoids dispersed throughout the middle layer, and a spongy polymer-rich region at the bottom.^{89,90}

When solvent/non-solvent diffusion occurs more slowly, macrovoids are replaced by a bicontinuous structure (Fig. 1.10, delayed liquid-liquid demixing). In this case, precipitation takes place gradually, as non-solvent permeates the polymer solution and forms numerous small pores. This morphology is largely homogeneous, but frequently has a denser bottom layer where the polymer solution contacts the casting plate.^{87,91}

Without prior experimentation, the likely morphology for a specific casting system is difficult to predict. Easily calculated properties, such as solvent/polymer interaction strength or solvent/non-solvent interaction strength, do not correlate with a specific membrane type, and predictive mass-transfer calculations are complex and time-consuming.^{86,92} In choosing solvents for membrane casting, researchers typically identify solvents that are compatible with the polymer and non-solvent, then move to empirical trials to observe the type of membrane formed and identify its likely applications.⁹³⁻⁹⁵

Compatible solvents can be predicted by comparing measured HSP values for polymers and predicted or measured HSP values for solvent candidates. The relative energy difference (RED) value for each solvent/polymer combination predicts whether the solvent is likely to be effective ($RED < 1$) or ineffective ($RED > 1$) for that polymer. As an example, three common membrane polymers and a selection of common solvents are shown in Table 1.2. From this data, it is apparent that dipolar aprotic solvents tend to be closer to these polymers in HSP space, and therefore better at dissolving them. However, this class of solvents tends to have undesirable hazards and many have been restricted under REACH (see Section 1.3.1). Therefore, green solvents to replace dipolar aprotic solvents in membrane casting applications are in demand.^{84,96,97}

Table 1.2: HSP RED for common solvents and membrane polymers

Solvent	RED		
	PI	PSU	PES
acetone	1.2	1.1	0.9
acetonitrile	1.1	1.7	1.3
benzene	1.4	1.3	1.6
n-butanol	1.1	1.4	1.4
chloroform	1.3	0.9	1.1
cyclohexane	1.6	1.6	1.8
DCM	1.1	0.7	0.7
diethyl ether	1.5	1.5	1.6
DMF	0.9	1.0	0.7
DMSO	0.8	1.1	0.7
ethanol	0.9	1.7	1.7
ethyl acetate	1.3	1.1	1.1
hexane	1.6	1.9	2.0
methanol	1.0	2.2	2.1
NMP	1.0	0.7	0.3
2-propanol	1.1	1.4	1.5
THF	1.2	0.8	0.9
toluene	1.4	1.2	1.4
water	1.2	4.5	4.4

1.5 Dihydrolevoglucosenone (Cyrene) as a Green Solvent

Dihydrolevoglucosenone, or CyreneTM, is a novel solvent that has recently received a great deal of attention as a green replacement for conventional dipolar aprotic solvents.⁹⁸ Its use as a solvent was first discovered at the University of York in 2014, and it was subsequently co-developed with Circa Group, who are currently scaling it to commercial quantities.⁹⁹

Cyrene is produced in two synthetic steps from cellulose, using a novel hydrogenation process that makes its production cost-economical (Fig. 1.11). While insufficient data is available to calculate the mass intensity of the process, the hydrogenation step has ideal atom economy and laboratory yields of over 90%.¹⁰⁰ The liquid emissions from manufacture of Cyrene have been studied and found to have little environmental effect.¹⁰¹

Cyrene is currently registered under Annex VIII of REACH, which allows import of up to 100 tonnes/year into the EU.¹⁰² REACH registration testing showed that Cyrene has no significant toxicity, mutagenicity, or other major hazards. Its only hazard is serious

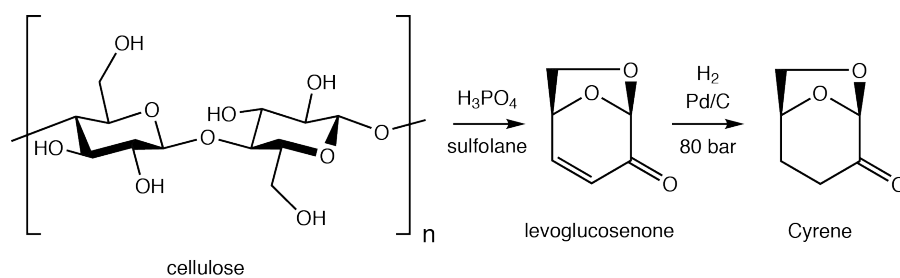


Figure 1.11: Cyrene can be synthesized from cellulose in two synthetic steps.

eye irritation, the exposure risk of which is lowered due to Cyrene's high boiling point of 227°C.¹⁰³ Finally, Cyrene is readily biodegradable under standard REACH screening, theoretically making its end-of-life disposal more environmentally friendly, though no data has yet been released for more realistic conditions.

In addition to its green credentials, Cyrene has very promising solubility parameters (Fig. 1.12). It is nearly identical to traditional solvent NMP in HSP space, suggesting that it will behave similarly to NMP and other dipolar aprotic solvents. In the KAT space, only two parameters— β and π^* —are relevant for aprotic solvents, as α (hydrogen bond donating ability) is effectively zero. Both of these scales show Cyrene to be in the dipolar aprotic solvent space, quite close to NMP, DMF, and other traditional solvents of this class. This similarity to dipolar aprotic solvents is rare for a green solvent, making Cyrene an interesting candidate to explore for replacement of dipolar aprotic solvents.¹⁰⁰

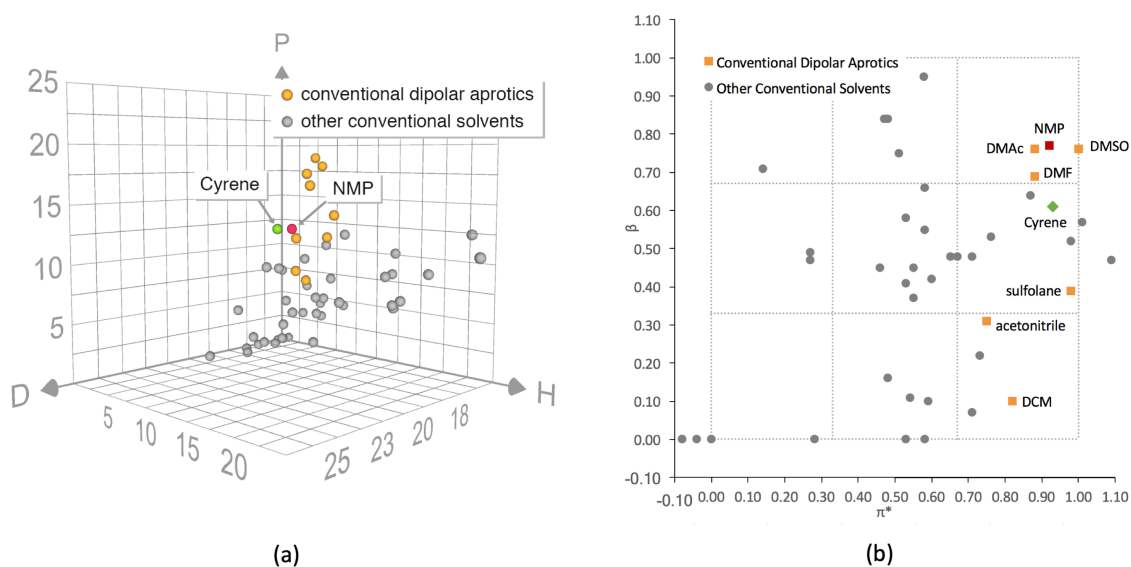
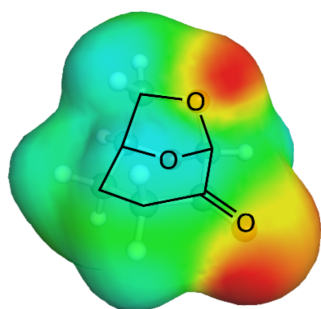


Figure 1.12: Cyrene (green) compared with traditional dipolar aprotic solvents (orange) and other conventional solvents (grey) in (a) HSP space, and (b) KAT space, excluding α as it is 0 in apolar solvents

Since manufacture of Cyrene began, new applications for this solvent have been discovered. Its utility as a reaction medium for organic synthesis has been explored in the Menschutkin reaction and a model fluorination,¹⁰⁰ Sonogashira cross-coupling and Cacchi-type annulation,¹⁰⁴ synthesis of metal-organic frameworks (MOFs),¹⁰⁵ synthesis of ureas,¹⁰⁶ Suzuki-Miyaura coupling,¹⁰⁷ and amide coupling.¹⁰⁸ These studies have also highlighted some drawbacks in use of Cyrene as a solvent for synthesis—namely, it is unstable to acids or bases, and its high boiling point can make it challenging to remove from reactions via traditional evaporative methods.⁹⁸ The stability issue has been addressed in one study by replacing the reactive ketone moiety with a cyclic ketal, but this introduces new challenges, such as a significantly higher melting point.¹⁰⁹

As is typical in solvent research, studies of Cyrene for applications outside of synthesis have only seldom been conducted. Interestingly, Cyrene performs very well in exfoliation of graphite to produce graphene, outperforming the standard NMP or DMF by an order of magnitude.^{110,111} This is due in part to the high viscosity of Cyrene (Fig. 1.13), which presents an advantage in this specific application. These results suggests that applications in advanced materials may be worth exploring, particularly as they do not require rapid evaporation of the solvent. As far as polymer studies, Cyrene's ability to swell cross-linked polymer resins was explored by Lawrenson *et al.* as a facet of peptide synthesis,¹¹² but otherwise materials applications are largely unreported.



Physical Properties of Cyrene	
Melting Point	< -20°C
Boiling Point	227°C
Flash Point	108°C
Viscosity (μ)	14.5 mPa · s
Density (ρ)	1.25 g/cm ³
Vapour Pressure	0.28 hPa

Figure 1.13: Structure and electron density of Cyrene, along with selected physical properties

In this work, applications of Cyrene outside of organic synthesis will be explored. As green solvents for polymer dissolution are crucial to the bioeconomy, Cyrene will be tested in dissolution of synthetic as well as natural polymers. Cyrene's ketal derivatives, known as Cygnets, will be investigated as blends for polymer applications to overcome their high melting point. Finally, polymer applications of a new class of bio-derived

chemicals will be explored in order to highlight another potential green solvent. This exploratory work is intended to open doors for new areas of research, widening the investigation of green solvents for polymer dissolution. It is hoped that some of these new areas will be useful in industrial applications, while others will spark further study that leads to new polymer dissolution solvents.

CHAPTER 2

GREEN SOLVENTS FOR DISSOLUTION OF POLYVINYLIDENE DIFLUORIDE

Polyvinylidene difluoride (PVDF) is a chemically inert thermoplastic polymer that is commonly used in applications where resistance to reactive chemicals is important. It is particularly popular in lithium-ion batteries. With the rapid expansion of the lithium-ion battery industry to service consumer electronics and electric cars, green manufacture and recycling of these batteries has become critical to the circular economy. However, the solvent typically used to dissolve PVDF for manufacture and recycling of PVDF batteries is *N*-methyl-2-pyrrolidinone (NMP), which is reprotoxic and now restricted under REACH. This chapter explores green replacements for NMP in dissolution of high molecular-weight PVDF for battery applications.

2.1 Background

As the global economy gradually transitions from fossil fuel power to renewable energy, the need for high-capacity rechargeable batteries grows more urgent. The increasing adoption of electric vehicles makes the demand especially pressing (Fig. 2.1). With this sharp increase in lithium-ion battery demand, it is important to examine the sustainability of their manufacture, use, and disposal. Some issues, such as energy costs of manufacturing and recycling, as well as abundance of the required elements (e.g. lithium and cobalt), have been addressed in several sources.^{113–116} Solvent usage, on the other hand, is a concern that is rarely addressed in depth.

In both manufacture and recycling of lithium-ion batteries, the solvent of choice is NMP.^{118,119} This solvent requires shielded, explosion-proof equipment when used industrially, as well as strong ventilation to reduce vapour concentration.¹¹⁸ Additionally, the reprotoxicity of NMP has resulted in its REACH restriction, requiring manufacturers to capture and recycle NMP rather than release it into the air.¹²⁰ All of these protective measures are expensive to implement and maintain. Replacing NMP with a safer, greener solvent would remove the need for such measures, reducing costs and improving safety.

The main driver for using NMP is the necessity of dissolving PVDF, which is commonly used as a polymer binder in the electrodes of lithium-ion batteries (Fig. 2.2).¹²¹

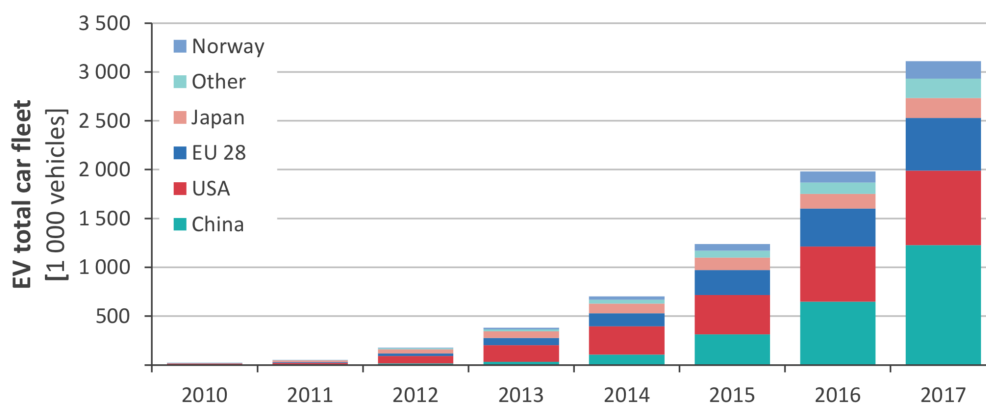


Figure 2.1: Use of electric vehicles (EV) is growing rapidly around the world.

Source: 2018 European Commission report on lithium-ion batteries.¹¹⁷

It serves to hold the active material and any conductive additives against the current-collecting metallic film, while withstanding heating and electrical cycling in the presence of lithium salt and organic carbonates. This stability, while critical to the operation of the battery, makes PVDF quite difficult to dissolve.

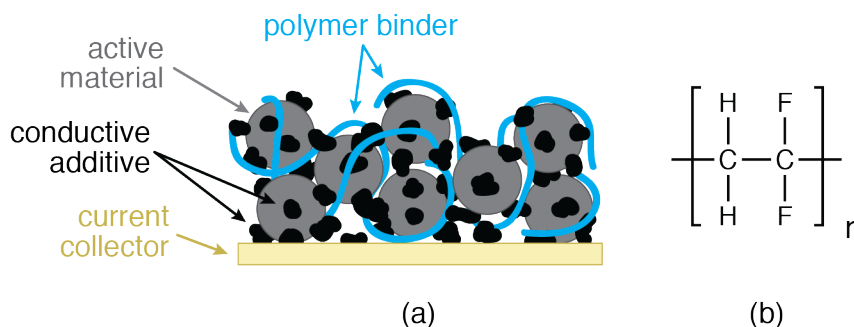


Figure 2.2: (a) Cathode portion of a lithium-ion battery, showing application of polymer to bind active materials and additives to current-collecting foil (b) Chemical structure of PVDF

Solvents for dissolution of PVDF have been studied extensively, primarily for their effects on membrane formation.^{93,122–131} Some progress has been made towards greener solvents for PVDF membranes.^{84,132} However, the PVDF used for battery applications (e.g. Solef® 5130) has an extremely high weight-averaged molecular weight (M_w) of 1,000–1,200 kDa,¹³³ which is at least double the M_w of the PVDF used for membrane applications. This could cause significant changes in its solubility behaviour, as well as the morphology of any materials made with this polymer. It is therefore important to study this specific grade of PVDF in applications such as battery recycling and manufacture. Solubility studies were initiated with computational modelling to give an idea of potential

green solvents.

2.2 Modelling PVDF Dissolution

2.2.1 Solubility Prediction

Hansen Solubility Parameters (HSP) are a popular means of assessing the solubility of a polymer. As described in Section 1.2.5, HSP divide solubility behaviour into three components (δ_D , δ_P , and δ_H), which can be plotted three-dimensionally to visualise the solvent space. Though they do not present a complete picture of solvation, they are frequently useful for predicting polymer dissolution. Measuring the HSP of a polymer by testing which solvents can dissolve it allows generation of a solubility sphere (Fig. 1.4). This can then be used to predict other compatible solvents from the HSP database, speeding up solvent selection by allowing rapid computational screening.

Some HSP values for PVDF have been previously reported, but as solubility of a polymer can vary significantly with molecular weight, a new dissolution model was developed here specifically for Solef® 5130. To develop a predictive HSP sphere, several methods were attempted. Figure 2.3 shows each attempt, listing first the center coordinates of the sphere, then the “core” values which indicate quality of fit (± 0.75 in any coordinate is considered a bad fit, ± 0.25 in all coordinates is considered a good fit), then the sphere radius.⁵⁰

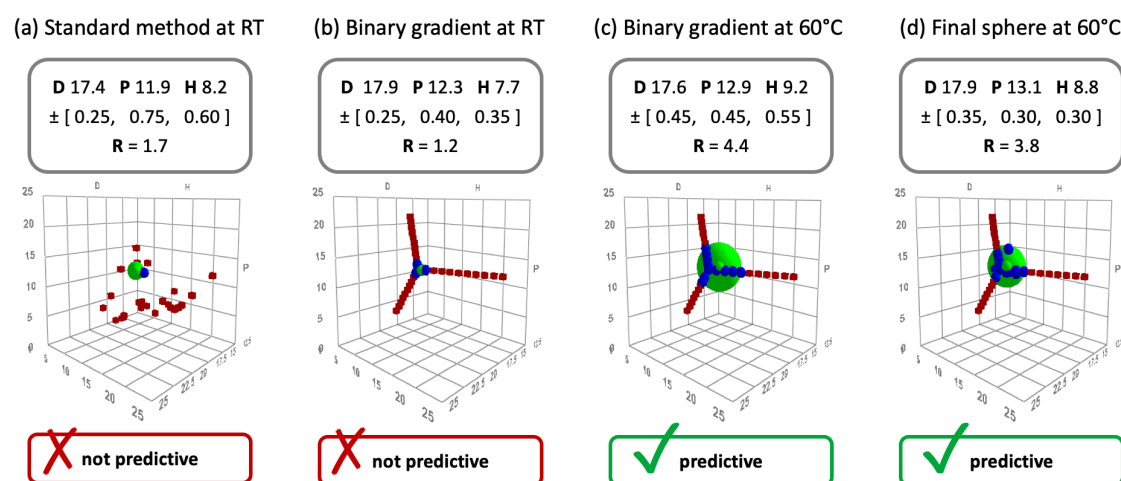


Figure 2.3: Modelling work to generate a predictive HSP sphere for PVDF dissolution, showing sphere center coordinates \pm “core” values indicating fit, and sphere radii. Fit is considered good when all core values are below 0.75.

First, the traditional method of HSP sphere construction was attempted. A number

of readily-available solvents were selected to cover a wide area of HSP space. These test solvents were combined with 10% w/v PVDF (a high polymer loading suitable for battery applications) and mixed for three days at room temperature. This method identified only two solvents (NMP and dimethylacetamide (DMAc)) that could dissolve PVDF, giving insufficient data to construct a good model and resulting in a small sphere and bad fit (Fig. 2.3a). This model was not predictive, meaning that solvents within the boundaries of the sphere did not dissolve PVDF.

Next, a binary gradient approach was used, combining three non-solvents (benzyl benzoate, ethylene carbonate, and methanol) with a good solvent (NMP) in various proportions to more precisely probe the boundaries of the sphere in three directions.¹³⁴ HSPiP predicts the parameters of solvent blends by using a simple linear combination of the individual solvent parameters; this allows creation of a range of test solvents whose HSP values move outward from the central good solvent in precise steps. This technique is less common, but theoretically should give a precise idea of the sphere size and location. However, this method also failed at room temperature, giving a sphere that was too small and not predictive (Fig. 2.3b). The conclusion from these two initial experiments was that despite the three-day test duration, kinetic effects were likely impacting the results and giving false negative results for compatible solvents. To address this, heating was adopted into the testing protocol, in the hope of expanding the HSP sphere and identifying more solvents to dissolve 10% w/v PVDF.

A temperature of 60°C was selected to provide moderate heating while keeping energy use fairly low. Heating and stirring overnight gave a much improved result, with a sphere that proved predictive for single solvents, though the core values indicate that the fit is not ideal (Fig. 2.3c). These results also suggest that for PVDF, especially the high- M_w PVDF used here (1,000–1,200 kDa) heating is of critical importance in dissolution—kinetic effects are apparently dominant in most of the tested solvents, and the traditional test without heating presents an inaccurate picture of solvent compatibility. Several conventional single solvents were then added to the model to narrow down the sphere slightly, resulting in a final sphere with better fit and a radius of 3.8 (Fig. 2.3d).

This sphere proved quite similar to that presented in a 1988 publication from Bottino *et al.*, who used PVDF with a M_w of 450 kDa (Fig. 2.4).¹³⁵ This confirms the validity of the new model, while also showing that a large increase in M_w only results in a small change in HSP.

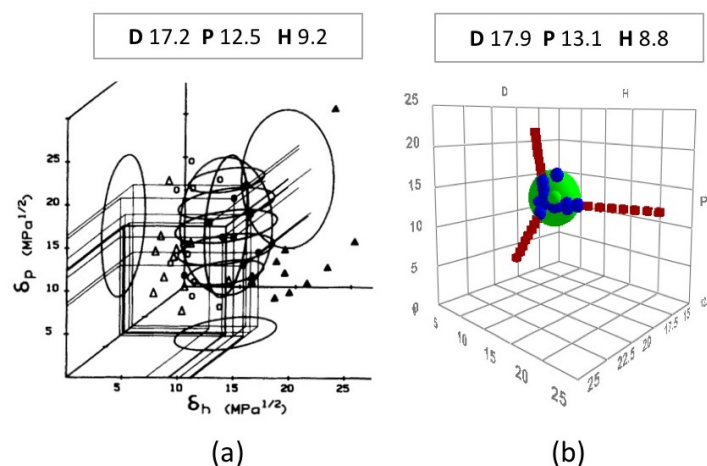


Figure 2.4: HSP spheres to predict PVDF dissolution, as found in a) Bottino's work of 1988,¹³⁵ b) this work.

After constructing a solubility model, a database of 224 commercially available green solvents was constructed in order to identify candidates that could be used for PVDF dissolution. The database was drawn from four sources: the CHEM21 Solvent Selection Guide,⁴¹ Moity's 2012 work on sustainable solvents,¹³⁶ Jessop's 2012 work on solvents for green chemistry,⁵⁴ and the Inkemia catalogue of green solvents.¹³⁷

Solvents from these sources were considered to be sustainable if they were bio-derived and lacking serious hazards (i.e. excluding solvents that would be considered hazardous or highly hazardous by CHEM21 guide). Sustainable candidates were combined into a database of Hansen parameters, drawing from the existing HSPiP database if possible, or generating automatically predicted parameters (using the built-in Y-MB algorithm) from simplified molecular-input line-entry system (SMILES) codes if not. This database was used in combination with the predictive sphere above to produce a list of likely PVDF solvents, which were then empirically tested. The relative energy difference (RED) of each solvent candidate is the simplest indicator of likely compatibility (Eq. 1.14). An RED below one indicates the solvent is within the polymer's solubility sphere and will likely dissolve it, while an RED greater than one indicates likely incompatibility.

A key feature of HSP for polymer dissolution is the ability to create functional solvent blends by combining two non-solvents with appropriate parameters. Accordingly, the list of solvent candidates for this project included single solvents as well as binary blends. Every single-component solvent with $RED < 1$ proved empirically able to dissolve PVDF, with the exception of acetic anhydride (Table 2.1). As acetic anhydride hydrolyses readily in atmospheric moisture to form acetic acid, it is likely that the stock solvent used—

Table 2.1: Results of single-solvent dissolution trials for PVDF

Solvent	MVol	RED	Success?
N-Methyl-2-Pyrrolidone (NMP)	96.6	0.50	yes
N,N-Dimethyl Formamide (DMF)	77.4	0.55	yes
N,N-Dimethyl Acetamide (DMAc)	93	0.56	yes
Cyrene	101.6	0.78	yes
γ -Valerolactone (GVL)	97.1	0.80	yes
Acetic Anhydride	95	0.82	no
Dimethylsulfoxide (DMSO)	71.3	0.88	yes
Cyclopentanone (CP)	89.1	0.98	yes
γ -Butyrolactone (GBL)	76.5	1.00	yes
Glycerol Carbonate	83.2	3.40	no

Solvents with RED < 1 are predicted to dissolve PVDF. Samples were prepared with 10% w/v PVDF and stirred at 60-100°C overnight.

which had been opened many months before this experiment—was contaminated with a significant amount of acetic acid. This would change its HSP significantly, bringing it out of the solubility sphere. Discounting this anomalous result, the single solvents predicted by HSP could successfully dissolve PVDF. Glycerol carbonate was tested as an example of a sustainable solvent well outside of the solubility sphere, and indeed did not dissolve PVDF.

Table 2.2: Results of blended solvent dissolution trials for PVDF

Solvent 1	Solvent 2	Vol% 1	Vol% 2	RED	Success?
p-Cymene	Glycerol Carbonate	54	46	0.01	no
5-HMF	GVL	37	63	0.06	yes
Isobutanol	Propylene Carbonate	44	56	0.13	no
CP	Water	89	11	0.13	yes
Cyclohexane	Glycerol Carbonate	48	52	0.14	no
DMF	Cyrene	58	42	0.18	yes
Acetic Acid	Propylene Carbonate	49	51	0.20	no
DMAc	Cyrene	58	42	0.22	yes
CP	Glycerol	81	19	0.27	yes
CP	Ethylene Glycol	80	20	0.28	no
Acetonitrile	Benzyl Alcohol	52	48	0.41	no

Solvents with RED < 1 are predicted to dissolve PVDF. Samples were prepared with 10% w/v PVDF and stirred at 60-100°C overnight. Solvent abbreviations used here for brevity: 5-HMF = 5-hydroxymethylfurfural, GVL = γ -valerolactone, CP = cyclopentanone, DMF = N,N-dimethylformamide, DMAc = N,N-dimethylacetamide

However, the blended solvents were less predictable (Table 2.2). Blends of a successful single solvent with a non-solvent tended to work, while blends of two non-solvents did

not work. In some cases, even blends with a successful solvent did not work, as seen with cyclopentanone (CP) and ethylene glycol. From this, we can conclude that dissolving PVDF requires certain solvent characteristics that cannot be accurately predicted for blends. Thus, the utility of the HSP model for PVDF is currently limited to single solvents. Rasool *et al.* had similar difficulties when attempting to dissolve PVDF in green solvents for membrane preparation.¹³⁸ In that case, the polymer used had a MW of 534 kDa, showing that the unpredictability of blends for PVDF dissolution is not limited to the extremely high-MW PVDF used in this study. While this phenomenon could be related to the inability of Hansen parameters to predict complex solvent interactions such as preferential solvation, the fact that HSP can predict blends for many other polymers suggests that the cause is more likely some unusual characteristic of PVDF, such as high crystallinity.

The results of the modelling study and dissolution trials identified four potential green solvent candidates, which were then tested and compared against NMP in a variety of ways.

2.3 Properties of PVDF Solutions

2.3.1 Final Candidates

The best green solvent candidates for PVDF dissolution are summarized in Table 2.3 and Figure 2.5. NMP is included as an example of a standard non-green PVDF solvent. Dimethylsulfoxide (DMSO), γ -valerolactone (GVL), dihydrolevoglucosenone (Cyrene) and CP are all bio-derived and fairly safe. Cyrene, as described in Section 1.5, is derived from cellulose in two steps and considered non-hazardous with the exception of eye irritation.⁹⁸ Its reactivity with bases and strong acids can lead to instability issues in some applications.¹⁰⁴ It is currently REACH registered for use of up to 100 tonnes/year in the EU. The boiling point of Cyrene is 25°C higher than that of NMP, making it harder to remove when evaporation is required. Its density is about 20% higher. The most notable difference, however, is the viscosity—with a room-temperature viscosity almost nine times higher than NMP, Cyrene may behave differently in dissolution and application of PVDF solutions.

DMSO is produced through catalytic oxidation of dimethyl sulfide, which is a byproduct of the Kraft wood pulping process.^{69,141,142} While it is fully registered under REACH, allowing over 1,000 tonnes/year to be used in the EU, and considered non-hazardous, its

Table 2.3: Green solvent candidates for PVDF dissolution compared with traditional solvent NMP

Solvent	δ_D	δ_P	δ_H	Viscosity (25°C, mPa s)	Density (g/cm ³)	BP (1 atm, °C)	Water Content (%)
NMP	18.0	12.3	7.2	1.67 ¹³⁹	1.03 ¹³⁹	202	0.21
DMSO	18.4	16.4	10.2	1.99 ¹³⁹	1.10 ¹³⁹	189	0.06
GVL	16.9	11.5	6.3	2.20 ¹¹⁰	1.05 ¹¹⁰	207	0.24
Cyrene	18.8	10.6	6.9	14.5 ¹¹⁰	1.25 ¹¹⁰	227	0.18–0.96
CP	17.9	11.9	5.2	1.29 ¹¹⁰	0.95 ¹⁴⁰	131	0.18

skin penetration ability, strong odour in wastewater treatment, and generation of SO_x upon incineration can be causes for concern.^{41,143–145} Its density and boiling point are within 10% of the NMP values, while viscosity is 20% higher, suggesting its polymer dissolution behaviour could be moderately different.

GVL is derived from the conversion of cellulosic biomass to glucose and then levulinic acid.¹³⁸ It is considered non-toxic, has low volatility, and does not appear to readily form peroxides.^{138,146,147} However, GVL is not currently REACH-registered, limiting its use in the EU to under 1 tonne/year. There is no data readily available on health hazards such as mutagenicity and reprotoxicity, leaving some questions about its overall safety. The closely-related compound γ -butyrolactone (GBL) was also predicted to dissolve PVDF, but was ruled out on the basis of it being restricted in some countries, as it is converted in the body to controlled drug γ -hydroxybutyrate (GHB).¹⁴⁸ GVL is chemically similar, but less potent as a drug and therefore less restricted, though it may still raise concerns in some industries. GVL is very close to NMP in density and boiling point, but like DMSO, its viscosity is somewhat higher (about a 30% increase).

Finally, CP is typically synthesised from petrochemical precursors, but can be produced efficiently from hemicellulose-derived furfural.^{149,150} It is considered a flammable liquid and irritant, but is fully REACH-registered, allowing use of over 1,000 tonnes per year in the EU.¹⁵¹ As it has no significant toxicity or waste disposal issues, CP can be considered a green option in applications where risk of fire can be controlled.¹⁵² This candidate is the only one with a boiling point and viscosity considerably lower than those of NMP, though its density is similar. The boiling point, in particular, represents a drop of 71°C, suggesting that CP will evaporate much faster and may not be suitable for applications where low volatility is important.

Of these green candidates, GVL, CP, and Cyrene are not well-studied in the literature.

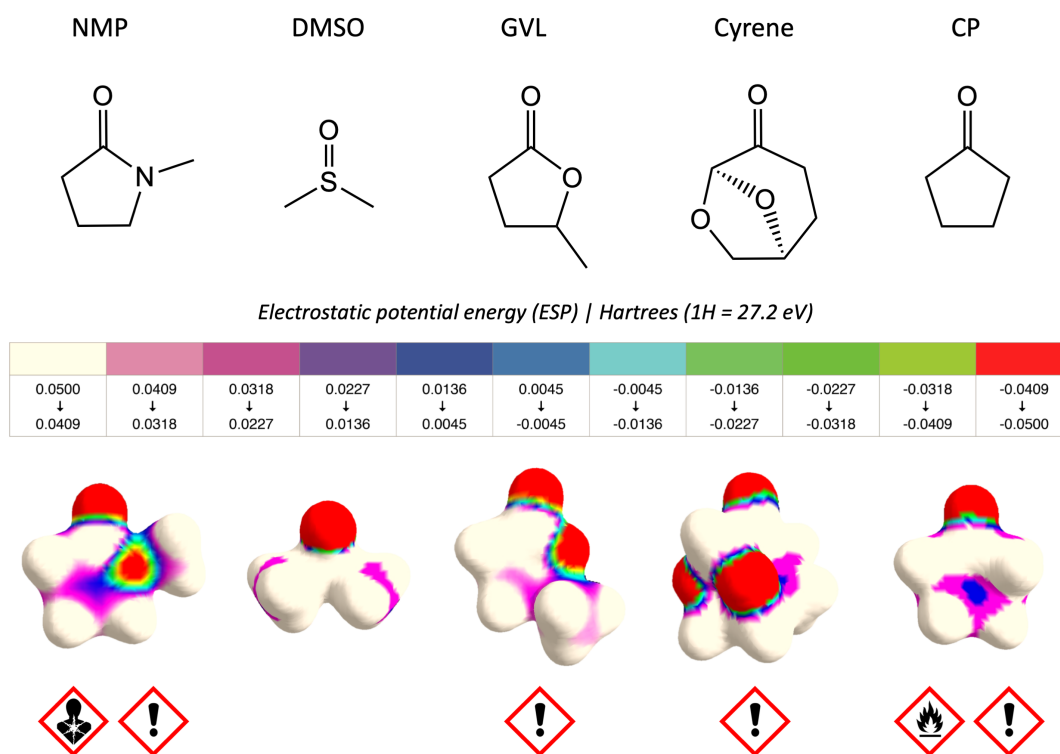


Figure 2.5: Final solvent candidates for PVDF dissolution, depicted as structural formulae and ESP surfaces, with associated GHS symbols below.

GVL is reported as a solvent for a co-polymer of PVDF and hexafluoropropylene,^{153,154} and is mentioned briefly in patents as a PVDF solvent for electrodes or membranes,^{155,156} but its properties are not well-reported. CP has been reported as a solvent for PVDF-trifluoroethylene copolymers,^{157,158} a co-solvent for PVDF or its copolymers in the presence of propylene carbonate,^{159,160} and is briefly mentioned as a single solvent for pure PVDF, but again, no exploration of the properties of PVDF dissolved in CP is available.¹⁶¹ Cyrene is the most novel of these solvents, and is only reported in two interactions with PVDF: membrane formation with PVDF ($M_w = 322$ kDa),¹³² and ability to dissolve PVDF nanofiltration membranes.¹⁶² DMSO, on the other hand, is well-known as a PVDF solvent, and has been studied in casting of PVDF membranes^{130,163,164} and other applications.¹⁶⁵

These four green solvents were therefore studied for their ability to dissolve high molecular weight PVDF designed for battery applications, and their unique properties were assessed and compared with those of solutions in NMP. Each solvent can dissolve at least 10% w/v PVDF, with NMP and DMSO achieving this at room temperature over several hours, and GVL, Cyrene, and CP with heating to 60-100°C in under two hours. The behaviour of these PVDF solutions varies quite a bit, as depicted in Fig. 2.6 and

described below.

2.3.2 Dissolution Differences Between Solvents

There are significant differences in the PVDF dissolution behaviour of each green solvent candidate (Fig. 2.6). As a baseline, dissolution in NMP begins immediately at room temperature, gelling the outermost layer of PVDF and forming a film that forces the bulk of the polymer to clump and strongly adhere to the glass vial. This phenomenon slows dissolution significantly, and even with heating and magnetic stirring it can take several hours for the PVDF to fully dissolve. When dissolution is complete, the solution is a clear, colorless, viscous liquid at room temperature. This gelation phenomenon is known in other polymers, such as polyvinylpyrrolidone (PVP), where beginning at a high pH to prevent dissolution, and then lowering it until the solvent becomes compatible, prevents clumping and increases the overall dissolution rate by orders of magnitude.⁷⁹

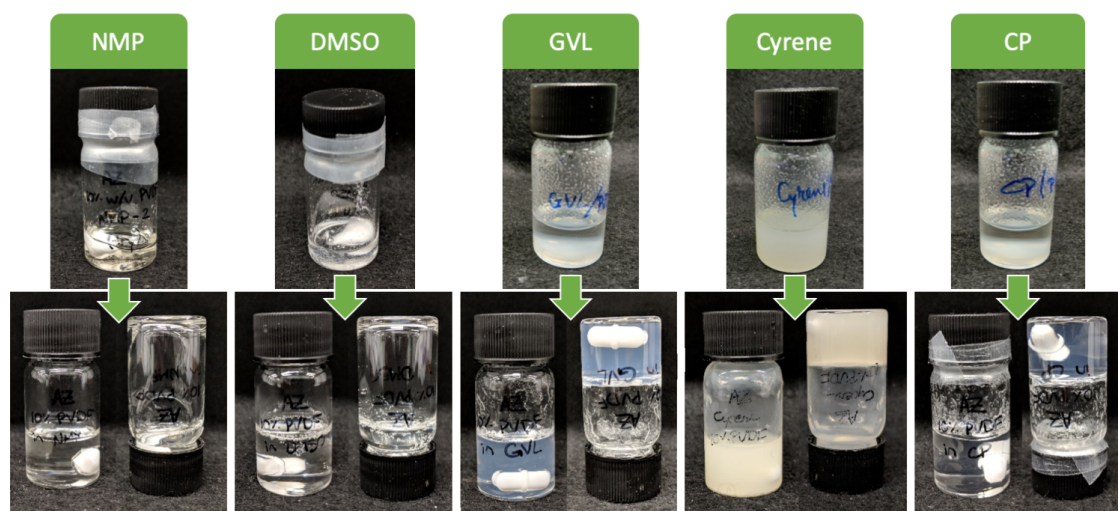


Figure 2.6: 10% w/v PVDF is shown before and after dissolution in each solvent. NMP and DMSO show distinctive clumping behaviour, while GVL, Cyrene, and CP disperse PVDF.

The first green solvent candidate, DMSO, behaves quite similarly to NMP. Dissolution of PVDF begins immediately at room temperature, but the bulk of the polymer clumps, and full dissolution takes several hours even when heated. Additionally, there can be small, completely transparent clumps that persist even when dissolution appears complete, making it difficult to judge whether all of the polymer has dissolved. When the PVDF is fully dissolved, the solution is very similar to an NMP solution—a clear, colorless, viscous liquid at room temperature.

The other three green solvents—GVL, Cyrene, and CP—are much better at dispersing PVDF. Dissolution in these solvents does not occur at room temperature, even after several weeks. GVL and CP must be heated (60°C was the minimum heating attempted) to activate dissolution, and Cyrene requires heating to 100°C. However, even when heated, these solvents do not display the clumping behaviour seen in NMP and DMSO. Instead, the PVDF powder disperses throughout the solvent when shaken or stirred, and the individual particles gradually swell and dissolve over the course of 1–2 hours heating and stirring. This process of gradually heating the solvent can be viewed as analogous to the pH switch used for PVP. By using a solvent that is initially worse (i.e. no dissolution at room-temperature), and heating until it becomes compatible, the clumping issue is avoided and overall dissolution rate is greatly increased. This may present an advantage in recycling situations, where rapid and complete dissolution of PVDF is desired.

2.3.3 Gel Behaviour

GVL, Cyrene, and CP all form a strong gel with 10% w/v PVDF when cooled to room temperature (Fig. 2.5). Gelation of PVDF in ketone and lactone solvents has been previously reported, suggesting that it is the ketone moiety in these three solvents that is responsible for this behaviour.^{166–168} All of these gels exhibit thermoreversible sol-gel transitions, indicating that physical, rather than chemical, cross-linking is occurring.¹⁶⁹ In Cyrene and CP, the gelation occurs rapidly upon cooling, while the GVL solution sets slowly, taking 24 hours to fully gel. This presents some opportunity for processing the GVL solution as a room-temperature liquid, while Cyrene and CP must be kept hot to maintain their liquid forms.

At the 10% w/v concentrations tested here, CP produces a gel that is mostly clear with very slight turbidity, GVL forms a cloudy gel, and the Cyrene gel is completely opaque. This suggests varying levels of polymeric aggregation within the cooling solutions, with the more opaque gels likely having larger aggregates and regions of higher polymer density causing increased light scattering.^{170,171} This variance in aggregate size could affect the applications of these gels, with the more turbid ones being potentially unsuitable for applications where smooth, continuous application of PVDF is required (i.e. film formation). However, for applications that require less homogeneity, such as battery binders, either type of gel would likely be suitable. Application as conductive gel electrolytes, which are highly desirable for battery applications, could also be restricted

by an overly dense macromolecular morphology—an open, porous structure is necessary to allow ionic conduction.^{154,172}

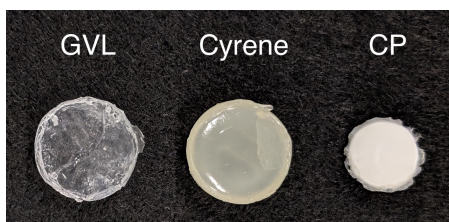


Figure 2.7: Gels prepared with 10% w/v PVDF in CP, GVL, and Cyrene. After being stored in sealed vials for several days, CP samples show considerable shrinkage.

These gels also exhibit differences in long-term stability. The lower boiling point of CP (Table 2.3) results in rapid drying of the gel, even in a sealed vial (Fig. 2.7). CP evaporation causes dramatic shrinking of the substance, going from a clear, colorless gel to an opaque white pellet. Gels made with GVL and Cyrene are far more stable, showing no obvious change even after several weeks. Therefore, gels made with GVL or Cyrene would be more suitable for applications that require a long-lasting gel.

The minimum gelator concentrations (MGC) were measured in order to identify the working liquid range for each solvent, with polymer concentration intervals of 1% w/v (Table 2.4). These values denote the minimum concentration of PVDF necessary to form a gel. While GVL has the highest MGC, it also has a continuous sol-gel transition, with lower concentrations forming a weaker pseudo-gel that gradually flows under gravity. Cyrene and CP have sharp sol-gel transitions, remaining obviously liquid at concentrations below the MGC.

Table 2.4: Minimum gelator concentrations for PVDF solvents

	MGC (% w/v)
GVL	7
Cyrene	1
CP	3

2.3.4 Rheometry of Gels and Solutions

Rheological properties of polymer solutions can be important in determining the limits of their applicability, as well as giving hints about the solvent-solute interaction. The rheological properties of these 10% w/v PVDF solutions were assessed in several ways. For gelled samples, amplitude sweeps were performed at 25°C to assess the strength of

the gel. The gel samples were also heated to 100°C to assess their viscosity as liquids. For liquid samples, viscosity was assessed at both 25°C and 100°C. Tests were performed in triplicate, using a fresh sample for every trial.

The amplitude sweep of each gel shows the variance of both the shear storage (G') and shear loss (G'') moduli with increasing shear strain (Appendix A.1). When G' exceeds G'' , the gel is behaving like a solid; G'' exceeding G' indicates the material is acting as a viscoelastic fluid.¹⁷³ The crossover point, at which G' intersects G'' , represents the maximum shear strain the sample is capable of handling before the gel structure breaks down. This point serves as a measure of the gel strength. By this metric, Cyrene and GVL samples performed similarly (Fig. A.1 and A.2), with the gel breaking between 10 and 20% shear strain. The CP gel, on the other hand, did not break until reaching over 100% shear strain, indicating that this gel is much stronger than the other two.

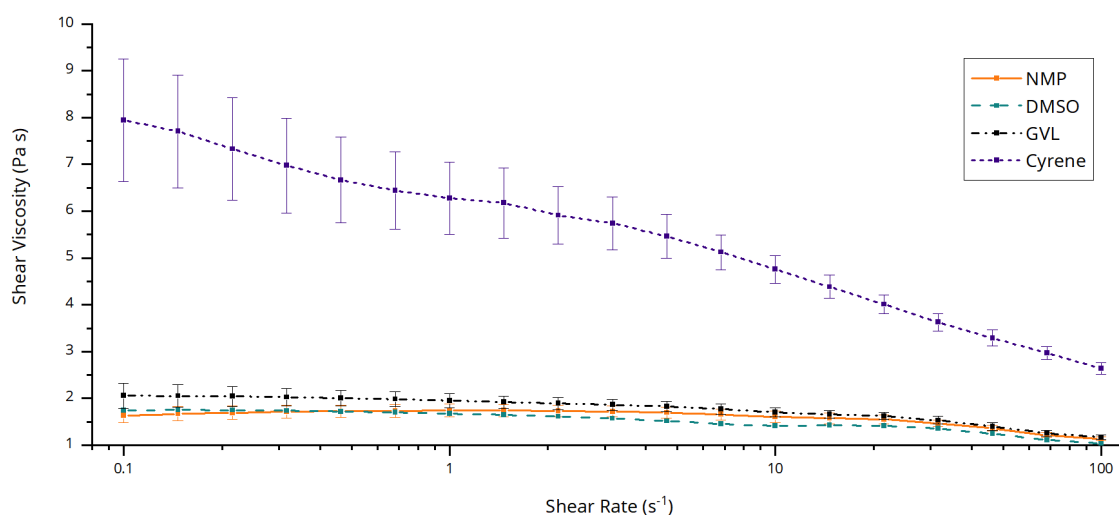


Figure 2.8: Viscosity of 10% w/v PVDF in various solvents at 100°C. Results presented as averages of three independent trials \pm standard error.

Viscosity comparisons between solvents were performed at 100°C, allowing study of all solvents except CP, which proved too volatile for elevated-temperature trials. For each trial, the shear rate was gradually increased from 0.1 s⁻¹ to 100 s⁻¹, and the shear viscosity measured 7 times per decade in a logarithmic progression (Fig. 2.8). All samples showed a viscosity decrease with increased shear (shear thinning). Results for NMP, DMSO, and GVL are self-consistent with low error (see also Fig. A.6, A.7, A.8), but Cyrene samples display a large error margin. This could potentially be due to the variable water content of Cyrene. While the other three solvents were kept over molecular sieves to ensure consistent water content, Cyrene is unstable to molecular sieves and could not be dried

in this way. While Cyrene is not hygroscopic, its water content did vary from 0.18–0.96% between batches (Table 2.3), which could cause some difference in PVDF interaction.

NMP, DMSO, and GVL solutions behave quite similarly to one another in high-temperature viscosity trials. GVL samples display a slightly higher viscosity than the other two, while DMSO samples show slightly more pronounced shear thinning. Cyrene solutions, on the other hand, display a viscosity that is roughly four times higher than the other solvents. This is likely due to the high viscosity of pure Cyrene (14.5 mPa s, Table 2.3), which is well above the viscosities of pure NMP (1.67), DMSO (1.99), and GVL (2.20). The same trend of viscosities is maintained in the PVDF solutions, with $\text{Cyrene} > \text{GVL} > \text{DMSO} > \text{NMP}$.

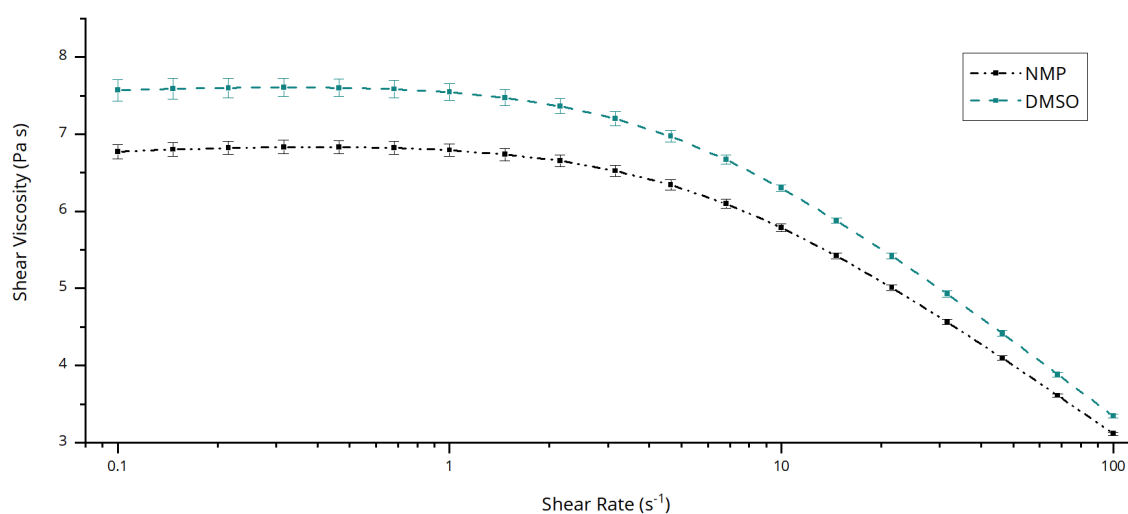


Figure 2.9: Viscosity of 10% w/v PVDF in various solvents at 25°C. Results presented as averages of three independent trials \pm standard error.

At 25°C, only NMP and DMSO samples could be measured (Fig. 2.9), as GVL, Cyrene, and CP formed gels at this temperature. DMSO proved to form a slightly more viscous solution, maintaining the expected trend based on pure solvent viscosities, but otherwise behaves very similarly to NMP.

The differences in dissolution behaviour among the four green solvent candidates suggest that they could have advantages over NMP in practical applications. This was investigated by observing the behaviour of each solution when cast as a film, which could be useful for both electronics and membrane applications.

2.4 Practical Applications

2.4.1 Membrane Casting

Research in this section was carried out in collaboration with Roxana Milesco.

Given its high thermal stability and chemical resistance, PVDF is popular in membranes for separations, including uses such as purification of water and gases, food processing, environmental protection, and more.⁸³ In these applications, the most common manufacturing technique is casting from solution and inducing phase separation to form a polymer film.⁸⁵ When a non-solvent is used to encourage phase separation, the process is known as non-solvent induced phase inversion (NIPS). The mechanics of this process are described in more detail in Section 1.4.1. Solvent properties can greatly impact the morphology of the membrane, and therefore its performance in various applications.^{86,174}

Membrane preparation via NIPS was chosen as an industrially relevant application test that could be performed with available equipment. Samples were prepared using 10% w/v solutions of PVDF in each of the four green solvent candidates, as well as NMP for comparison. Each solution was cast onto a glass plate, which was immediately immersed in a water bath for phase inversion (Fig. 1.9). With the exception of CP, all solutions were heated to 100°C to dissolve, then cast directly from hot solution onto a gently warmed plate. CP solution was too volatile to heat to 100°C, and was instead heated to 60°C to dissolve and cast onto a cold plate to reduce evaporation. The prepared membranes were then dried under vacuum and analysed via scanning electron microscopy (SEM) and attenuated total reflection Fourier transform infrared (ATR FT-IR) spectroscopy. This allowed examination of their pore morphology, which is critical in membrane applications, and crystallinity, which can be affected by solvent polarity. Additional membranes from NMP, DMSO, and GVL were cast at room temperature (Fig. A.10), while Cyrene and CP gelled too quickly for room-temperature casting, but comparisons between solvents were performed with hot-cast membranes to reduce differences due to thermal effects.^{175,176}

Visually, there are obvious differences between the solvents (Fig. 2.10). Samples made from NMP, DMSO, and GVL are quite similar, forming opaque white pliable films with wrinkled surfaces. Each has its own characteristic surface striations. These films are relatively quick to form when placed in the water bath, taking 10-20 seconds to completely solidify, though GVL films formed more slowly than NMP and DMSO. Upon

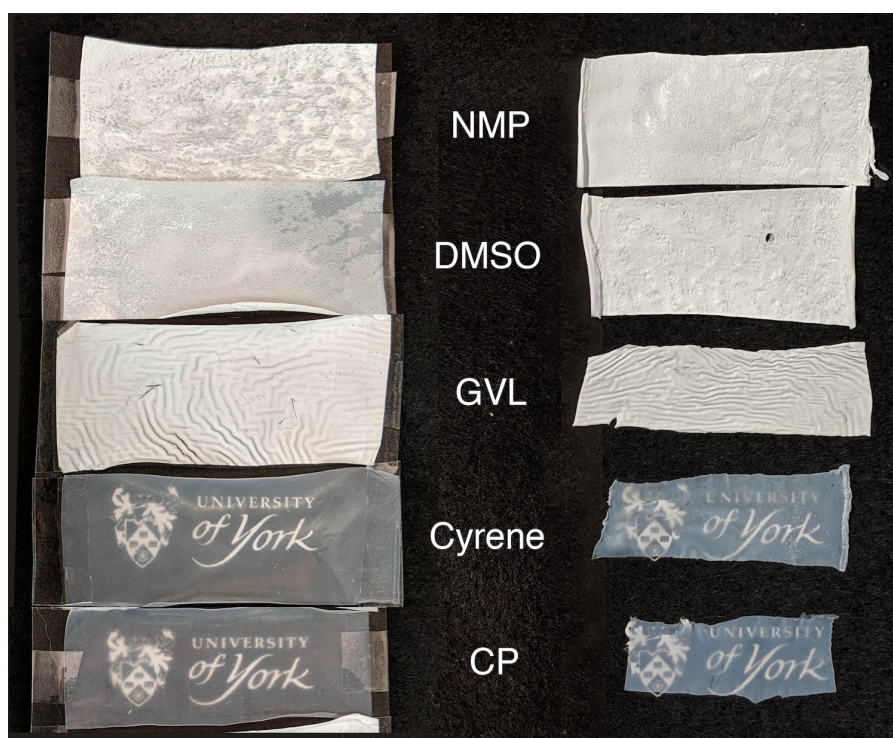


Figure 2.10: Membranes prepared with 10% w/v PVDF in five solvents, photographed atop logo graphic before (left) and after (right) vacuum drying.

drying, NMP and DMSO undergo very little shrinkage, while GVL shrinks slightly. All of these samples remain flexible after drying.

Cyrene and CP, on the other hand, form translucent, almost colorless films with smooth surfaces. When placed in the water bath, these samples solidify quite slowly, taking over 60 seconds each. Figure 2.10 shows the membranes immediately after being removed from water, before drying. After drying, the Cyrene and CP films undergo considerable shrinkage, becoming cloudier and more brittle.

It is worth noting that while these films were prepared with 10% w/v PVDF, this high concentration is not necessary. Lower concentrations of PVDF in these solvents may yield different film properties, and are a good target for future studies.

By SEM, the microscopic basis for the visual differences between films becomes apparent. Films cast from NMP and DMSO (Fig. 2.11) range from 140-180 μm thick and display the irregular macrovoids, finger-like pores, and smooth, dense surface skin that are characteristic of PVDF membranes.⁸⁸ The formation of these structures is caused by rapid liquid-liquid phase separation (*demixing*) of the polymer solution—that is, when the PVDF solvent and the water bath interchange quickly, the polymer becomes more concentrated in specific areas and less concentrated in others, eventually precipitating in

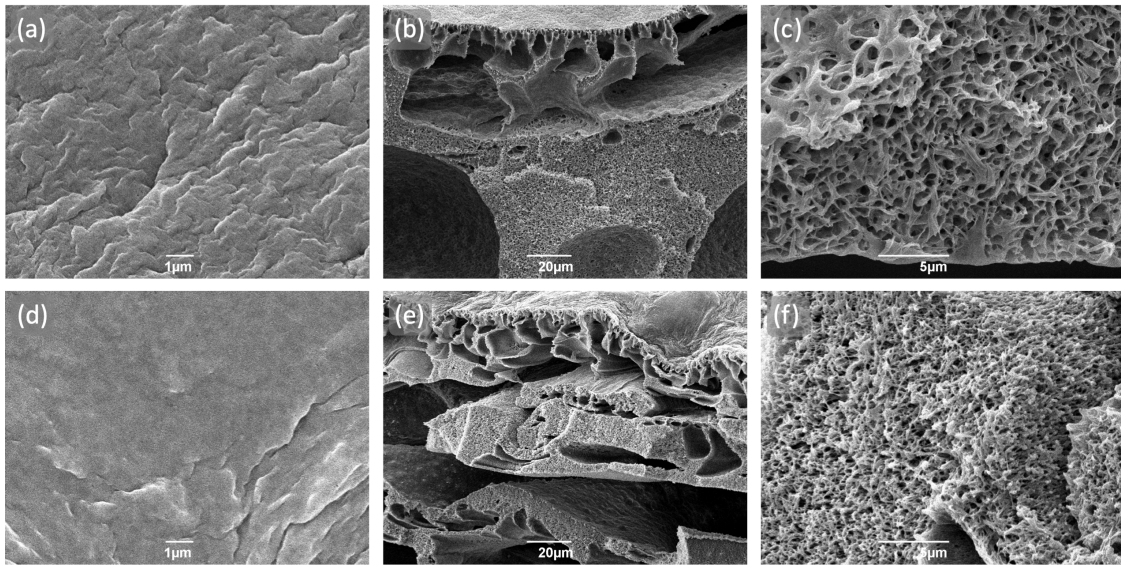


Figure 2.11: SEM micrographs of films prepared with 10% w/v PVDF in NMP and DMSO, showing (a) NMP surface (10,000x), (b) NMP cross-section (800x), (c) NMP cross-section (5,000x), (d) DMSO surface (10,000x), (e) DMSO cross-section (800x), (f) DMSO cross-section (5,000x)

an irregular, highly porous morphology with a smooth surface skin (Fig. 1.10).^{85,88,89,92,177}

The inhomogeneity seen here is the likely source of the opacity of the membranes, as the structure is not sufficiently ordered to allow light to pass through. Similarly, the pliability of the membrane could result from the capacity of these porous structures for flexing without breaking. For filtration applications, the large size and high incidence of voids in these cross-sections does not necessarily indicate that these membranes will have a high flux. Because PVDF membranes have a dense top skin, flux is typically determined by the presence of pores in the top layer, rather than the interior.⁸⁶

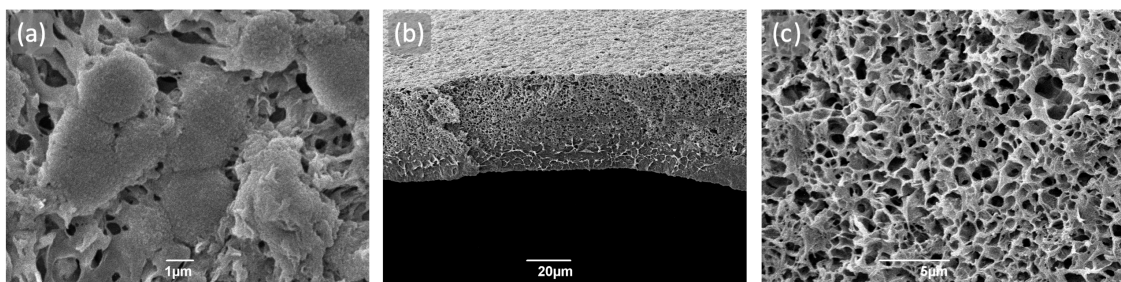


Figure 2.12: SEM micrographs of films prepared with 10% w/v PVDF in GVL, showing (a) Surface (10,000x), (b) Cross-section (800x), (c) Cross-section (5,000x)

GVL films, on the other hand, display a different morphology (Fig. 2.12). These membranes are much thinner, measuring roughly 40-45 μm thick, and lack the finger-like

pores and macrovoids of the NMP and DMSO samples, instead displaying a spongy, fairly dense structure (*bicontinuous*) with a porous and irregular surface. The internal spongy structure of the GVL film is quite similar to the denser regions of the NMP and DMSO films, but its regularity, lack of macrovoids, and the noticeably slower speed of film formation suggests that liquid-liquid phase separation occurs more slowly in GVL. This bicontinuous morphology has been previously associated with delayed demixing in other solvents, supporting this explanation.⁸⁵ The GVL membrane has fewer defects than those formed from NMP and DMSO, suggesting that PVDF membranes cast from GVL may be mechanically stronger. Again, the porosity of the internal structure likely contributes to both the opacity and the flexibility of the film.

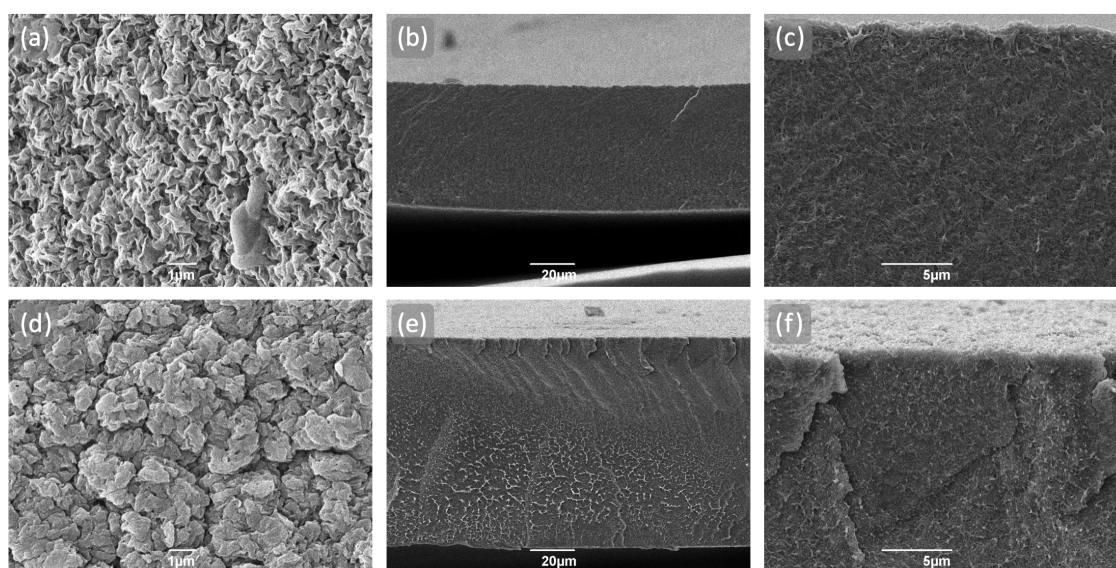


Figure 2.13: SEM micrographs of films prepared with 10% w/v PVDF in Cyrene and CP, showing (a) Cyrene surface (10,000x), (b) Cyrene cross-section (800x), (c) Cyrene cross-section (5,000x), (d) CP surface (10,000x), (e) CP cross-section (800x), (f) CP cross-section (5,000x)

Finally, membranes cast from Cyrene and CP appear very similar by SEM (Fig. 2.13), just as they do to the naked eye. Cyrene membranes are 60-65 μm thick, and CP membranes are 80-90 μm . Both solvents form very dense, non-porous morphologies with wrinkled surface layers. This morphology has neither the characteristics of liquid-liquid phase separation, nor solid-liquid phase separation, in which spherical or sheaf-like nodes of crystallisation would be expected.¹⁷⁸ However, neither does this film resemble a simple dried gel, which would likely show spherical nodules due to slow crystallisation.^{179,180} Instead, it appears that the polymer precipitated very slowly out of solution, forming a non-porous, optically translucent, brittle crystalline sheet.

While it might seem logical that the structure of the solvent, or its HSP, could be used to explain the structure of its membranes, this is not typically the case. A thorough examination of PVDF membranes in various solvents by Bottino *et al.* showed that neither solvent/polymer nor solvent/non-solvent interaction strengths correlate with membrane structure.⁸⁶ This is supported in these results as well—the strength of PVDF/solvent interactions should increase with decreasing Hansen distances (R_a , Table 2.5), with NMP > Cyrene/GVL > DMSO > CP. Obviously, this does not explain the membrane morphologies seen here. Similarly, the water/solvent interaction trend would suggest the porosity of the structures should follow DMSO > NMP > Cyrene/GVL > CP. While this trend is closer to resembling the hierarchy of porosities seen, Cyrene and GVL behave quite differently, which is not predicted here.

Table 2.5: Hansen distances (R_a) between solvent candidates and PVDF/water

Solvent	R_a	
	PVDF	Water
NMP	1.8	35.6
DMSO	3.7	32.6
GVL	3.6	36.4
Cyrene	3.6	36.4
CP	3.8	37.6

It is known that water exhibits complex behaviour that is not reliably predictable by HSP.⁵⁰ Indeed, the strength of water/solvent interactions predicted here does not seem to correlate with water/solvent miscibility. NMP, DMSO, and GVL are fully miscible with water,^{147,181,182} while CP is only slightly water-soluble.¹⁵¹ Cyrene will mix with water, but this is kinetically slow, and Cyrene will layer with water if combined gently. This actual water miscibility behaviour may be contributing to the observed membrane structures—reluctant interaction of solvent with water bath could slow diffusion of water into the polymer solution, preventing the formation of macrovoids and forcing slow crystallisation of the polymer into a non-porous layer. This solvent/non-solvent diffusion phenomenon, represented by the binary diffusivity, was shown by Bottino *et al.* to be the key correlation between solvent and membrane structure.⁸⁶ In addition, the rapid gelation of PVDF in Cyrene and CP upon cooling suggests that gelation would likely begin upon immersion in the cool water bath, further reducing diffusion of water into the polymer matrix.

When contrasting the morphologies of membranes formed in NMP and DMSO

versus GVL, miscibility cannot be the determining factor. Instead, the viscosity of the casting solution could be influencing the speed of liquid-liquid interchange.¹³² The GVL solution is slightly more viscous than NMP and DMSO (Fig. 2.8), potentially slowing the penetration of water into the polymer matrix and reducing the demixing rate. This phenomenon could explain the denser bicontinuous structure and the absence of large macrovoids formed by rapid demixing.

To further analyse the structure of the PVDF membranes, ATR-FTIR spectra of the surfaces were obtained (Fig. 2.14). Two crystalline phases of PVDF are evident: the non-polar α phase, which has a trans-gauche conformation and is kinetically favoured, and the polar β phase, which has an entirely trans conformation and is thermodynamically favoured.^{128,131,132}

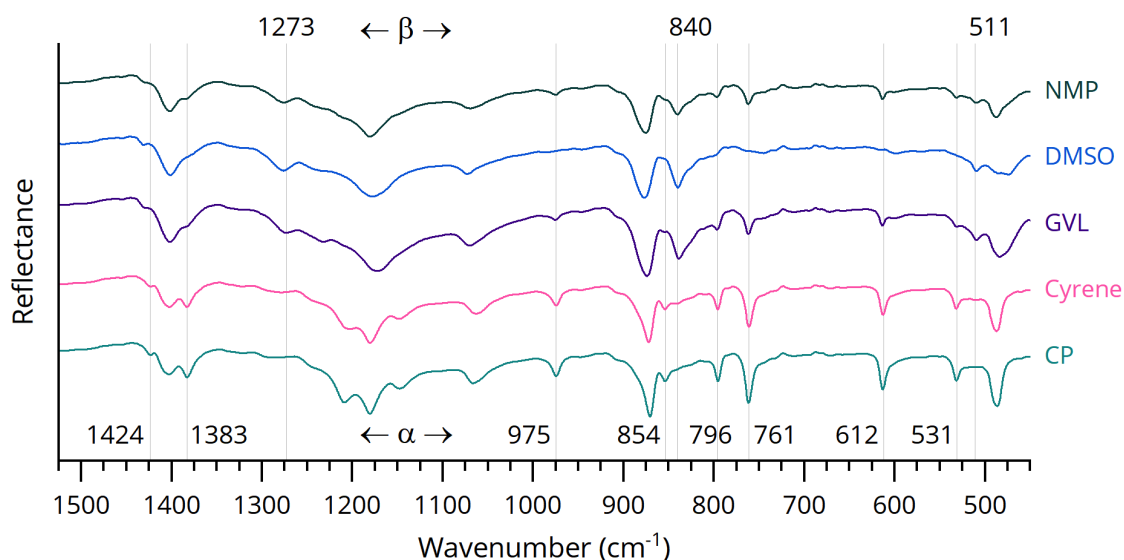


Figure 2.14: FT-IR spectra of 10% w/v PVDF films cast from solvent candidates and NMP, with arbitrary units of absorbance. Reference lines indicate characteristic peaks, with β -phase peaks across the top and α -phase peaks across the bottom (see text).

Of the solvents examined here, DMSO seems to yield entirely β -phase PVDF, showing characteristic peaks at 1273, 840, and 511 cm^{-1} . While NMP and GVL samples also show these β peaks, they have minor peaks associated with the α phase, indicating that the PVDF in these films is a mixture of the two. Cyrene shows almost entirely α peaks, with a hint of β character at 840 cm^{-1} . The CP sample yields entirely α peaks.

Past studies have suggested that more polar solvents will favour β phase development, and this is borne out here to some extent (Table 2.6).¹³² DMSO, which entirely favours β phase, has the highest δ_p at 16.4. NMP has the next highest δ_p at 12.3, and is

Table 2.6: Crystallinity of PVDF films and HSP of solvents

Solvent	δ_D	δ_P	δ_H	Phase
NMP	18.0	12.3	7.2	β (some α)
DMSO	18.4	16.4	10.2	β
GVL	16.9	11.5	6.3	β (some α)
Cyrene	18.8	10.6	6.9	α (some β)
CP	17.9	11.9	5.2	α

HSP are given in units of $MPa^{1/2}$

mostly β with a hint of α . However, CP's δ_P is close to that of both NMP and GVL, and considerably higher than Cyrene's, breaking the pattern.

Instead, the phase preference can be explained by a combination of polarity and hydrogen bonding. DMSO, with both a high δ_P and δ_H , favours the β phase exclusively. NMP and GVL are mid-range in both δ_P and δ_H , allowing formation of some α -phase polymer. Cyrene has a considerably lower δ_P and mid-range δ_H , encouraging formation of α phase with a bit of β . Finally, CP has a mid-range δ_P , which could enable β phase formation, but its unusually low δ_H instead promotes α .

2.5 Summary and Future Work

In conclusion, a number of green candidates have been identified for dissolution of high-MW PVDF, and the performance of each candidate was compared with conventional solvent NMP. Each solvent was tested for its ability to dissolve PVDF at 10% w/v, which is relevant for battery manufacturing and recycling, as well as its ability to form membranes for separation applications. The key findings are summarised in Table 2.7.

Each solvent presents a different set of hazards and properties. DMSO performs similarly to NMP in all respects, dissolving PVDF at room temperature while exhibiting the clumping behaviour that slows dissolution significantly. These systems can take several hours to dissolve PVDF, and DMSO in particular forms optically transparent clumps that make it difficult to ascertain whether dissolution is complete. The DMSO/PVDF solution is liquid at room temperature, with a slightly higher viscosity than the NMP/PVDF solution (Fig. 2.9). In membrane preparation, both NMP and DMSO form flexible, opaque films that do not show significant shrinkage upon drying. Their internal structures are inhomogeneous, with numerous irregular macrovoids that are typical of rapid liquid-liquid demixing. These results suggest that DMSO could be a good drop-in replacement for

Table 2.7: Summary of PVDF solvent candidate properties

Solvent	Hazards	Dissolution		Gelation		Membrane
		Temp (°C)	Speed	Min % w/v	Shrinkage	
NMP	reprotoxic irritant	25	slow	-	-	flexible opaque macrovoids
DMSO	none	25	slow	-	-	flexible opaque macrovoids
GVL	unknown	60	fast	7.0	low	flexible opaque bicontinuous
Cyrene	irritant	100	fast	1.0	low	brittle transparent non-porous
CP	flammable irritant	60	fast	3.0	high	brittle transparent non-porous

NMP in PVDF dissolution. However, despite its lack of hazards, DMSO is controversial in industry due to significant odour issues in wastewater treatment, generation of SO_x upon incineration, and its ability to bring organic compounds through the skin barrier. These issues may affect its adoption as a green solvent.

In GVL, PVDF disperses readily, avoiding the clumping behaviour seen in DMSO and NMP. Though this solvent requires heating to achieve dissolution (60°C was used here), the overall process takes less than two hours. The GVL/PVDF solution was found to be slightly more viscous than DMSO or NMP solutions at 100°C. Upon cooling, GVL/PVDF gradually gels over the next day, eventually forming a translucent, thermoreversible gel. GVL requires 7% w/v PVDF to form a stable gel, though lower concentrations result in pseudo-gelatinous samples, indicating a continuous sol-gel transition. Rheological trials indicate this gel breaks between 10 and 20% shear strain. The GVL/PVDF gel sample is stable for weeks under ambient conditions, suggesting it may be applicable industrially (for example, as part of a gel electrolyte in a battery). Membranes cast from GVL/PVDF are also flexible and opaque, but do not display the inhomogeneous structure found in NMP and DMSO. Instead, this solvent forms a homogeneous bicontinuous structure, potentially adding mechanical strength while retaining porosity.

Overall, GVL could serve as an alternative to NMP for PVDF dissolution, though

the gelation behaviour may prove problematic for drop-in replacement. However, the gradual nature of the gelation, as well as its thermoreversibility, suggests that issues could be avoided in industrial processes that employ gentle heating. Additionally, as GVL dissolution of PVDF occurs more quickly and reliably due to the lack of clumping, GVL may actually present an improvement in battery recycling applications, where the goal is to separate the PVDF from the other components of the electrode. The main barrier to GVL as a green solvent is its regulatory status—it is not registered under REACH, meaning that its use in the EU is limited to less than 1 tonne/year. The registration process is time-consuming and expensive, presenting an obstacle to larger-scale use. Additionally, while GVL has been shown to be non-toxic and non-volatile, other hazards are currently unreported, so it cannot be presumed safe. Further safety data is needed before recommendations can be made about GVL as an alternative solvent.

Cyrene behaves similarly to GVL in dissolution of PVDF, though it must be heated to roughly 100°C for dissolution to occur at an appreciable rate. Dispersion is similarly easy, and lack of clumping allows PVDF dissolution within 2 hours. The Cyrene/PVDF solution is 3-6 times more viscous at 100°C than the three solutions described above, probably due to the relatively high viscosity of pure Cyrene. Cyrene/PVDF forms an opaque gel immediately upon cooling, making it a challenge to handle this solution at room temperature. Like with GVL, the gelation is thermoreversible and stable for weeks under ambient conditions, and the gel was found to sustain 10–20% shear strain before breaking. Unlike GVL, the gel formed is completely opaque, suggesting considerable aggregation of the polymer and perhaps limiting applications. Cyrene can form a gel with a much lower concentration of polymer, showing a sharp sol-gel transition below 1% w/v PVDF. Upon attempting membrane casting from a hot Cyrene/PVDF solution, a thin, clear film is formed. This turns translucent white and brittle upon drying, and by SEM appears to have a homogeneous, non-porous cross-section.

Because of this morphology, Cyrene does not appear to be a suitable solvent for PVDF membranes, though there may be other applications where translucency is more important than porosity. The ready gelation behaviour, particularly with low concentrations of PVDF, may be worth examining for applications such as battery electrolytes, where polymer aggregation may not pose a problem. Finally, due to its ready dispersion and rapid dissolution of PVDF, Cyrene may be useful for battery recycling, if the high temperature required for dissolution is industrially acceptable. As Cyrene is fully registered under

REACH Annex VIII, it can be used in the EU at up to 100 tonnes per year, and has been shown to have no probable hazards aside from eye irritation. Combined with its unusual PVDF interactions, this suggests that Cyrene should be explored further as a potential green solvent in this application.

Finally, CP also acts as a non-clumping solvent for rapid, heated PVDF dissolution. However, its high volatility relative to the other solvent candidates may cause issues in processing, as it gradually evaporates when heated, yet does not noticeably dissolve the polymer at room temperature. Viscosity of the heated solution could not be measured due to rapid evaporation at 100°C, and rapid gelation upon cooling prevented low-temperature viscosity measurements. Like Cyrene and GVL, CP forms a thermo-reversible gel with PVDF. The CP/PVDF gel is nearly colorless and transparent, and can handle over 100% shear strain before breaking, indicating considerable strength. CP requires only 3% w/v PVDF to form a gel, with a sharp sol-gel transition below this concentration. However, CP/PVDF gels are not stable under ambient conditions, with rapid solvent evaporation causing noticeable shrinking in the first few hours after gelation. In membrane casting attempts, CP performs very similarly to Cyrene, forming a transparent, non-porous film that becomes brittle when dried.

Of the four green candidates, CP seems the least promising. Its membrane behaviour limits a popular application, and its volatility makes it difficult to handle, particularly as a replacement for high-boiling NMP. Its flammability is a more significant hazard than any known for the other three candidates. However, CP is fully REACH-registered and has no waste disposal issues, so it may still be more practical than Cyrene, GVL, or DMSO in closed systems where volatility is not an issue.

To sum up, a potential drop-in replacement for NMP in PVDF dissolution has been identified, as well as several solvents that could be green replacements in specific applications. These are particularly promising in battery recycling, where their rapid dissolution of PVDF may represent an improvement over NMP; this is the logical next step in this study. In addition, the gelling candidates may present opportunities for improved dispersion of active ingredients and conductive additives for battery manufacturing, and perhaps form useful gel electrolytes. These present interesting areas for future study. The membrane properties of DMSO and GVL should be studied further, comparing their tensile strength and filtration abilities to those of NMP. Constructing phase diagrams for the PVDF/solvent/water systems of all four candidates could be theoretically interesting.

CHAPTER 3

CELLULOSE DISSOLUTION IN CELLULOSE-BASED SOLVENT

Cellulose is the most abundant biopolymer on earth, with the potential to form the basis for a renewable bioeconomy. Unfortunately, it is also notoriously difficult to dissolve. The high level of crystallinity and hydrogen bonding in cellulose make it resistant to common solvents. Indeed, cellulose solvent systems tend to be unusual combinations of salts and dipolar aprotic solvents, or alkalis and water, with some ionic liquids and deep eutectic solvents known to work as well.^{183,184} Currently, commercial systems for cellulose dissolution in the EU rely on *N*-methylmorpholine-*N*-oxide (NMMO), which is a flammable solid and oxidiser.¹⁸⁵ Cyrene could potentially replace NMMO as a cellulose solvent, providing a green alternative.

3.1 Background

Cellulose is found in the cell walls of almost all green plants, including trees, agricultural crops, seaweed, and microalgae (Fig. 3.1). The global mass of cellulose is estimated at 7×10^{11} tonnes, with up to 1.8×10^8 tonnes being produced by plants each year.^{186,187} Currently, only 1×10^5 tonnes are being used annually to produce paper, textiles, and other goods, leaving a vast quantity available as a renewable resource. Furthermore, cellulose is not a human food source, and is frequently considered a waste, making it an excellent feedstock from a sustainability perspective. Once dissolved, cellulose can be functionalised or otherwise treated to make textiles, plastics, fuels, and other economically critical products.^{188–191}

From a dissolution perspective, cellulose is extremely challenging. Its strong network of hydrogen bonds between hydroxyl groups (Fig. 3.1) makes it resistant to most attempts at dissolution. Historically, solvents that have proved harsh enough to overcome this bonding have also been dangerous to humans and the environment. The viscose process was the first commercial technology for cellulose dissolution, developed in the late 19th century, and is still in common use today. Indeed, though European plants have stopped using this technology due to its hazards, manufacture in China, India, and Southeast Asia is growing significantly.¹⁹² The viscose process relies on carbon disulfide, which is both

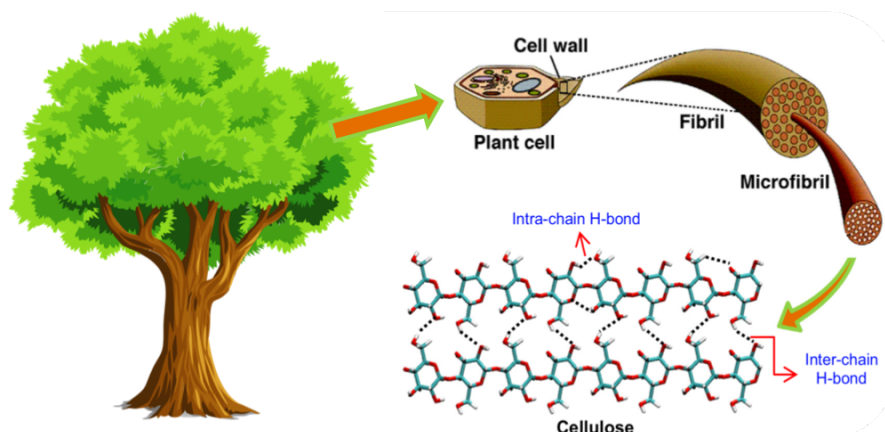


Figure 3.1: Cellulose originates from cell walls of plant biomass. Adapted from *Chem. Eng. Sci.*, **121**, Gupta, K.M. and Jiang, J., *Cellulose dissolution and regeneration in ionic liquids: A computational perspective*, 180–189, © 2015, with permission from Elsevier

neurotoxic and extremely flammable, resulting in regular accidents, chronic poisoning of workers, and environmental pollution.^{193–195} The viscose process also involves corrosive solutions of sodium hydroxide and sulfuric acid.⁸⁰

In the EU, textile manufacturing from cellulose is now achieved via the Lyocell process, which uses a solvent system of NMMO and water.¹⁹⁶ While NMMO solvation is an improvement over the viscose process, its oxidising properties present a risk of explosion during both storage and use.^{185,197} Synthesis of NMMO is far from environmentally friendly, relying on hazardous precursors (such as methylamine) and harsh conditions.¹⁹⁸ Additionally, the cellulose dissolution system must be heated above the melting point of NMMO, requiring high energy consumption.

While other cellulose solvent systems have been discovered, and will be discussed below, no truly green system has yet been commercialised. It is of critical importance to find a cellulose dissolution system that can safely and economically dissolve cellulose on a global scale, replacing the highly hazardous systems currently in use. As Cyrene is safe, sourced from cellulose, and similar to other dipolar aprotics used for cellulose dissolution, it is an attractive candidate for a replacement.

3.1.1 Solvent Systems

Various solvent systems can be used to dissolve cellulose, each having different advantages and limitations. Systems involving dipolar aprotic solvents are described here to form the basis for designing a Cyrene-based dissolution system. Figure 3.2 shows the most common dipolar aprotic solvents used in this application, allowing comparison

with Cyrene. Generally speaking, Cyrene is similar to the conventional solvents in that it is dipolar, aprotic, and amphiphilic. In the conventional solvents, oxygen and nitrogen or sulfur act as electronegative/hydrophilic centers, with terminal methyl groups providing hydrophobic influence. For Cyrene, electronegativity/hydrophilicity comes entirely from oxygen, and hydrophilic influence comes from methylene bridges in a seven-membered ring.

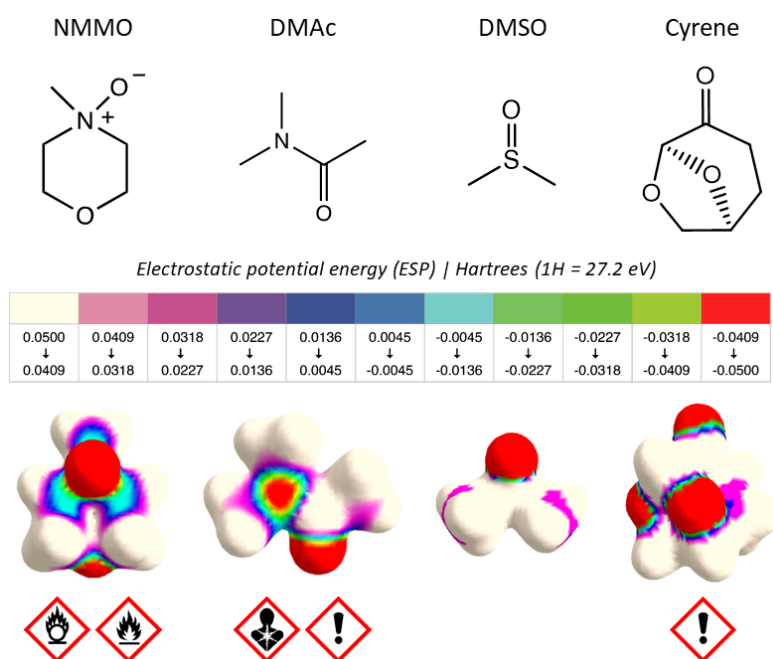


Figure 3.2: The most common dipolar aprotic solvents used in cellulose dissolution systems, depicted as structural formulae and ESP surfaces, with associated GHS symbols below.

NMMO and water. When heated above 85°C, a combination of NMMO and 20% w/w water can dissolve up to 20% w/v cellulose. The dominant interaction here is thought to be the formation of hydrogen bonds between cellulose hydroxyl groups and solvent N–O dipoles, disrupting the intermolecular hydrogen bonding in cellulose and forming stable solvent-cellulose complexes.¹⁹⁹ In this system, water serves to lower the melting point of NMMO from 170°C to 74°C, but also competes with cellulose to form hydrogen bonds with the solvent. Higher proportions of water lead to NMMO–water complexation and the loss of cellulose solubility. Currently, this system is used commercially in the Lyocell process to produce cellulose-based fibres.

DMAc/LiCl One of the most common laboratory-scale solvent systems for cellulose is 8% w/v lithium chloride (LiCl) in dimethylacetamide (DMAc), which can dissolve up to 16% w/v cellulose.^{200,201} This system relies on pretreatment of cellulose, typically involving mechanical disintegration, solvent exchange, or another activation method that relaxes the polymer chains and prepares them for dissolution.^{183,202} Notably, this system has only been reported to work with DMAc and NMP, despite testing with other dipolar aprotics.²⁰⁰ Unfortunately, DMAc and NMP are both either toxic or reprotoxic, making them difficult to work with safely on an industrial scale.²⁰³ Additionally, lithium is an increasingly scarce element, and would ideally be replaced with a more abundant element in this application.²⁰⁴ However, the DMAc system appears to work exclusively with lithium chloride, despite both other cations and halide anions being tested.²⁰⁰

DMSO/TBAF A lesser-known option for cellulose dissolution is the use of dimethylsulfoxide (DMSO) with tetrabutylammonium fluoride (TBAF). 10 – 20% w/v of TBAF trihydrate in DMSO was found to dissolve 2.5% cellulose within 15 minutes at room temperature, without requiring pretreatment.²⁰⁵ This system is thought to work similarly to the DMAc/LiCl system, with the fluoride anion dominating dissolution while the cation is presumably stabilised by the solvent dipoles. TBAF is a very powerful hydrogen-bond acceptor, which enables it to interact with hydroxyl groups on cellulose. The addition of water to this system induces gelation and halts dissolution, probably due to competing hydrogen bonding interactions. DMSO containing benzyltrimethylammonium fluoride monohydrate was shown to dissolve 1% cellulose, while tetramethylammonium fluoride proved an unsuitable additive due to its insolubility in DMSO.¹⁸³ There have been no recent publications improving upon this system, so it may be limited to low weight percentages of cellulose. Additionally, quaternary ammonium fluorides like TBAF are typically very expensive, which may reduce industrial interest in this system.

Dipolar Aprotics as Diluents Ionic liquids (ILs) and quaternary ammonium chlorides are capable of dissolving cellulose on their own, but this can be expensive and slow. By contrast, adding a small mole fraction of IL to a dipolar aprotic solvent can promote rapid dissolution of 10% w/v cellulose.²⁰⁶ This method is particularly effective with nitrogen- or sulfur-containing solvents, but also works with *t*-butanol, γ -valerolactone (GVL), and γ -butyrolactone (GBL).^{207,208} Similarly, quaternary ammonium chlorides can be diluted with DMAc to dissolve up to 10% w/v cellulose without pretreatment.²⁰⁹

3.1.2 Swelling and Dispersion

In many cases, attempts at cellulose dissolution result instead in swelling of the polymer or colloidal dispersion of cellulose aggregates.²¹⁰ These results are worth examining as hints for cellulose dissolution, as well as on their own merit.

Swelling Swelling of cellulose can sometimes be a stepping stone to dissolution. For example, in the case of the NMMO and water solvent system, the ratio of NMMO to water determines whether the solvent will dissolve cellulose quickly, swell it and then dissolve it, or swell it without dissolving it.²¹¹ Careful microscopic examination of modes of swelling can help decipher whether the solvent system is promising (Fig. 3.3).

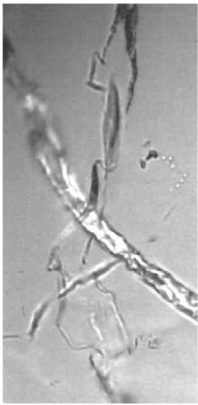
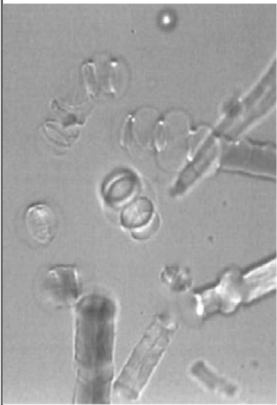
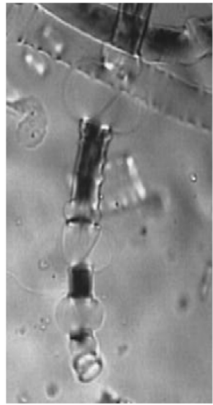
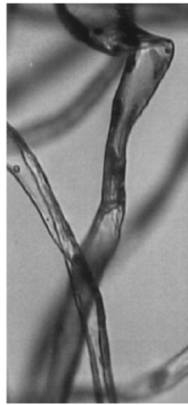
Content of water	< 17%	19 – 24%	25 – 35%	> 35%
Swelling and dissolution mechanism	Dissolution by disintegration in spindle (Mode 1)	Swelling by ballooning, dissolution (Mode 2)	Swelling by ballooning, no dissolution (Mode 3)	Homogeneous swelling, no dissolution (Mode 4)
10 µm •—•	Wood fibre 	Wood fibre 	Wood fibre 	Cotton fibre 

Figure 3.3: Different swelling and dissolution modes of cellulose fibres in varying ratios of NMMO/water. Reprinted from C. Cuissinat and P. Navard, *Macromolecular Symposia*, 2006, **244**, 1–18 with permission from John Wiley and Sons © 2007

In very good solvents, as in NMMO with less than 17% water content, the cellulose fibres immediately begin to break apart and dissolve, with no apparent swelling step. With 19 – 24% water, the NMMO system becomes slightly less effective, and a slower dissolution process is seen. In this case, the cellulose swells inhomogeneously, forming ‘balloons’ of swollen fibre that grow and gradually ‘burst’, or dissolve. With more than 25% water, the NMMO system ceases to dissolve cellulose, instead forming balloons separated by areas of unaffected fibre. With some tweaking of parameters or additives,

this solvent system may eventually dissolve cellulose, as it is penetrating the fibres enough to cause ballooning. Finally, with over 35% water, the cellulose fibres exhibit homogeneous swelling, but no ballooning or dissolution. This type of swelling indicates a bad solvent, and is not likely to lead to dissolution.

Dispersion While swelling can indicate the potential for dissolution, dispersion is sometimes an independent goal of cellulose science. Cellulose dispersions can be used industrially as additives to food, cosmetics, and pharmaceuticals, or serve as binders or thickeners.²¹² A stable dispersion, or colloid, is not necessarily a predictor of dissolution, but instead indicates that the cellulose molecules have been suspended in solution by one or more stabilising forces. These forces can include van der Waals forces, charged repulsion, excluded volume repulsion, or even simple entropy.²¹³ If these forces are strong enough, the cellulose suspension can become stable in the long term, making it useful in industrial and consumer applications.

3.1.3 General Principles of Dissolution

Cellulose is a natural linear polymer composed of hundreds to thousands of glucose monomers (Fig. 3.4).¹⁸⁹ Like any polymer, its characteristic properties arise from its monomer backbone and its molecular weight.⁷⁹ The large number of hydroxyl groups in the cellulose backbone (three per monomer) give it extensive hydrogen bonding ability and rigid crystalline regions. The large variation in degree of polymerisation (DP)—from 300 to 10,000 repeating units, depending on the source—makes it critical to consider the molecular weight of cellulose samples used across dissolution studies.¹⁸⁹

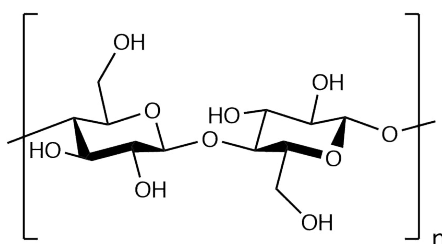


Figure 3.4: Cellulose is a polysaccharide composed of repeating units of glucose.

Unlike most polymers, cellulose does not seem to adhere to a normal understanding of dissolution. The many different solvent systems for cellulose have very little in common, and there is no clear consensus on the principles behind their efficacy. While many cellulose researchers refer to strong hydrogen-bonding interactions between cellulose

and solvent as the main driving force for dissolution, this is inconsistent with the fact that water is a cellulose anti-solvent.⁸⁰ Medronho *et al.* make a convincing argument for the amphiphilicity of cellulose having a strong impact on its dissolution.^{210,214} This suggests that amphiphilic solvents (those having both hydrophilic and hydrophobic parts) would promote dissolution.

Some studies vaguely refer to the crystallinity of cellulose as a barrier to dissolution, but amorphous cellulose does not appear to be any easier to dissolve than crystalline.²¹⁴ In fact, most cellulose is composed of both crystalline regions and amorphous regions (Fig. 3.5), and the crystalline regions may become amorphous as they dissolve. Ghasemi *et al.* have suggested that disruption of crystallinity and disentanglement of amorphous polymer chains are distinct phenomena that must be accomplished in sequence to dissolve cellulose, and any functional solvent system must be able to achieve both.^{215,216}

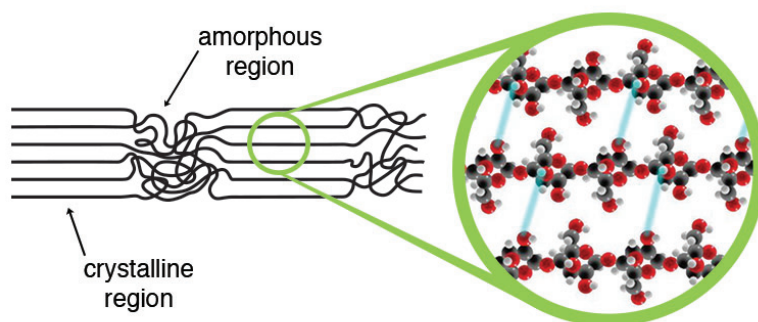


Figure 3.5: Cellulose microfibrils are composed of crystalline regions with strong inter-chain hydrogen bonding (inset, hydrogen bonds in blue), and amorphous regions with entangled chains

A particularly confusing and unexplained trend in cellulose dissolution is the tendency for low temperatures to promote dissolution in certain solvent systems, which would seem to contradict both kinetic and thermodynamic principles of mixing. This could be due to conformational changes in the polymer chain that favour a more polar conformation at low temperatures, therefore promoting low-temperature dissolution in polar solvents.⁸⁰ Another theory posits a self-assembled inclusion complex of cellulose and solvent components, with rigid chains of cellulose in solution that aggregate at higher temperatures.²¹⁷ No mechanism for this phenomenon has been conclusively proven yet.

From the perspective of basic physical principles, cellulose must comply with thermodynamic principles of solvation—the mixed state must be of a lower Gibbs energy

than two separated phases. As discussed in Section 1.2, both enthalpy and entropy of solvation contribute to the overall energy. In cellulose, it has been proposed that the entropic term is particularly important.²¹⁴ The glucose monomer, as well as related short-chain oligomers, tend to be very water-soluble, which is to be expected from the high concentration of hydroxyl groups. Longer chain lengths, beginning with DP = 8, become practically insoluble. This suggests that chain rigidity arising from constraints upon rotation reduces the entropy of the cellulose-water mixture. Another consideration in aqueous cellulose behaviour is the presence of hydrophobic regions in the cellulose chain. This can cause cluster formation in the presence of water, stabilising supramolecular cellulose structures. Both of these effects have been proposed to cause a negative entropic term, which could explain the anomalous low-temperature dissolution of cellulose in aqueous systems.²¹⁸

Finally, any discussion of cellulose dissolution is made more complicated by the need to distinguish between thermodynamic and kinetic effects. Thermodynamic arguments, such as favourable interactions, are intuitively easier to understand, making them very popular in the literature. However, if a dissolution process is kinetically slow, dissolution may not be evident on the experimental timescale even with positive thermodynamic interactions. Therefore, solvent systems that do not appear to dissolve cellulose are not necessarily non-solvents, but could just be kinetically slow.

With all of these principles in mind, the suitability of Cyrene as a potential cellulose solvent was assessed.

3.1.4 Potential of Cyrene for Cellulose Dissolution

First, Cyrene's solubility parameters were compared to those of the dipolar aprotic solvents used for cellulose dissolution (Table 3.1). NMMO is presented here as the typical cellulose dissolution mixture with 23.5% w/w water, with solubility parameters adjusted accordingly. In general, Cyrene is in the region of the other dipolar aprotics, while being rather far removed from the NMMO/water mixture. This is due to the significant increase in hydrogen bonding ability (δ_H) that comes with the addition of water.

Adding water to Cyrene could bring its solubility parameters closer to the mixture of NMMO and water, but there is more complexity in the Cyrene/water system due to ready formation of a geminal diol (Figure 3.6).²¹⁹ The Hansen Solubility Parameters (HSP) of such a system could be predicted via linear combination, representing it as a ternary

Table 3.1: Solubility parameters for traditional dipolar aprotics and Cyrene

	δ_D	δ_P	δ_H	D-Cyrene	α^a	β	π^*	Δ -Cyrene
Cyrene	18.9	12.4	7.1	0.0	0.00	0.61 ^b	0.93 ^b	0.00
NMMO/H ₂ O	18.3	16.1	16.6	10.2	0.30 ^c	0.75 ^c	1.13 ^c	0.39
DMAc	16.8	11.5	10.2	5.1	0.00	0.76 ^d	0.88 ^d	0.16
NMP	18.0	12.3	7.2	1.6	0.00	0.77 ^d	0.92 ^d	0.16
DMSO	18.4	16.4	10.2	5.1	0.00	0.76 ^d	1.00 ^d	0.17
GBL	18.0	16.6	7.4	4.5	0.00	0.49 ^d	0.87 ^d	0.13
GVL	16.9	11.5	6.3	4.0	0.00	0.60 ^e	0.83 ^e	0.10

D-Cyrene = distance from Cyrene in the Hansen space, Δ -Cyrene = distance from OME₃₋₅ in the KAT space. HSP values were drawn from HSPiP database or predicted by HSPiP. ^aAssumed to be zero for aprotic solvents. ^bSherwood *et al.*¹⁰⁰ ^cHauru *et al.*, for 23.5% w/w H₂O in NMMO at 30°C ^dKamlet *et al.*⁵³ ^eJessop *et al.*⁵⁴

mixture of Cyrene, the geminal diol, and water. However, due to the complexity of the system, this prediction may not be reliable. Instead, this system is best explored experimentally, with various blends of Cyrene/water being tested for their efficacy in cellulose dissolution. This system should have increased amphiphilicity and increased hydrogen bonding ability, making it a more likely cellulose solvent, but the presence of water could inhibit dissolution nonetheless.

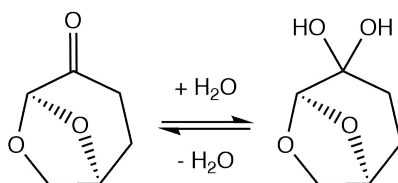


Figure 3.6: In the presence of water, Cyrene forms a geminal diol in an equilibrium that depends on the ratio of Cyrene to water.

Returning to predicted solvent similarity, the HSP of Cyrene are remarkably similar to NMP, and fairly similar to the other dipolar aprotic solvents. By Kamlet-Abboud-Taft (KAT) solvatochromic parameters, Cyrene is very close to all of the single solvents, but particularly close to GVL.

By looking in more detail at the individual KAT parameters, it is apparent that Cyrene's hydrogen bond accepting ability (β) is almost identical to that of GVL, while the polarity parameters (π^*) are less similar. For the other solvents, this is reversed, with Cyrene's π^* parameter being closer. However, it is not clear which of these parameters is more important, as the hydrogen bonding and polarity (especially as it relates to

amphiphilicity) could both affect cellulose dissolution. It is enough to conclude that by KAT parameters, it appears that Cyrene could be a viable replacement for some of the dipolar aprotic solvents used with additives for cellulose dissolution.

Structurally, Cyrene is quite similar to NMMO and the other common cellulose solvents (Fig. 3.2), with oxygen atoms that serve as centers of high electronegativity and boost the solvent's polarity. Additionally, Cyrene has four adjacent sp^3 carbon atoms that serve as a hydrophilic region, providing the desired amphiphilicity. However, the bridged bicyclic structure of Cyrene adds rigidity that is not present in the other solvents, perhaps making it more difficult for Cyrene to intercalate between cellulose chains.

Cyrene's low vapour pressure and high boiling point (227°C)¹⁰³ could be advantageous in recycling the solvent system, making it more economical to adopt on an industrial scale. After adding an anti-solvent (typically ethanol) to force cellulose precipitation, the anti-solvent could be separated from Cyrene via distillation, allowing reuse of Cyrene and any high-boiling cosolvents.²⁰⁷

In both solubility parameters and physicochemical properties, Cyrene appears to be a suitable candidate for cellulose dissolution. Tests were performed with Cyrene and various additives to assess its real-world performance in this application.

3.2 Methodology

There is still no consensus on standard methods for investigation of cellulose dissolution, despite many publications in the field. When investigating this area, researchers must select or develop methods for:

- pretreatment of cellulose,
- overcoming kinetic barriers to dissolution,
- checking whether dissolution has occurred, and
- analysing regenerated cellulose post-dissolution.

Cellulose Pretreatment A number of mechanical or chemical pretreatments are available to improve the solubility of cellulose, with the general hypothesis being that these treatments untangle polymer chains to reduce solvent resistance.²⁰² Cellulose can be steamed, boiled, soaked in ammonia, ball-milled, homogenised, and treated with acid or alkali solution.^{200,215,220,221} The most common laboratory pretreatment seems to be solvent exchange, beginning with water and gradually replacing with the desired solvent

(Fig. 3.7).^{200–202} As this process can be easily scaled up or down as needed, does not adversely impact the cellulose quality, and involves no harsh chemicals, it was selected as the pretreatment method for this work.

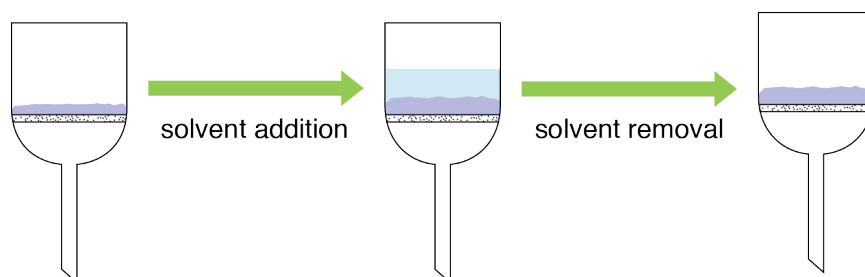


Figure 3.7: Cellulose can be pretreated to improve chance of dissolution. Water is added to cellulose and allowed to soak for 5 min, then removed via vacuum filtration. Process is repeated once with ethanol and three times with test solvent.

Overcoming Kinetic Barriers In much of the cellulose literature, various approaches are taken to overcome kinetic barriers and speed dissolution. The most commonly used method is conventional heating, but microwave heating and ultrasonication have also been used.²²² As prolonged heating can result in degradation of both cellulose and Cyrene, ultrasonication was chosen as the primary method for speeding dissolution in this work. As mentioned above, cooling can also speed dissolution in dipolar aprotic solvents, but this is more likely due to conformational changes than a kinetic effect. This was also tested here by cooling samples to -30°C overnight.

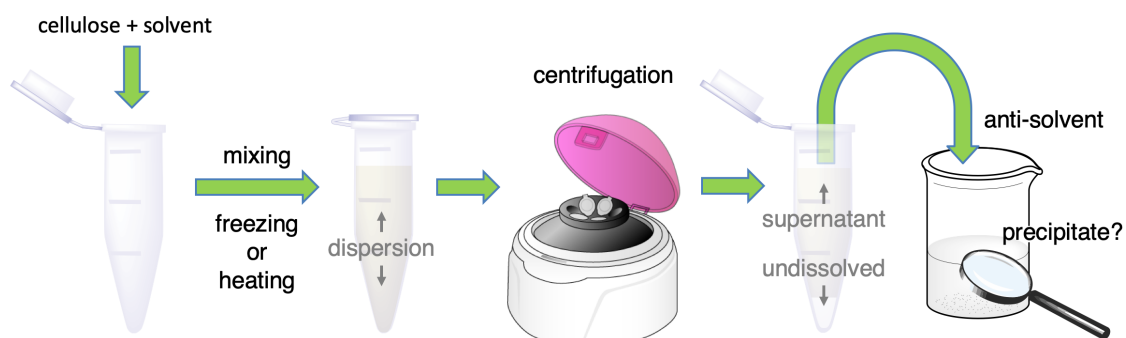


Figure 3.8: General procedure for cellulose dissolution experiments. Centrifuge image from DBCLS licensed under CC BY 4.0

Checking for Dissolution Even the seemingly simple task of checking whether any cellulose has dissolved can be quite complex. While NMR spectroscopy is the workhorse

of chemical analysis, in cellulose dissolution it is rarely used—diluting a sample with deuterated solvent in the normal way would make the cellulose too dilute to detect, but preparing neat NMR samples would require cost-prohibitive (or nonexistent) deuterated versions of each test solvent. Many researchers check for optical clarity as an indicator that all cellulose has dissolved. Some use optical microscopy for this purpose,²²³ others perform turbidity measurements,²²⁴ and many rely simply on visual inspection.²⁰⁷

For this exploratory work, the chief interest was in assessing whether any fraction of the cellulose had dissolved, which ruled out optical clarity as an option (clarity relies on the entirety of the cellulose dissolving). Instead, each sample was centrifuged to remove any undissolved cellulose, and anti-solvent added to the supernatant (Fig. 3.8). If solid precipitate was formed at this point, the solvent system was considered to be successful.

Analysing Regenerated Cellulose When cellulose has been regenerated (e.g. precipitated from supernatant), it is important to analyse it to ensure that the sample was truly dissolved, rather than simply dispersed. This is easily done by X-ray diffraction (XRD) or infrared (IR) spectroscopy. An X-ray diffractogram or IR spectrum will clearly show the differences between crystalline phases of cellulose (Fig. 3.9).^{225,226} Typically, cellulose regenerated from solution changes crystalline phases, shifting from cellulose I to II.^{199,210}

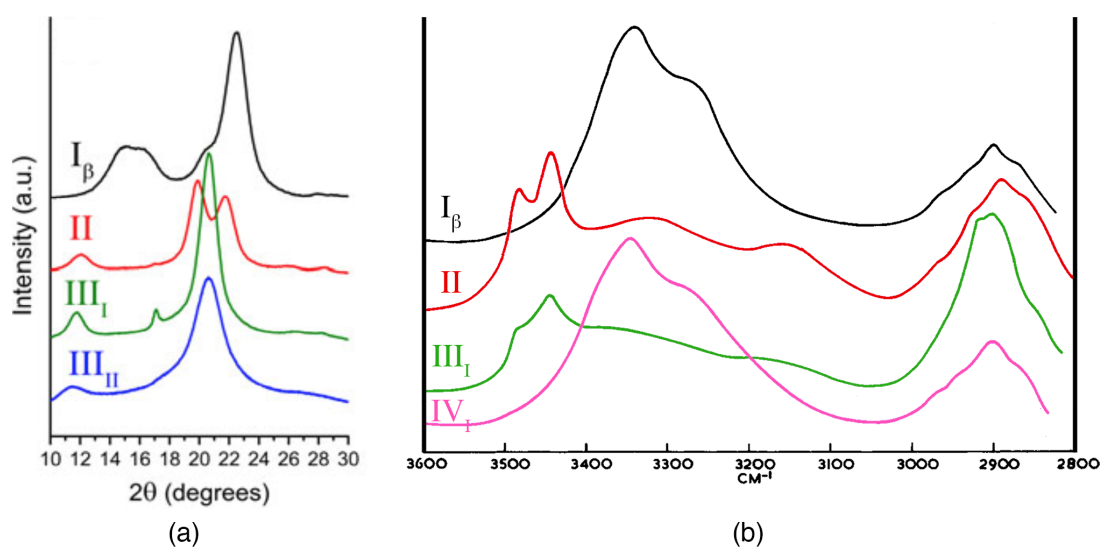


Figure 3.9: Crystalline phases of cellulose by (a) XRD and (b) IR. Adapted from C. M. Lee et al., *Cellulose*, 2013, **20**, 991–1000 with permission from Springer Nature © 2013 and H. J. Marrinan and J. Mann, *Journal of Polymer Science*, 1956, **21**, 301–311 with permission from John Wiley and Sons © 1956.

3.3 Results and Discussion

3.3.1 Design of Dissolution Systems

While solvents can be compared by predicting or measuring their solubility parameters, the additives used for cellulose dissolution have no easy metrics for comparison, as HSP predictions are not yet reliable for ionic compounds.⁵⁰ Additive structures tend to be drastically different, preventing direct qualitative comparisons. Because of the diversity and unpredictability of cellulose solvent additives, it was decided that experimenting with a wide range of additives was the best approach. The potential additives were chosen based on compounds that worked with dipolar aprotic solvents in the literature, as well as closely-related alternatives (e.g. substituting bromide for chloride, tetramethyl for tetrabutyl, etc.).

Table 3.2: Solubility of dissolution additives in Cyrene

Additive	Solubility	
	Cyrene	Cyrene/Water
lithium fluoride	no	no
lithium chloride	no	>50% water
lithium bromide	yes	yes
zinc fluoride	no	no
zinc chloride	degraded	yes
zinc bromide	degraded	yes
tetrabutylammonium fluoride hydrate	degraded	no
tetrabutylammonium chloride	yes	yes
tetrabutylammonium tribromide	degraded	degraded
tetrabutylammonium iodide	yes	<50% water
tetrabutylammonium acetate	degraded	yes
tetrabutylammonium hydrogen sulfate	yes	yes
tetramethylammonium fluoride tetrahydrate	degraded	degraded
tributylmethylammonium chloride	yes	yes
trimethyloctylammonium chloride	yes	yes
tetraoctylammonium bromide	yes	<20% water
propylene carbonate	yes	yes
glycerol carbonate	yes	yes

The solubility of each additive candidate was tested in Cyrene (Table 3.2). The concentrations of additive were chosen based on common literature methods for these or

similar additives in dipolar aprotic solvents, and are detailed in Table A.1. Each candidate was also tested in nine mixtures of Cyrene and water, beginning with 10% w/w water in Cyrene and increasing in 10% intervals to 90% water. Table 3.2 indicates which of these mixtures could successfully dissolve each additive, with *yes* indicating all Cyrene/water mixtures were successful. In some cases, the additive reacted with Cyrene to form a viscous or solid mixture, which was considered to be degradation. Adding water to Cyrene mitigated this effect for some additives, while in others the apparent degradation persisted even in mixtures of Cyrene and water. Solvent systems with degradation were not tested in cellulose dissolution trials, but in cases of water-mitigated degradation, the compatible water systems were tested.

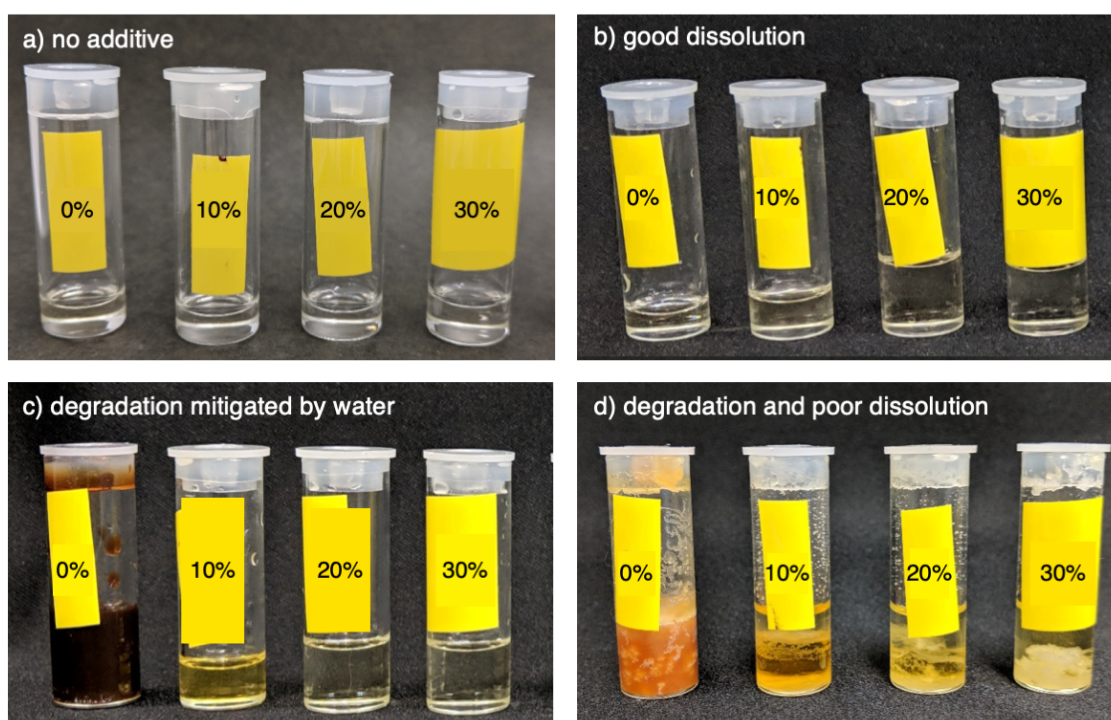


Figure 3.10: Examples of additive dissolution attempts in Cyrene, with water content ranging from 0-30%. Sample shown are Cyrene/water with a) no additive, b) tetrabutylammonium hydrogen sulfate, c) zinc chloride, and d) tetramethylammonium fluoride tetrahydrate.

Selected examples of attempted solvent systems from Table 3.2 are pictured in Figure 3.10 to demonstrate the high variance of results across additives. With no additives, water and Cyrene form a clear, colorless solution that appears stable at room temperature. Dissolution of additives was considered 'good' when the solutions were completely clear and no precipitation was observed over several days. In cases where water was found to mitigate the apparent degradation of Cyrene, the pure Cyrene sample changed colour

dramatically and became viscous or solid, but addition of even 10% water resulted in a clear solution with mild colour change, and 20% water or more gave good dissolution with minimal colour change. This was observed in the cases of zinc chloride and bromide, as well as tetrabutylammonium acetate. In these cases, the salt is likely being preferentially solvated by water, reducing the reactivity of the salt as well as the frequency of contact with Cyrene. Finally, a number of additives were found to be completely unsuitable for use with Cyrene, either degrading or failing to dissolve in all samples. For example, tetrabutylammonium fluoride hydrate (pictured here) was found to transform Cyrene to an orange solid, and addition of water resulted in very poor dissolution.

Examining the results in Table 3.2 for trends, simple inorganic salts tend to be insoluble in Cyrene. Unfortunately, this rules out Cyrene/LiCl (a direct analogue to DMAc/LiCl) as a promising dissolution system, as lithium chloride requires at least 50% water in Cyrene to dissolve. However, lithium bromide was tested as a Cyrene-soluble alternative.

For quaternary ammonium salts, a range of cations and anions were tested. Tetrabutylammonium cations are the most common and readily available, and had fair solubility in Cyrene. Tetrabutylammonium chloride, in particular, was readily soluble in both Cyrene and Cyrene/water mixtures. Unfortunately, tetrabutylammonium bromide was not available at the time of testing, and the tribromide variant was substituted instead. This should be followed up at a later date, as the tribromide anion behaves differently from monobromide. Two salts with fluoride anions were selected for their strong hydrogen bond accepting ability, but unfortunately proved quite reactive with Cyrene (as expected, due to its instability to bases).¹⁰⁴ Tetrabutylammonium acetate and hydrogen sulfate were chosen as examples of salts with bulky anions, in order to test the effect of anion size on dissolution.

Propylene carbonate and glycerol carbonate were also tested as unusual additive candidates. These were selected on the basis of an HSPiP prediction, using Dextran C as the target solute. This polymer is similar to amorphous cellulose, not microcrystalline cellulose, but it is the closest related polymer for which HSP values are available.⁵⁹ A combination of water, Cyrene, and geminal diol was used as the solvent, and HSPiP was used to find the best additive to bring the mixture closer to the HSP of Dextran C. Propylene carbonate and glycerol carbonate were predicted to be the best green options.

After testing solubility of all additives above, the successfully dissolved solvent

systems were progressed to cellulose dissolution testing.

3.3.2 Cellulose Dissolution Trials

Research in this section was carried out in collaboration with Noriyuki Isobe.

Each successful additive from above was tested in ratios from 0% w/w water in Cyrene (i.e. pure Cyrene) to 100% (i.e. pure water) (Table 3.3). Additive concentrations were based on typical values drawn from literature related to that additive (see Table A.1). DMSO and DMAc solvent systems were included as controls, allowing comparison between behaviour of Cyrene and conventional dipolar aprotics for each additive. Mixtures of Cyrene and water with no additives were also tested to check whether Cyrene could behave like NMMO and dissolve cellulose in the presence of water.

To begin with, the general method depicted in Figure 3.8 was used, mixing each sample via inversion and shaking before cooling to -30°C overnight. Each cellulose sample (10 mg, or 1% w/v cellulose/solvent) was pretreated using solvent exchange to maximise chances of dissolution. After freezing, the quality of the cellulose dispersion was assessed by observing the speed with which the dispersion settled (Table 3.3). If a dispersion settled quickly, it was considered to be of poor quality, while slower-settling dispersions were more promising. Though this is not a predictor of dissolution, it does give some idea of the level of interaction between cellulose and solvent system, as well as predicting whether any solvent system might give industrially useful colloidal dispersions. Samples where the settled cellulose was visibly swollen were marked as such, and it is suspected that these samples are close to dissolution (though unfortunately, this only occurred in DMSO control samples).

It should be noted that samples with more than 40% water in Cyrene only gave dispersions of fair or poor quality, as expected due to water's anti-solvent nature. However, samples with 10-30% water in Cyrene were able to give good dispersions, and even in some cases improve upon the 0% result, suggesting that the geminal diol of Cyrene may indeed be contributing positively to cellulose-solvent interaction. However, as these observations are qualitative, no definite conclusions can be reached.

After observing the cellulose dispersion quality, each sample was centrifuged for ten minutes to remove the undissolved cellulose (Fig. 3.8). The supernatant was carefully decanted and combined with ethanol as an anti-solvent, checking for precipitate as evidence of dissolution. Only one of the Cyrene solvent systems tested was successful in

Table 3.3: Dispersion quality in cellulose dissolution trials

Additive	Water Content (w/w)										Control Solvent		
	0%	10%	20%	30%	40%	50%	60%	70%	80%	90%	100%	DMSO	DMAC
none	fair	fair	fair	fair	fair	fair	poor	poor	poor	poor	poor	poor	poor
[Li] ⁺ [Cl] ⁻	-	-	-	-	-	fair	poor	poor	poor	poor	poor	good	dissolved
[Li] ⁺ [Br] ⁻	fair	good	good	fair	fair	fair	poor	poor	poor	poor	poor	poor	poor
[Zn] ²⁺ [Cl] ₂ ⁻	-	good	good	good	fair	poor	poor	poor	poor	poor	poor	poor	-
[Zn] ²⁺ [Br] ₂ ⁻	-	good	good	good	good	fair	poor	poor	poor	poor	poor	poor	poor
[NBu ₄] ⁺ [Cl] ⁻	good	good	good	good	fair	poor	poor	poor	poor	poor	poor	swollen	-
[NBu ₄] ⁺ [I] ⁻	poor	poor	poor	-	-	-	-	-	-	-	-	poor	poor
[NBu ₄] ⁺ [Ac] ⁻	-	good	fair	fair	fair	poor	poor	poor	poor	poor	poor	dissolved	dissolved
[NBu ₄] ⁺ [HSO ₄] ⁻	fair	fair	poor	fair	poor	fair	poor	poor	poor	poor	poor	poor	poor
[NBu ₃ Me] ⁺ [Cl] ⁻	good	good	fair	fair	good	fair	poor	poor	poor	poor	poor	good	dissolved
[NMe ₃ Oct] ⁺ [Cl] ⁻	fair	fair	fair	fair	poor	poor	poor	poor	poor	poor	poor	swollen	-
propylene carbonate	good	good	good	fair	fair	fair	poor	poor	poor	poor	poor	poor	poor

Quality of dispersion was judged by speed of settling, with slower settling indicating better dispersion. Dashes indicate systems that were immiscible or degraded.

dissolving cellulose—tetrabutylammonium chloride ($[\text{NBu}_4]^+[\text{Cl}]^-$, or TBAC) in pure Cyrene. The lack of dissolution in the corresponding 10% water/Cyrene system suggests that water is indeed acting as an anti-solvent in Cyrene, despite presence of the geminal diol. Roughly 3 mg of cellulose were regenerated from Cyrene/TBAC, meaning that 0.3% w/v cellulose had been dissolved.

The regenerated cellulose from this sample was analysed via XRD to assess whether the cellulose was fully dissolved, or only dispersed (Fig. 3.11a). The TBAC/Cyrene system produces regenerated cellulose that is very similar to a 1:1 superimposition of cellulose I and II. From this, it can be deduced that the content of cellulose II in the regenerated sample is roughly 40-60%, and the behaviour observed is not full dissolution, but a mixture of dissolution, swelling, and dispersion. This is similar to the behaviour of cellulose in an aqueous solution of zinc chloride, which has been used in the past for processing of cellulose.^{227,228} Therefore, the Cyrene/TBAC system could be useful as a green solvent system for cellulose processing.

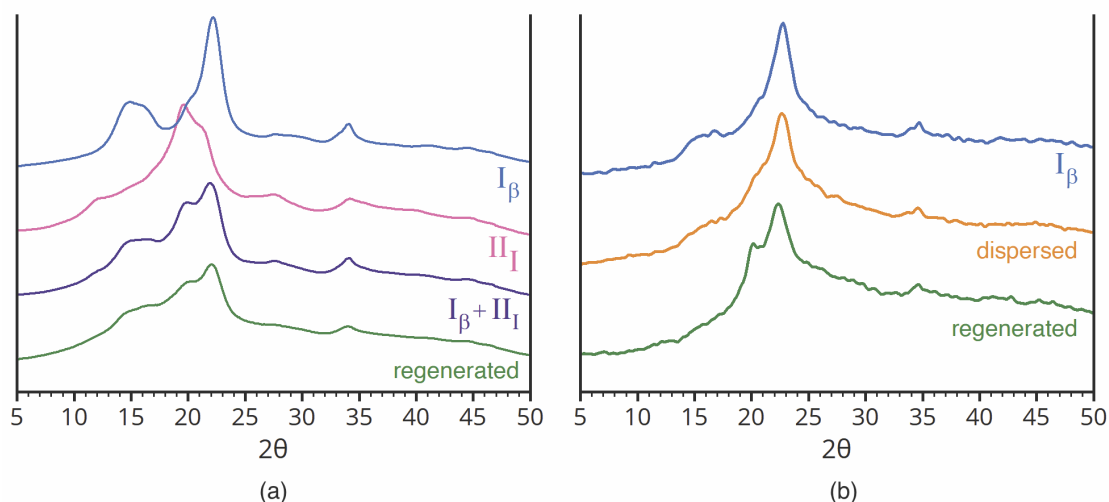


Figure 3.11: XRD spectra of microcrystalline cellulose (I_β) and treated samples. (a) Cellulose II can be superimposed in a 1:1 ratio with Cellulose I to give a spectrum very similar to that of the regenerated cellulose. (b) Large-scale cellulose dissolution trials yielded a dispersion of cellulose I and a regenerated mixture of cellulose I and II.

To check whether conventional industrial methods could achieve similar results in this solvent system, a larger-scale dissolution attempt was made using mechanical mixing and conventional heating at 80°C over 24 hours. This treatment resulted in an orange-brown mixture that was much harder to separate, needing 3 – 4 hours of centrifugation to obtain a clear supernatant. The foggy supernatant that results from

shorter centrifugation appears to be a dispersion of cellulose I (Fig. 3.11b, dispersed). The cellulose regenerated from the clear supernatant appears to be a mix of cellulose I and II, as seen previously, though perhaps with less cellulose II (Fig. 3.11b, regenerated). Possibly, the prolonged heating breaks the cellulose polymer chain into shorter fragments that are more stable as a dispersion due to entropic effects. This could be investigated via gel permeation chromatography (GPC) to confirm the chain length of the dispersed cellulose. It is known that highly charged colloidal dispersions are more resistant to centrifugation due to electrostatic repulsion; it is possible that chloride ions on the surface of the cellulose chains are contributing to the stability of this dispersion.²²⁹

To further probe the capabilities of the Cyrene/TBAC solvent system, it was investigated with a variety of processing methods aimed at overcoming kinetic barriers and speeding dissolution.

3.3.3 Improving Cellulose Dissolution

The TBAC/Cyrene solution was very viscous, making it difficult to mix and perhaps slowing cellulose dissolution due to decreased mobility of free TBAC ions and reduced kinetics.²³⁰ To combat this, DMSO was introduced as a relatively green, low-viscosity cosolvent, preparing mixtures of Cyrene and TBAC with 5 – 20% v/v DMSO before adding cellulose (Fig. 3.12a). These samples were then treated with the standard dissolution method described above, shaking to mix and cooling to -30°C overnight. While Cyrene/TBAC and DMSO mix readily, addition of DMSO reduced the solubility of cellulose to practically zero, despite a visually obvious reduction in viscosity of the solvent system. This could be due to a reduced concentration of TBAC salt in the solvent system, but adding more salt with the DMSO would again increase viscosity, making this solution non-viable.

Next, sonication was used with the Cyrene/TBAC system to aggressively increase mixing and speed dissolution, attempting to overcome the viscosity issue by a different method. Sonication (ultrasound treatment) uses high-frequency sound waves input directly into the mixture to induce *cavitation*, or the formation of microscopic gas bubbles that rapidly expand and burst.²³¹ Cavitation rapidly mixes the sample, but also releases energy in the form of heat and light that can degrade both solvent and polymer, and even break glass sample vials if unchecked.²³² For this reason, sonication of small samples without cooling is impractical for more than a few minutes—the sample rapidly overheats,

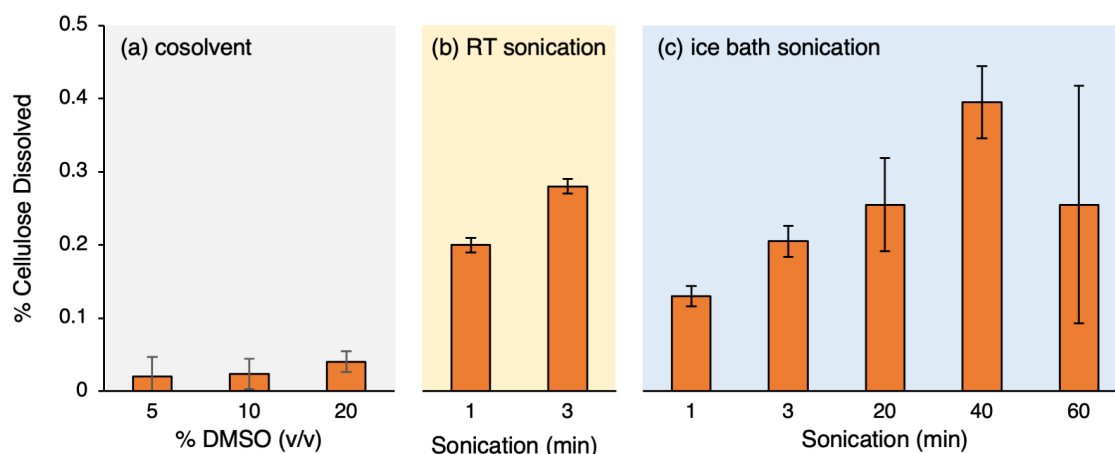


Figure 3.12: Attempts at improvement of cellulose dissolution in Cyrene/TBAC system using (a) DMSO as a cosolvent, (b) sonication at room temperature, and (c) sonication in an ice bath. Results are presented as average of 2-3 trials \pm standard deviation.

even when pausing sonication periodically to allow for heat dissipation.

Nevertheless, samples were sonicated briefly without cooling (Fig. 3.12b) and compared to samples sonicated in an ice bath from 1 – 60 minutes (Fig. 3.12c). Sonication was achieved via a titanium alloy microtip (2 mm diameter) inserted directly into the sample, using a VCX-130 ultrasonic processor. While this instrument is capable of delivering 130W of power, amplitude was set to 60%, limiting maximum power delivery to 78W. Actual power delivery could vary depending on viscosity of the solution—in future trials this could be actively monitored to ensure consistent sonication. The results show that sonication without cooling is slightly more effective than sonication in ice, though the ice bath allows for longer periods of sonication that ultimately perform better. It should be noted that these trials did not test whether uncooled sonication resulted in degradation of polymer, which would be of concern in industrial applications. Trials with DMAc/LiCl have shown that temperatures above 150°C shorten the polymer chain and reduce cellulose quality, though it is not clear what the temperature of concern would be in this Cyrene/TBAC system.²⁰⁰ The high variance in the 60-minute samples is due to experimental error in one trial. This could be corrected with another repetition, and it is expected that the upward trend in dissolution would then persist into the 60-minute range.

Regardless, the maximum dissolution achieved thus far with the Cyrene/TBAC system is below 0.5% w/v cellulose. This must be improved significantly to make it a viable commercial competitor, but the potential of this system has been uncovered and

performance can likely be further improved.

3.4 Summary and Future Work

The potential of Cyrene in cellulose dissolution has been shown with this work, though for industrial application this system requires significant improvement in quantity of cellulose dissolved. Industrial cellulose solvent systems are capable of dissolving up to 20% w/v cellulose. Cyrene has been shown here to dissolve almost 0.5% w/v cellulose in combination with TBAC, which is too low to be competitive. When regenerated, the dissolved cellulose is a mixture of phases I and II, showing that the dissolution behaviour is complex. However, the stability and optical clarity of the dissolved material suggests that this system could be suitable for processing cellulose. Furthermore, the stable dispersion achieved via prolonged mixing could have industrial processing uses.

The Cyrene/TBAC system is moderately green, given the status of TBAC as a relatively environmentally friendly quaternary ammonium salt.²³³ It is particularly compelling that Cyrene can be derived from cellulose in two steps, then used to dissolve cellulose. However, TBAC is not renewably-sourced, nor is it registered under REACH, so it is possible that more data will emerge on its toxicity and environmental properties. Its use in the EU is limited to under 1 tonne/year, pending registration. Future work should look at other additives that are both renewable and benign, potentially including naturally-sourced deep eutectic solvents and green co-solvents, while also considering REACH registration status. While DMSO did not appear to promote dissolution in this system, it is entirely possible that a different co-solvent could both reduce viscosity and increase dissolution.

Future work should also include revisiting some of the samples that appeared to give good dispersions in initial trials, and attempting sonication, heating, or higher concentrations of salt to investigate whether dissolution can be achieved. The solubility of TBAC in Cyrene was found in a late trial to be close to 50% w/w, while only 40% was used for the trials in this research. Increasing the salt concentration to maximum could increase availability of free ions in solution, potentially boosting cellulose solubility for TBAC and other additives. If other systems can be identified for cellulose dissolution in Cyrene, perhaps the basis of the dissolution behaviour can be uncovered and used to predict other additives. In this work, systems utilising dipolar aprotic solvents were prioritised for their potential similarity to Cyrene, but the popularity of cellulose dissolution in

aqueous systems of urea/thiourea with sodium or lithium hydroxide suggests another avenue to pursue.^{223,234}

Microwave heating trials would also be interesting, as microwaves have been shown to accelerate cellulose dissolution in some cases.²³⁵ Microwave heating is a more efficient alternative to conventional heating, and may be able to avoid some of the degradation that is suspected in the larger-scale heating trials attempted here. The cellulose obtained from large-scale heating trials and sonication trials should be analysed via GPC for degradation of the polymer chains, comparing it to any results obtained from microwave trials.

In order for the Cyrene/TBAC system to be economical and part of the circular economy, it should be recyclable. Processing methods that degrade the solvent and prevent recycling should be avoided. To that end, small-scale recycling trials should be attempted, along with NMR analysis of the solvent system after each trial to assess stability. This would provide enough information to decide whether heating and mechanical mixing, room-temperature sonication, or sonication in an ice bath is preferred.

To conclude, this research has shown that it is possible to dissolve cellulose in a Cyrene-based solvent system, albeit in very small quantities. There may be potential for additional dissolution of cellulose with modification of this solvent system, and much future work remains to be done in order to explore its capabilities.

CHAPTER 4

BLENDING SOLVENTS FOR NOVEL PROPERTIES

While Cyrene has potential as a green solvent, some of its properties present unusual challenges. In particular, its reactive ketone moiety is labile to acids and bases, limiting its applicability as a solvent.¹⁰⁴ Replacing the problematic ketone group with a more stable ketal yields a series of Cyrene derivatives known as Cygnets, some of which have intriguing solvation properties.¹⁰⁹ In particular, Cygnet 0.0, which is formed by the reaction of Cyrene with ethylene glycol in the presence of an acidic catalyst, is predicted to behave similarly to dichloromethane (DCM). Unfortunately, this derivative is also highly crystalline, with a melting point above 70°C. This makes it more difficult to handle as a solvent. By blending Cygnet 0.0 with Cyrene, it may be possible to access the DCM-like properties of this Cygnet while keeping the low melting point of Cyrene, opening new applications. In addition, the blending of solvents can lead to unpredictable properties, potentially changing the performance in unexpected ways.

4.1 Background

In addition to being used as a solvent, Cyrene can be used as a platform molecule to create other potentially useful compounds. One motivation for derivatisation of Cyrene is to reduce its reactivity—Cyrene's ready formation of dimer in the presence of base, as well as its sensitivity to strong acids, limits its use in certain applications.¹⁰⁴ In addition, creating new compounds from Cyrene expands the palette of green, bio-based chemicals. As the synthesis of Cyrene from cellulose takes only two steps, compounds made in one step from Cyrene are only three steps removed from the raw feedstock. This creates opportunity for using green chemistry to create a range of molecules that can be easily produced from cellulose, but have a diverse range of functional groups and applications, opening new opportunities for cellulose as a feedstock.

The Cygnets, in particular, are ketals of Cyrene that are accessed via the reaction of Cyrene with various diols in the presence of an acidic clay catalyst (Fig. 4.1).¹⁰⁹ This reaction is simple and efficient, using a heterogeneous catalyst and producing only water as a byproduct. Cygnets are named for the length of their pendent carbon chains (e.g.

Cygnets 0.0 has no carbon chains on the ketal, while Cygnets 1.1 has two methyl groups). As they are structurally close to Cyrene, these compounds are considered potential green solvent candidates. They are attractive in this application partly due to their increased stability—without the reactive ketone moiety, the Cygnets are more resistant to acids and bases than Cyrene. They are predicted to be non-toxic and non-mutagenic, though more safety testing must be performed before they can be considered safe.¹⁰⁹

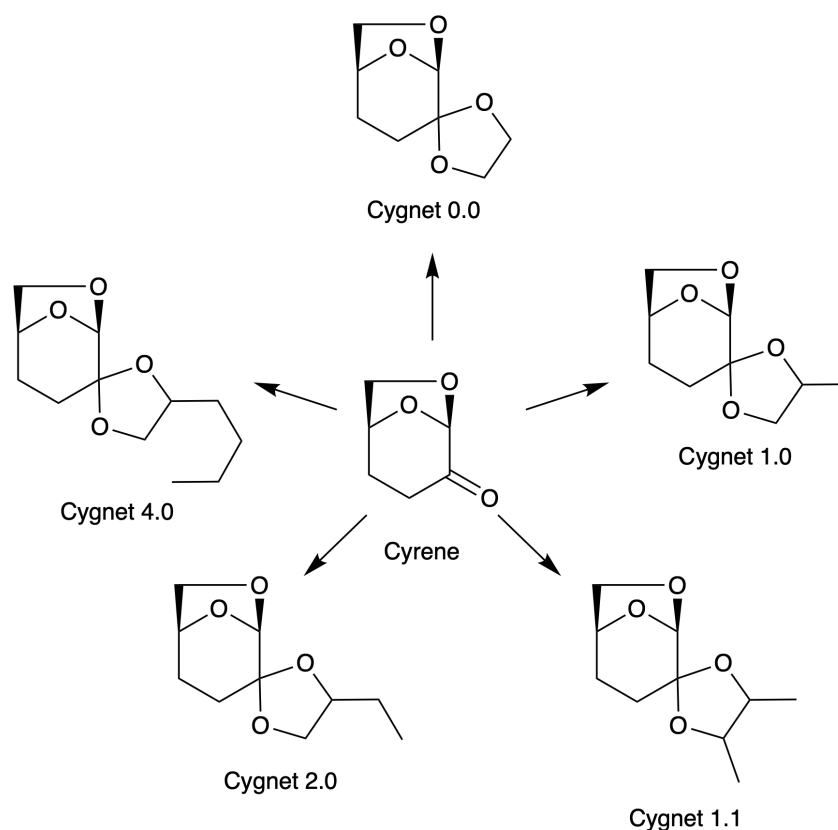


Figure 4.1: Five different Cygnets have been synthesised from Cyrene to date, with nomenclature based on length of ketal carbon chains.

As solvents, Cygnets present their own unique challenges. While Cyrene has a melting point below -20°C , making it easy to handle as a liquid under standard conditions, Cygnets have melting points that are considerably higher. All variants presented here are solid or near-solid at room temperature. Cygnets 0.0 is the most thoroughly investigated of the Cygnets. It presents as a needle-like crystalline solid at room temperature and has a melting point near 70°C . The other Cygnets have not been synthesised in sufficiently high purity to measure their melting points, but they are all solid at room temperature. Their other physical properties, including viscosity and density, have not yet been investigated.

While having a melting point below 100°C is the common threshold for ionic liquids

to be considered potential solvents, it can be difficult to replace solvents in industrial processes with higher-melting alternatives, especially if the process requires the solvent to be liquid at a low temperature. Therefore, blending Cygnets with other solvents could be of interest, yielding liquid solvents with potentially novel solvent properties. For this work, Cyrene was chosen as the liquid component of the blend, though theoretically any green solvent could be used. Though this re-introduces the issue of Cyrene’s instability, there are not many options for stable green solvents with high dipolarity. After ruling out solvents with toxicity and flammability issues, dimethylsulfoxide (DMSO) is left as the only other REACH-registered choice, and its ability to penetrate the skin barrier often raises concerns in industrial settings.⁴¹

Because Cyrene is the precursor for Cygnet synthesis, Cyrene/Cygnet blends could be conveniently synthesised by using diol as a limiting reagent. Removal of water with a drying agent, followed by filtration to remove drying agent and catalyst, presents an attractive single-step synthetic option that theoretically requires no purification. Neither Cyrene nor Cygnet had been reported in blends prior to this work, making this a novel area to explore.

Table 4.1: Predicted HSP for Cygnet 0.0 and related solvents

Solvent	δ_D	δ_P	δ_H
Cyrene	18.8	12.4	7.1
NMP	18.0	12.3	7.2
Cygnet 0.0	18.3	8.2	6.9
DCM	17.0	7.3	7.1

HSP values in MPa^{1/2}.

Cygnet 0.0 is of particular interest as a solvent, as its Hansen Solubility Parameters (HSP) are predicted to be very close to those of DCM (Table 4.1), which is unprecedented for a green solvent. The polarity parameter, δ_P , is much lower in Cygnet 0.0 than in Cyrene, bringing it closer to DCM. This is probably a result of the electronegative ketone moiety being replaced with a five-membered ring with methylene groups facing outwards, making the molecule overall less polar. Blending Cygnet 0.0 with Cyrene could create a range of cellulose-derived solvents with tunable solubility parameters.

For testing polymer-related applications of this blended system, the casting of filtration membranes was chosen as a proof of concept. Polymer membranes are applied in filtration processes in a wide range of industries, and their properties depend strongly

on the solvent(s) used in their preparation.⁸⁷ Despite extensive research in non-solvent induced phase inversion (NIPS) membrane casting over the last two decades, membranes are still largely prepared using hazardous conventional solvents that possess the desired properties.

A blend of Cygnet and Cyrene could conceivably act like DCM in dissolving polymers for NIPS membrane casting (see Section 1.4.1 for details of this process), with potential improvements. The decreased volatility of Cygnet/Cyrene compared to DCM would reduce solvent evaporation during the casting process, increasing the reliability of membrane production.^{81,91} Additionally, Cygnet and Cyrene are both water-miscible, allowing water to penetrate into the membrane during NIPS to form the pores that are critical to the membrane's performance. The presumed safety (pending further investigation) of this solvent system would be particularly beneficial in casting water filtration membranes, as any solvent left behind in the membrane would be non-toxic and safe for water filtration. Therefore, the use of Cygnet/Cyrene blends in membrane casting was attempted here as a test of their applicability in polymer processing, first by predictive methods and then empirically.

4.2 Greening of Cygnet Synthesis

Previously-reported syntheses of the Cygnet compounds involve refluxing the reagents in toluene for 24 hours, which is not in keeping with green chemistry principles.¹⁰⁹ For large-scale industrial uses, it is critical that the synthetic route is safe, energy-efficient, and produces as little waste as possible. While ideally, the preferred synthetic route for Cygnet/Cyrene blends would involve less than one equivalent of diol, allowing *in situ* creation of the blend, for this initial experimental work it was decided to begin with the purified form of Cygnet. This allowed study of the properties of pure Cygnet as well as its Cyrene blends.

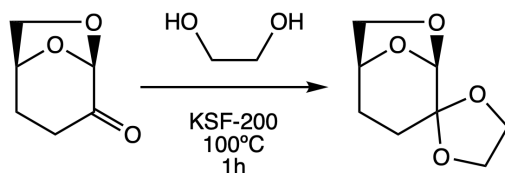


Figure 4.2: Improved synthesis for Cygnet 0.0. The use of toluene has been eliminated, the amount of catalyst reduced, and the reaction temperature lowered.

In order to “green” the Cygnet synthesis, kinetic trials were conducted with reduced

temperature, various solvents, and reduced catalyst loading. The most efficient synthetic procedure for Cygnet 0.0 proved to be solvent-free for one hour in an open flask, giving over 90% conversion, over 50% yield, and eliminating solvent waste and water waste (Fig. 4.2). The amount of acidic clay catalyst used was reduced by 68.8%, and the reaction temperature was lowered by 10°C.

Finally, the original workup featured an aqueous extraction followed by recrystallisation from heptane, generating significant amounts of petroleum-derived solvent waste. In the new procedure, the extraction step is skipped altogether, as the product crystallises after vacuum filtration and can then be recrystallized from minimal ethanol. The dramatic improvement in efficiency and ease of Cygnet synthesis will enable easier experimentation with the properties and applications of Cygnet 0.0. It could potentially be generalised to the other Cygnets, though their individual crystallisation behaviour could require alternative methods of purification.

4.3 Predicting Solubility Behaviour

4.3.1 HSP Predictions

While Cygnet 0.0 (Cygnet) is predicted to be close to DCM in the solvent space, it is a solid at room temperature, making it difficult to handle as a solvent. Combining it with Cyrene may create a solvent system that is liquid at room temperature, while still close to DCM in the solvent space. To investigate this possibility, HSP were used as a simple model to predict solvent behaviour for varying ratios of Cygnet and Cyrene. The goal was to identify blends with high potential for application.

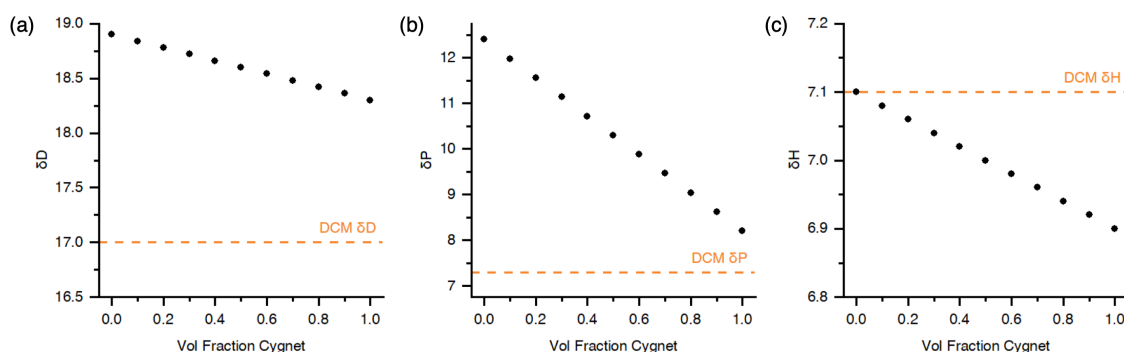


Figure 4.3: Hansen solubility parameters (MPa^{1/2}) as predicted for Cygnet-Cyrene mixtures. (a) Dispersion forces (δ_D), (b) dipolarity/polarizability (δ_P), and (c) hydrogen bonding ability (δ_H) are shown versus volume fraction of Cygnet in Cyrene. Values for DCM are included as dashed lines.

The HSPiP software predicts the solubility parameters of mixtures as a linear combination of the parameters for each individual component. Therefore, the predicted HSP for these binary mixtures form simple linear plots (Fig. 4.3). In δ_D (Fig. 4.3a) and δ_P (Fig. 4.3b), moving closer to pure Cygnet brings the solubility parameters closer to DCM, while the opposite is true for δ_H (Fig. 4.3c). The parameter with the most dramatic difference between Cygnet and Cyrene is dipolarity (δ_P). In dispersion (δ_D) and hydrogen bonding (δ_H), Cygnet and Cyrene are quite similar. The best solvent mixture, therefore, would be one where the polarity is as close as possible to Cygnet, while being fully miscible and retaining the low melting point of Cyrene. According to HSP, maximising the volume fraction of Cygnet would be ideal.

Naturally, the predictive power of this simple calculation is limited, as the properties of mixtures can change in a non-linear way. For example, in mixtures of formamide with other solvents, both dipolar aprotic and protic, the dielectric constants deviate greatly from the ideal linear model.²³⁶ Therefore, experimental studies must be performed to explore the actual behavior of the solvent mixtures.

4.3.2 KAT Measurements

Kamlet-Abboud-Taft (KAT) solvatochromic parameters were measured for binary mixtures of Cygnet and Cyrene and compared with those of DCM (Fig. 4.4). As both Cyrene and Cygnet are aprotic solvents, the hydrogen bond accepting ability (α) was not measured. While HSPiP predicts mixtures by volume fraction, experimentally it is much simpler to use weight fraction, as Cygnet is a solid at room temperature. The density of Cygnet is currently unknown, but is likely to be similar to that of Cyrene, so the volume fraction and weight fraction results are compared directly in this work.

All KAT parameter measurements were conducted at 60°C to enable measurement of samples that were solid at room temperature. This temperature was selected based on previously reported methods for measurement of Cygnet KAT parameters.¹⁰⁹ However, it proved to be insufficient for pure Cygnet, which remained a solid at this temperature. The melting point of Cygnet was found by DSC to be 71°C, which suggests that the previously reported KAT measurements were performed with a sample that contained some impurities. The maximum temperature on the Peltier apparatus used for performing high-temperature UV-Vis measurements was insufficient to fully melt Cygnet; therefore, KAT parameters for 100% Cygnet are not reported here. It is also suspected that the 90%

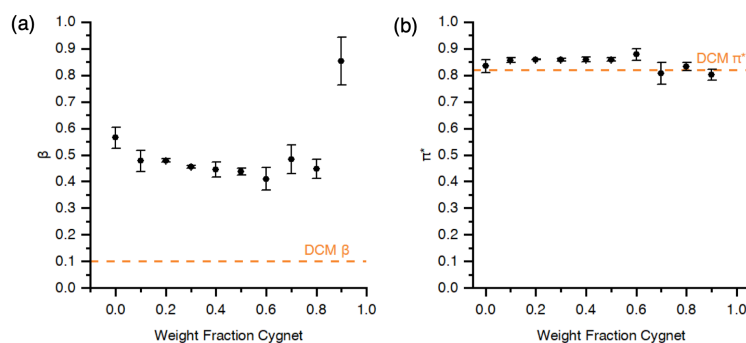


Figure 4.4: Measured KAT parameters for mixtures of Cygnet and Cyrene. (a) Hydrogen bond donating ability (β) and (b) dipolarity/polarisability (π^*) are shown vs. weight fraction of Cygnet in Cyrene. Values are given as average of three independent trials \pm standard deviation, with DCM values included as dashed lines.

Cygnet sample used to measure β may have begun to crystallise during the experiment, explaining the high error margin and the apparent jump in hydrogen bond donating ability. The DCM values reported here are known values for DCM at 25°C, and may be slightly different at elevated temperatures. However, the low boiling point of DCM makes high-temperature measurements impossible; the 25°C values are used here as a rough estimate for the sake of comparison.

Aside from the possibly erroneous 90% sample, the β (hydrogen bond donating ability) value of the mixtures appears to trend downwards from Cyrene towards 60% Cygnet, then slightly back up (Fig. 4.4a). It appears that 50-60% Cygnet in Cyrene gives the closest β value to DCM. Disregarding the potentially anomalous 90% Cygnet value, the maximum difference in β achieved by adding Cygnet to Cyrene was a drop of roughly 0.1, bringing it about 20% closer to the room-temperature DCM value. This is a fairly small difference, suggesting that addition of Cygnet may not have a sufficiently dramatic effect on membrane formation to justify its use.

For π^* (polarity/dipolarisability), the trend is even less pronounced (Fig. 4.4b). The values hover slightly above that of DCM from 0–60% Cygnet, then drop closer to DCM for 70-90% Cygnet. However, the differences in π^* values between all the blends are quite small, suggesting that the more important KAT parameter for bringing the solution closer to DCM is β . This is in direct contrast to the HSP values, for which the biggest difference was found in polarity.

The results here highlight the importance of combining computational and experimental solubility parameters to study solvent blends. While computationally predicted HSP show a simple linear trend in each parameter, and suggest that maximising the

proportion of Cygnet gives the best chance of a DCM-like blend, the experimentally measured KAT parameters are more complex. Both β and π^* show non-linear relationships with the weight fraction of Cygnet in Cyrene. KAT parameters imply the blend closest to DCM is in the range of 50-70% Cygnet, rather than 100%. This non-linear behaviour could be the result of complex interactions between the Cygnet and Cyrene molecules in the bulk solvent. However, it might also be due to preferential interaction of the solvatochromic dye molecules with one of the blend components, yielding a measurement of the cybotactic region surrounding the dye rather than the bulk mixture. If necessary, this could be further investigated using the preferential solvation model.^{60,61}

In the course of the KAT parameter experiments, it was found that 50% w/w Cygnet in Cyrene is the highest percentage of Cygnet that can be used at ambient temperature without rapid crystallisation. For ease of handling in both laboratory and industrial settings, this mixture was selected for further study. To ascertain whether this blend is suitable for membrane casting applications, its performance was tested in casting membranes from commonly used polymers.

4.4 Applications in Membrane Casting

4.4.1 Membrane Casting

Research in this section was carried out in collaboration with Roxana Milescu.

HSP values can be helpful in choosing polymers that are likely to dissolve in a given solvent. For this work, the HSP of Cyrene and 50% Cygnet 0.0 in Cyrene were compared with values for polymers commonly used in membrane applications for water filtration.⁸⁷ While the HSP of the Cygnet blend may not be entirely accurate, the estimate should be sufficient for a rough prediction of polymer dissolution. The HSP values and HSP distance (R_a) are given in Table 4.2 for each common membrane polymer, with the relative energy difference (RED) calculated for both Cyrene and Cygnet/Cyrene. RED values below 1 indicate the polymer will likely dissolve in this solvent, while values above 1 indicate poor dissolution. Values close to 1 are borderline cases.

The two polymers most likely to dissolve in both Cyrene and the Cygnet/Cyrene blend are polyethersulfone (PES) and polysulfone (PSU). These two were chosen as the best polymers for this initial proof of concept test. Additionally, polyimide (PI) was chosen as a borderline case to assess whether there is a difference in solubility. Each polymer was dissolved in Cyrene and 50% w/w Cygnet in Cyrene at 15–20% w/v. At

Table 4.2: HSP RED for common membrane polymers in Cyrene and Cygnet/Cyrene

Polymer	δ_D	δ_P	δ_H	R_a	RED	
					Cyrene	Cyg/Cyr
Polyethersulfone (PES)	19.0	11.0	8.0	8.0	0.21	0.18
Polysulfone (PSU)	19.8	11.2	6.2	11.3	0.21	0.24
Cellulose acetate	16.9	16.3	3.7	13.7	0.48	0.56
Poly(vinylidene fluoride) (PVDF)	17.0	12.1	10.2	8.0	0.61	0.61
Polyimide (PI)	24.3	19.5	22.9	21.6	0.95	1.00
Polyacrylonitrile (PAN)	22.4	14.1	9.1	8.0	0.93	1.09
Polytetrafluoroethylene (PTFE)	16.2	1.8	3.4	3.9	3.19	2.67
Polyamide (PA)	16.0	11.0	24.0	3.0	5.97	5.93

HSP values are in units of $\text{MPa}^{1/2}$, drawn from HSPiP database.⁵⁰

this concentration, there was no noticeable difference in solubility between PI, PES, and PSU.

A classic NIPS procedure (Fig. 1.9) was used to cast 500 μm membranes in both Cyrene and 50% w/w Cygnet in Cyrene, employing water as the antisolvent. Both of these solvents could be handled at room temperature, though in the case of the blend, Cygnet slowly crystallises out of solution over the course of several hours or days (depending on ambient temperature). Each polymer solution was cast at ambient temperature onto a glass plate using a steel blade, then immediately immersed in a room-temperature water bath to force precipitation of the polymer. After precipitation was complete, the membranes were removed and dried under vacuum. Membrane cross-sections were analysed by SEM to observe the morphological differences resulting from the addition of Cygnet to Cyrene.

Of the three polymers tested, PI membranes showed the most pronounced morphological differences between the Cyrene and Cygnet/Cyrene systems (Fig. 4.5). While PI in Cyrene forms numerous irregular macrovoids with diameters of 50-100 μm (Fig. 4.5a), the addition of Cygnet removes these irregular gaps entirely, instead forming regular, finger-like pores with diameters of 10-20 μm (Fig. 4.5d). These large-scale morphological features could impact water flux through the membrane, with the Cygnet/Cyrene membrane potentially allowing higher water flux due to increased surface area.²³⁷ The microstructures of the PI membranes appear to be similar in structure across solvent systems, but on different scales. In Cyrene, there is a sponge-like lattice with pores ranging from 2-8 μm in diameter (Fig. 4.5b-c). With the addition of Cygnet, this lattice shrinks

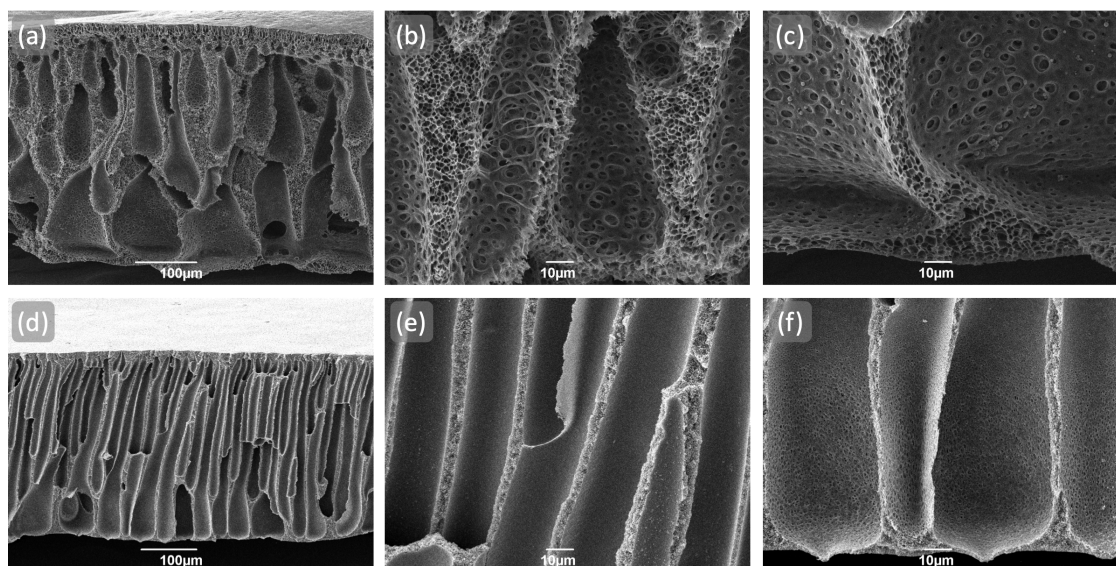


Figure 4.5: SEM images of 15% w/v PI membranes cast from Cyrene (a-c) and 50% w/w Cygnet in Cyrene (d-f).

considerably, with all pores becoming smaller than 1 μm in diameter (Fig. 4.5e-f). This difference in pore character could change the filtration performance of the membrane, allowing removal of smaller contaminants.

The factors affecting membrane morphology are complex, including both thermodynamic and kinetic effects. Flory-Huggins theory of polymer solutions can be used to describe the thermodynamic behaviour of the ternary polymer/solvent/antisolvent system, meaning that the energy of mixing depends on the concentration of each component of the mixture as well as specific inter-component interactions.²³⁸ To fully explain this behaviour, a phase diagram would need to be constructed to identify the gelation point of PI in each solvent, and binary interaction parameters would need to be calculated using activity coefficients for each solvent system and water. Additionally, in membranes with finger-like voids, membrane formation cannot be fully described by thermodynamics and kinetics, instead requiring consideration of phenomena such as syneresis, shrinkage, and stress relaxation.²³⁹ Performing this level of data collection and analysis is beyond the scope of this preliminary testing phase; therefore, the morphology differences are addressed qualitatively in this work.

Broadly speaking, macrovoid formation in polymer membranes is governed by the compatibility of the solvent with the antisolvent, and the viscosity of the polymer solution. Solvent-antisolvent compatibility can affect the extent to which water is able to flow into the cast membrane, with highly miscible systems tending to form more voids. High

viscosity of the polymer solution can reduce the rate of macrovoid formation, slowing movement of the polymer phase and resisting deformation.²⁴⁰ In the case of Cyrene or Cygnet/Cyrene and water, the thermodynamic compatibility of solvent/antisolvent is predicted to be quite similar across systems (Table 4.3).

Table 4.3: HSP and KAT parameters for Cyrene and 50% Cygnet blend

Solvent	δ_D	δ_P	δ_H	β	π^*
Cyrene	18.9	12.4	7.1	0.56	0.83
50% Cygnet in Cyrene	18.6	10.3	7.0	0.44	0.86
Water	15.5	16.0	42.3	0.49	1.14

Note: KAT parameters of blend were measured at 60°C, all other parameters at 25°C. HSP values in MPa^{1/2}.

The solubility parameters present conflicting evidence here (Table 4.3). δ_D and δ_H of Cyrene and the blend are almost identical, but the δ_P of Cyrene is slightly closer to that of water. In KAT parameters, the opposite is observed—the Cygnet blend is slightly closer to water in both β and π^* . Due to the large differences previously observed between the HSP predictions and the empirical KAT parameters, it appears that KAT parameters are more reliable for this blended solvent, and addition of Cygnet may bring Cyrene closer to the polarity of water. However, this effect is not very strong, and seems insufficient to explain the significant differences observed in the morphology of the PI membranes. It is important to note that these parameters say nothing about the kinetics of mixing, which could be different between the two systems.

The kinetics of mixing in these systems are more likely to be affected by the viscosity of the polymer solution. While viscosity of these systems has not yet been measured experimentally, the Cygnet/Cyrene blend appears significantly more viscous to the eye. This could account for the slower influx of water into the Cygnet/Cyrene/PI system and a resistance to horizontal expansion of the macrovoids, helping to explain the differences seen in the SEM micrographs above.

Polysulfone (PSU) membranes cast in Cyrene and Cygnet/Cyrene have morphologies that appear closely related to one another, each displaying a dense, spongy structure interrupted by finger-like macrovoids (Fig. 4.6). In Cyrene, macrovoids of roughly 100 μm diameter are formed; they tend to be separated by 50-100 μm of denser material and are mostly upright (Fig. 4.6a). They do not extend through the membrane, instead leaving the bottom half fairly homogeneous. With the addition of Cygnet, the macrovoids

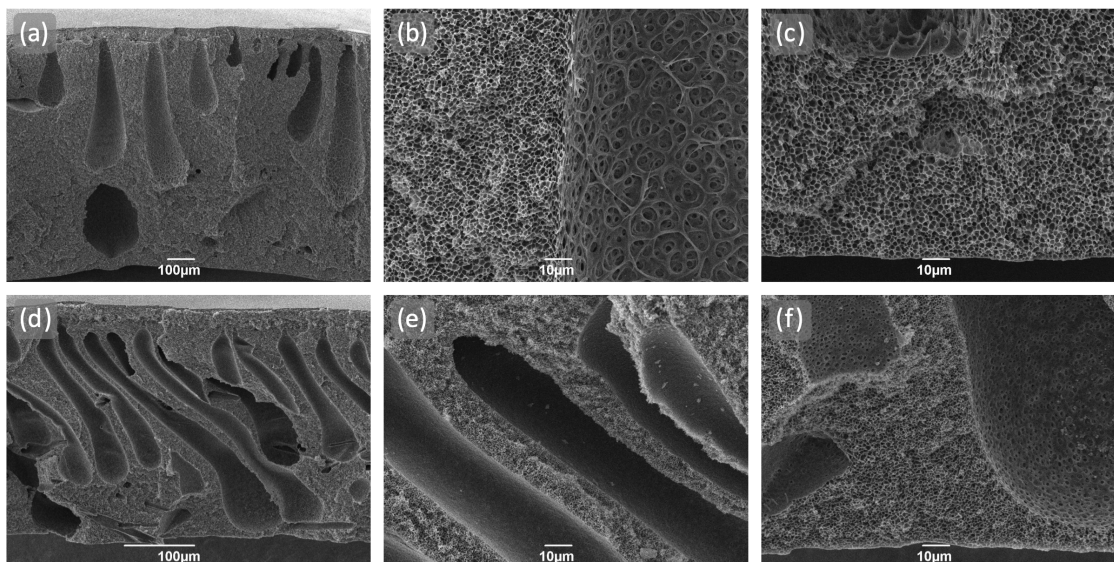


Figure 4.6: SEM images of 20% w/v PSU membranes cast from Cyrene (a-c) and 50% w/w Cygnet in Cyrene (d-f).

become more numerous and thinner, being only 20-50 μm in diameter and separated by only 10-20 μm (Fig. 4.6d). Additionally, these macrovoids penetrate to the bottom of the membrane and are noticeably tilted in one direction, probably due to the influence of the casting knife.²³⁷ It is worth noting that the dense, spongy portions of the PSU membrane have smaller pores in the Cygnet/Cyrene system, potentially changing the filtration capabilities of this membrane, as was also seen with PI. The increased number and surface area of the macrovoids again implies a potential for improved water flux through the membrane.²³⁷

In combination, these features suggest that the Cyrene polymer solution is more resistant to water influx, solidifying quickly upon formation of macrovoids and preventing them from penetrating to the bottom of the membrane. This appears to be the opposite of the behaviour seen in the PI membranes, which is not unexpected, as differences between polymers can strongly affect the performance of solvent systems.⁸⁷ In this case, it is possible that PSU in Cyrene forms a more viscous system that gels readily upon immersion in the water bath, nucleating precipitation in the bulk of the membrane and allowing only limited macrovoid formation. Addition of Cygnet could slightly improve polymer dissolution, forming a less viscous system that is easily penetrated by water.

With polyethersulfone (PES), on the other hand, the differences between solvent systems are not very pronounced (Fig. 4.7). Both Cyrene and Cygnet/Cyrene solvents form membranes that have large, irregular macrovoids toward the bottom, with similar,

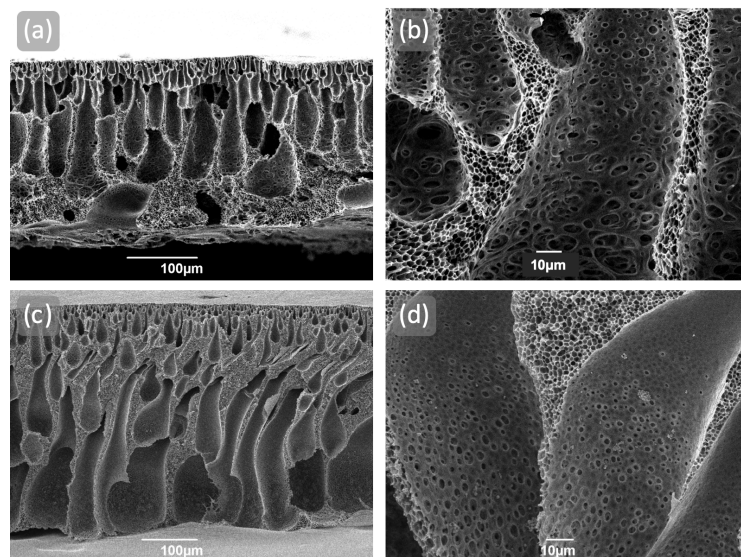


Figure 4.7: SEM images of 20% w/v PES membranes cast from Cyrene (a-b) and 50% w/w Cygnet in Cyrene (c-d).

but smaller, voids forming toward the top of the membrane. The primary difference in macrostructures is that the addition of Cygnet seems to reduce density of the bottom layer, with the macrovoids extending all the way down, rather than stopping about 50 μm from the bottom (Fig. 4.7c). The practical effect of the thinner bottom layer in Cygnet/Cyrene membranes is likely to be increased water flux, as the thin skin will provide less resistance.²³⁷ PES membranes formed in Cyrene appear to have a lacy microstructure with pores from 3-10 μm in diameter (Fig. 4.7b). When Cygnet is added, the overall microstructure appears similar, but with smaller pores roughly 1-5 μm in diameter (Fig. 4.7d). This effect is consistent in all three polymers, and will likely change the selectivity of the membrane for certain contaminants.

The difference in macrostructures could again be the result of slightly better polymer solubility in the case of the Cygnet/Cyrene blend. In pure Cyrene, the bottom layer begins to gel before water can penetrate completely into the membrane. In Cygnet/Cyrene, liquid-liquid separation occurs quickly throughout the membrane, creating areas of lower polymer concentration and forming large numbers of macrovoids.

4.5 Summary and Future Work

The work in this chapter has shown that a novel blend of Cyrene and its derivatives can behave in unexpected ways. The ketal derivatives of Cyrene, which were previously reported as more stable solvent options, present challenges due to their solidity at room

temperature. While these may be viable as solvents in specific applications, many industrial solvent uses require ambient temperature liquids. Mixing the simplest of these derivatives, Cygnet 0.0, with Cyrene was expected to create a liquid solvent with properties closer to those of DCM. While HSP predict a significant change in dipolarity from the addition of 50% w/w of Cygnet to Cyrene, experimental work with KAT parameters indicated only a small change in dipolarity. Hydrogen bond donating ability, the other KAT parameter of interest, showed a greater change, though still only 20% of the difference between Cyrene and DCM. These differences could reflect non-linear polarity of the bulk mixture, or preferential solvation of the dye by one component of the mixture.

To assess whether the addition of 50% Cygnet to Cyrene made a practical difference in solvent behaviour with polymers, water filtration membranes were cast with PI, PSU, and PES using the traditional NIPS process. Each polymer performed differently, with PI showing pronounced morphological differences on the macro scale, PSU showing moderate differences, and PES showing only slight differences. Fully explaining these variations would require in-depth assessment of each solvent system and polymer, taking into account phase diagrams, individual interactions between solvent, polymer, and antisolvent, and collecting data on viscosity and other properties of the polymer solutions. Qualitatively speaking, it appears that the addition of Cygnet impacts the viscosity of the polymer solutions, potentially causing their structural differences. On a smaller scale, the addition of Cygnet appears to shrink the micropores of each membrane, potentially allowing these membranes to be tailored for different contaminants. Depending on the application and the value added from these structural changes, blending Cygnet with Cyrene could be industrially useful.

To follow up on the membrane work from a practical standpoint, it is important to cast membranes using lower concentrations of Cygnet in Cyrene and observe the effect on morphology and pore size. This could determine whether this system is useful for applications where easy tuning of pore size is desired. It would be interesting to also compare the blended system with pure Cygnet, observing whether membranes cast in Cygnet/Cyrene blends appear similar to those cast in pure Cygnet, or if the blended system creates unique properties. To test this, membranes would have to be cast at 80-90°C in all solvent systems, as casting temperature can strongly impact membrane morphology.⁸⁷ Additional membranes could be cast at different thicknesses, polymer

concentrations, and casting temperatures to test how the blended solvent behaves in a range of conditions. Finally, all prepared membranes should be tested in actual water filtration trials, measuring the impact of morphology and pore size on water flux and filtration capabilities. This would give a clearer idea of whether there is value added by the use of Cygnet/Cyrene blends rather than Cyrene alone. Compared to DCM, both Cyrene and the Cygnet blend offer much slower solvent evaporation, allowing more reproducible membrane casting with less worker exposure to hazardous solvents.

The theoretical basis of differences between these solvent systems could be investigated via construction of a ternary phase diagram, allowing deeper examination of the thermodynamics of the membrane precipitation process.⁸⁷ At a more detailed level, the activity coefficients of each solvent-nonsolvent system could be calculated. Viscosity measurements of both the solvent systems and the polymer solutions would allow more informed discussion of the kinetics of precipitation.

In a broader sense, there is a great deal of related work that could be performed in the area of Cygnets and other Cyrene derivatives. While only one class of Cyrene derivative (and indeed, only one compound of that class) was considered here, there are numerous other derivatives, such as the other Cygnets as well as lactones, enones, and alcohols, that could have potential as blended solvents with novel properties.⁹⁸ Each class of derivatives could be considered as blends with Cyrene as well as other green solvents. The different Cygnets need further characterisation, particularly with respect to their physical properties, e.g. viscosity, density, melting and boiling points. Performing these characterising measurements could better inform choices about potential applications for these solvents. Prior to exploring more polymer-related applications, an economic assessment should be done to estimate the cost of manufacturing Cygnet 0.0. This would determine whether it is a practical option to use at high volumes, or whether its use in blends should be limited to low concentrations in order to make it economical.

CHAPTER 5
APPLICATIONS OF OXYMETHYLENE DIMETHYL ETHERS AS NOVEL
SOLVENTS

5.1 Background

While there is an urgent need for green dipolar aprotic solvents such as Cyrene, other classes of solvents are also lacking in suitable replacements. Ether solvents, for example, are almost universally ranked as somewhere between problematic and highly hazardous by the CHEM21 solvent selection guide, indicating a lack of safe options.⁴¹ As a class, they tend towards low flash point, high volatility, peroxide formation, water solubility, and environmental persistence, making them difficult to use and dispose of safely. A green ether solvent would ideally have:

- high flash point or low volatility,
- low water solubility,
- no peroxide formation,
- good toxicological properties,
- low environmental persistence, and
- a practical synthetic route from renewable feedstocks.

Figure 5.1 shows several conventional (top row) and neoteric (bottom row) ether solvents, with basic physical properties summarised in Table 5.1. Of these, only anisole (e) and *tert*-amyl methyl ether (TAME, f) qualify as “recommended” under CHEM21.

The conventional ether solvents range from problematic (b,d) to hazardous (c) and highly hazardous (a). Novel candidates g-i, while generally having fewer hazards, are ranked as problematic due to low auto-ignition temperature and/or peroxide formation ability.^{41,262} When considering feedstock, 2-methyltetrahydrofuran (MeTHF, i) is the only renewably-sourced candidate, though still problematic due to its oral toxicity and flammability. In short, there are no truly green ether solvents available. New candidates must be explored in order to add more safe or bio-derived options to the palette.

Oxymethylene dimethyl ethers, or OMEs, are a class of linear ethers with the molecular formula $\text{H}_3\text{CO}-(\text{CH}_2\text{O})_n-\text{CH}_3$ (commonly abbreviated OME_n to indicate chain length). A range of OMEs (typically $1 < n \leq 6$) have been studied in depth for their use as

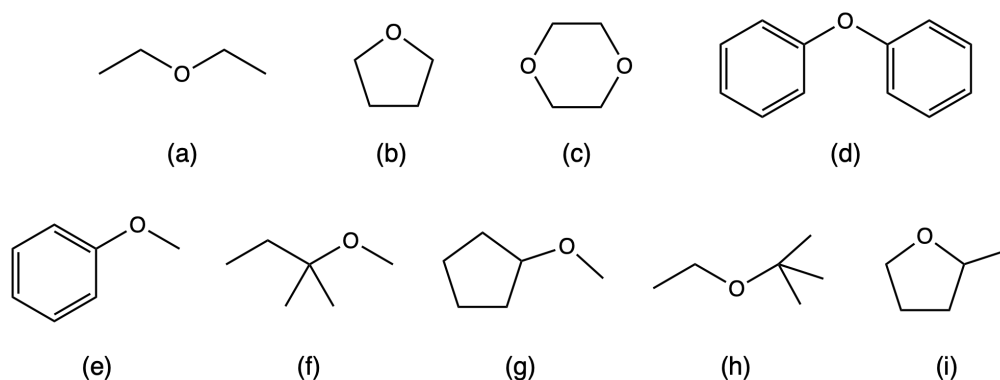


Figure 5.1: Structures of traditional and neoteric ether solvents. (a) Diethyl ether, (b) tetrahydrofuran (THF), (c) 1,4-dioxane, (d) diphenyl ether, (e) anisole, (f) *tert*-amyl methyl ether (TAME), (g) cyclopentyl methyl ether (CPME), (h) ethyl *tert*-butyl ether (ETBE), and (i) 2-methyltetrahydrofuran (MeTHF).

Table 5.1: Physical properties of ether solvents

	MP (°C)	BP (°C)	FP (°C)	ρ (g/cm ³ , 15°C)	η (cP, 25°C)	γ (mN/m, 20°C)
Diethyl ether	-116 ²⁴¹	35 ²⁴¹	-40 ²⁴¹	0.71 ²⁴¹	0.24 ²⁴²	18 ²⁴³
THF	-108 ²⁴⁴	65 ²⁴⁴	-17 ²⁴⁴	0.89 ²⁴⁴	0.45 ²⁴⁵	26 ²⁴⁵
1,4-dioxane	10 ²⁴⁶	100 ²⁴⁶	12 ²⁴⁶	1.03 ²⁴⁶	1.10 ²⁴⁷	37 ²⁴⁶
Diphenyl ether	25 ²⁴⁸	259 ²⁴⁸	115 ²⁴⁸	1.07 ²⁴⁸	3.49 ²⁴⁹	-
Anisole	-37 ²⁵⁰	155 ²⁵⁰	52 ²⁵⁰	1.00 ²⁵⁰	1.08 ²⁵¹	35 ²⁵²
TAME	-20 ²⁵³	85 ²⁵⁴	-7 ²⁵⁴	0.77 ²⁵⁴	0.42 ²⁵⁵	20 ²⁵⁵
CPME	-140 ²⁵⁶	106 ²⁵⁶	-1 ²⁵⁶	0.86 ²⁵⁶	0.55 ²⁵⁷	25 ²⁵⁷
ETBE	-97 ²⁵⁸	72 ²⁵⁸	-19 ²⁵⁸	0.74 ²⁵⁸	0.50 ²⁵⁹	72 ²⁵⁸
MeTHF	-20 ²⁶⁰	78 ²⁶⁰	-10 ²⁶⁰	0.85 ²⁶⁰	0.60 ²⁵⁷	25 ²⁶¹

ρ = density, η = dynamic viscosity, γ = surface tension

diesel fuel additives.^{263–266} Their applications outside the fuel sector have not previously been explored in any depth, with the exception of a few reports that are very limited in scope.^{267,268} However, OME₁, also known as dimethoxymethane or methylal, is a common industrial solvent, with applications in coatings, paint strippers, adhesives, degreasers, and more.²⁶⁹ As longer-chain OMEs are likely to share some solubility properties with OME₁, it is logical that they might also be applicable as solvents. Their wide liquid range and low viscosity (Table 5.2) confirms their practicality for solvent applications.

Compared to the ether solvents in Table 5.1, the physical properties of OMEs fall within the acceptable range, though their viscosities are higher than most. It is worth

noting that the high boiling and flash points of OMEs predict a relatively high auto-ignition temperature, bringing them in line with less hazardous ethers such as anisole and diphenyl ether. Indeed, auto-ignition points for these OMEs are reported to be between 230-240°C.²⁷⁰ The peroxide formation potential of these compounds has not been reported, nor is there any data yet available on their toxicological properties. These characteristics must be investigated to ascertain the overall safety of these solvent candidates. Current data is insufficient to assign a ranking for OMEs with the CHEM21 system.

Table 5.2: Physical properties of OMEs

	MP (°C)	BP (°C)	FP (°C)	ρ (g/cm ³ , 15°C)	η (cP, 25°C)	γ (mN/m, 20°C)
OME ₃	-43 ²⁷¹	156 ²⁷¹	20 ²⁷²	1.04 ²⁷¹	1.13 ²⁷²	29 ²⁷¹
OME ₄	-10 ²⁷¹	202 ²⁷¹	77 ²⁷²	1.08 ²⁷¹	1.88 ²⁷²	31 ²⁷¹
OME ₅	18 ²⁷¹	242 ²⁷¹	103 ²⁷²	1.11 ²⁷¹	2.93 ²⁷²	33 ²⁷¹
OME ₃₋₅	-19 ²⁷³	157-259 ²⁶⁴	70 ²⁷⁰	1.07 ²⁶⁴	-	31 ²⁷⁰

ρ = density, η = dynamic viscosity, γ = surface tension

From a feedstock perspective, OMEs can be synthesised from methanol, opening pathways for production via biomass-derived syngas or captured CO₂ and renewable H₂. Figure 5.2 shows a general overview of OME synthesis, a process which produces a mixture of oligomers. The method of synthesis strongly influences the distribution of chain lengths in this mixture; consequently, there are a wide variety of well-explored methods for this synthesis. Options include traditional aqueous acid catalysis,²⁷⁴ anhydrous heterogeneous catalysis,²⁷⁵ a low-energy anhydrous route,²⁷⁶ electrolysis,²⁷⁷ ionic liquid catalysis,²⁷⁸ and direct gas-phase oxidation of methanol,²⁷⁹ among others.

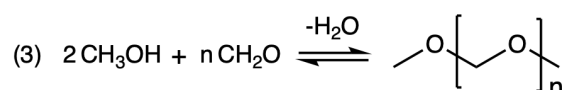
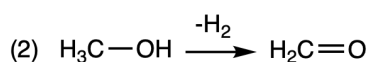
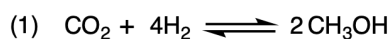


Figure 5.2: A general scheme for synthesis of OMEs ($n > 1$) from CO₂ and H₂.

Choosing the appropriate synthetic route and conditions allows tuning of the ratio of product chain lengths, tailoring the oligomer mixture to a desired application. The chain

length distribution can then be narrowed via molecular size reforming, recycling the side products and isolating the desired OMEs via distillation.²⁸⁰ However, this process is energy-intensive and costly, particularly for the traditional aqueous synthetic route. For solvent applications, costs must be kept low enough to compete with traditional solvents. For example, modelling by White *et al.* indicates that the synthesis of a mixture of OME₃₋₅ from a gaseous formaldehyde/methanol stream would cost \$951 per ton, when produced at a scale of 35 kt/year.²⁸¹ By comparison, a 2006 report on the chemical market estimated the cost of acetone at roughly \$900-1300 per tonne, and toluene at \$560-600 per ton, which makes OME₃₋₅ competitive with low-cost solvents even when produced at a fairly small scale.²⁸²

To investigate solvent applications of OMEs, the cost-competitive OME₃₋₅ mixture was selected as a model. Its solubility parameters were predicted with HSPiP and measured with solvatochromic dyes, giving an idea of likely solvent applications.

5.2 Predicting Solubility Behaviour

GC-MS analysis of a commercially-available OME₃₋₅ mixture indicated that the bulk of the mixture was composed of OME₃ (43%), OME₄ (24%), OME₅ (10%), and a branched derivative of OME₁ (10%) by mass (Figure 5.3, Table A.2). The rest of the mixture is made up of smaller fractions (< 5% each) of longer-chain OMEs and their derivatives (D-OME_n). This composition was used as a basis for predicting Hansen Solubility Parameters (HSP) of the mixture to quantify its likely solubility behaviour.

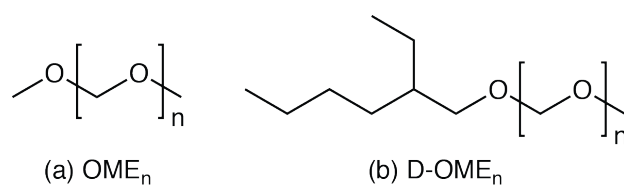


Figure 5.3: The investigated mixture is composed predominantly of OME₃₋₅ (a, 77%), OME_{n>5} (a, 5%), and derivatives (b) of varying chain lengths (15%).

For each component of the mixture over 1% by mass, HSP were predicted from simplified molecular-input line-entry system (SMILES) codes using the native HSPiP predictive algorithm (Y-MB). These values were then linearly combined using the proportions determined by GC-MS. Comparing the resulting values with those of other ether solvents indicates which traditional solvents OME₃₋₅ could potentially replace (Table 5.3). TAME and ETBE are excluded here due to lack of data. The D-OME value denotes how

far each solvent is from OME₃₋₅ in the three-dimensional Hansen space; lower values indicate similar solvents. The δ_D (dispersion parameter) is reasonably similar to those of the non-aromatic ether solvents, reflecting the presence of 5 – 7 linear carbons per molecule in the bulk of the mixture. The high δ_P (polarity parameter) of OME₃₋₅ suggests it could be considerably more polar than other ether-type solvents, which is likely due to the high oxygen content of the longer-chain OMEs. Finally, the δ_H (hydrogen bonding parameter) for OME₃₋₅ is fairly typical for an ether solvent.

Table 5.3: Solubility parameters for OME mixture and other ethers

	δ_D	δ_P	δ_H	D-OME	α^a	β	π^*	Δ -OME
OME ₃₋₅	15.6	7.1	6.1	0.0	0.00	0.36 ^b	0.55 ^b	0.00
1,4-dioxane	17.5	1.8	9.0	7.1	0.00	0.37 ^c	0.55 ^c	0.01
CPME	16.7	4.3	4.3	4.0	0.00	0.53 ^e	0.42 ^e	0.21
THF	16.8	5.7	8.0	3.3	0.00	0.58 ^d	0.59 ^d	0.22
2-MeTHF	16.9	5.0	4.3	3.8	0.00	0.58 ^e	0.53 ^e	0.22
Anisole	17.8	4.4	6.9	5.2	0.00	0.22 ^c	0.73 ^c	0.23
Diphenyl ether	19.4	3.4	4.0	8.7	0.00	0.13 ^c	0.66 ^c	0.25
Diethyl ether	14.5	2.9	4.6	5.0	0.00	0.47 ^c	0.27 ^c	0.44

D-OME = distance from OME₃₋₅ in the Hansen space, Δ -OME = distance from OME₃₋₅ in the KAT space. HSP values were drawn from HSPiP database or predicted by HSPiP with units of MPa^{1/2}. ^aAssumed to be zero for aprotic solvents. ^bThis work. ^cKamlet *et al.*⁵³ ^dByrne *et al.*²⁸³ ^eJessop *et al.*⁵⁴

Another useful predictor of solubility behavior is Kamlet-Abboud-Taft (KAT) parameters, which are measured by using three solvatochromic dyes that probe a solvent's intermolecular interactions (Figure 1.5).⁵³ By observing these dyes via UV-Vis spectroscopy, the hydrogen bond acidity (α), hydrogen bond basicity (β), and dipolarity/polarisability (π^*) can be calculated. As they measure slightly different characteristics, these parameters cannot directly be compared with HSP, but comparing KAT parameters across solvents can be useful.

KAT parameters for the OME₃₋₅ mixture were measured and compared with known values for conventional ether solvents and greener options such as 2-MeTHF and cyclopentyl methyl ether (CPME) (Table 5.3). Values for Δ -OME indicate how far each solvent is from OME₃₋₅ in the three-dimensional KAT space, giving an experimental predictor of how similar the two solvents are, with lower values suggesting increased similarity. Generally speaking, the KAT parameters of OME₃₋₅ are well within the expected range for ether solvents, with neither β nor π^* standing out. This confirms that this

mixture will likely act as a suitable substitute for conventional ether solvents. Notably, the OME KAT parameters are nearly identical to those of 1,4-dioxane, suggesting that these two solvents will behave very similarly in most solvation phenomena.

When working with ether solvents, their ability to coordinate to salts and organometallic compounds can sometimes be of particular importance. Application-specific measurements of Lewis basicity may therefore be more relevant than β in certain cases, e.g. Grignard reactions. While beyond the scope of this work, measurement of values such as the donor number (SbCl_5 affinity) or BF_3 affinity may be useful in determining other potential applications of OMEs.^{284,285}

OME₃₋₅ was tested here as a replacement for tetrahydrofuran (THF), which is one of the most commonly used ethers, and 1,4-dioxane, which is closest in the KAT space. The applications tested ranged from organic reactions to polymer dissolution.

5.3 Use as Organic Reaction Medium

Solvents are a major source of concern in the pharmaceutical and fine chemicals industry, where solvent use accounts for 80-90% of mass in a typical batch reaction.²⁸⁶ The pharmaceutical industry is actively seeking new green solvents, as demonstrated by the proliferation of solvent replacement research published by this industry in the last several years.^{39,144,152,287-289} A few reactions where OME₃₋₅ could replace conventional solvents were therefore investigated to establish its utility as an organic reaction medium.

5.3.1 Suzuki-Miyaura Coupling

As proof of OME applicability in pharmaceutical synthesis, the Suzuki-Miyaura coupling was selected. This palladium-catalysed reaction is a workhorse of the pharmaceutical industry, where it is firmly established as one of the most popular C–C bond-forming methods.¹⁰⁷ It is commonly performed in solvents such as 1,4-dioxane and THF, making it a likely match for the solubility parameters of OME₃₋₅. Two representative Suzuki-Miyaura couplings were carried out to test the solvent performance of OME₃₋₅ in this key pharmaceutical reaction (Fig. 5.4).

The results in OME₃₋₅ were compared against 1,4-dioxane, which is closest to OME₃₋₅ in the KAT space, and CPME, which was selected as a readily-available example of a safer neoteric ether. The reaction in Fig. 5.4a was chosen as an example of a very basic Suzuki reaction, in which cross-coupling and homocoupling are indistinguishable, as both form

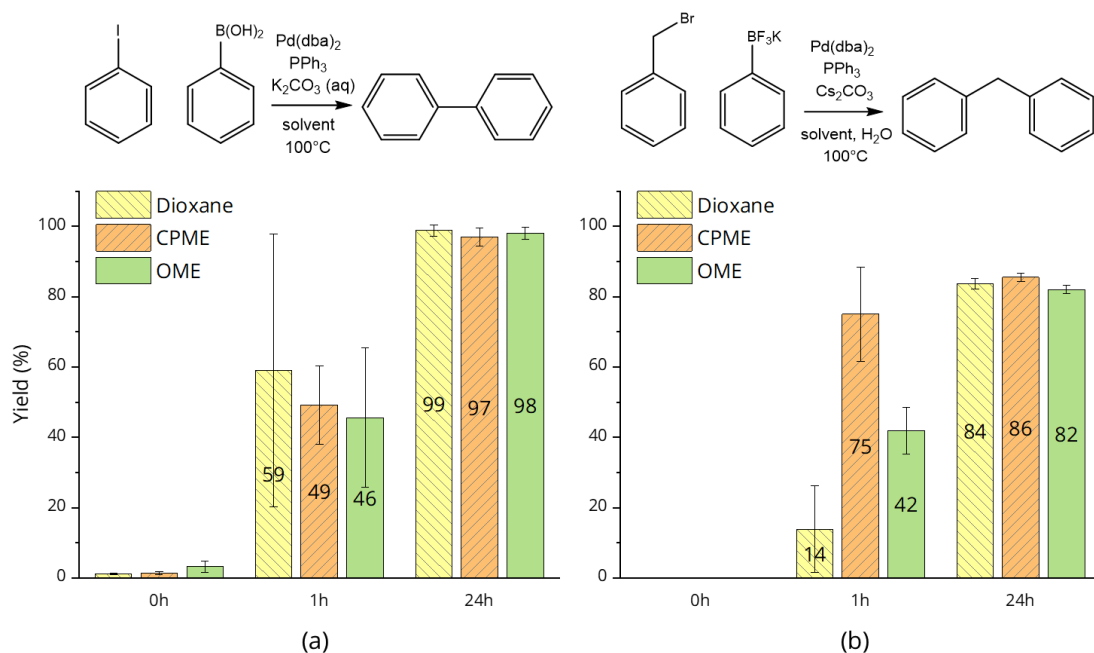


Figure 5.4: Reaction yields of Suzuki-Miyaura coupling reactions to produce a) biphenyl and b) diphenylmethane in 1,4-dioxane, CPME, and OME₃₋₅ solvents. Yields were calculated by GC-FID following calibration for each product. Results are presented as the average of three independent trials \pm standard deviation.

biphenyl products. By comparison, the reaction in Fig. 5.4b produces diphenylmethane as the cross-coupling product and biphenyl as the homocoupling product. The competing reactions can result in lower yield, and outcomes can vary significantly depending on the properties of the ether solvent. In particular, CPME is known to outperform traditional ether solvents in this coupling, giving the fastest reaction and the least homocoupling.²⁹⁰

In biphenyl coupling reaction 5.4a, all three solvents equally promoted formation of the biphenyl product. The speed of reaction was similar in all solvents, but reactions in dioxane seemed to proceed more erratically in the first hour, while CPME and OME₃₋₅ yielded more consistent reaction rates across three repetitions. After 24 hours, the yields were practically indistinguishable.

For the diphenylmethane coupling 5.4b, reactions in dioxane proved considerably slower than in the other two solvents. After 24 hours, all three solvents performed similarly, with CPME having a slight advantage. There are slight differences in formation of the homocoupling products: while dioxane formed more biphenyl than the other two solvents, OME₃₋₅ formed the most dibenzyl (Fig. 5.5).

While there is currently insufficient toxicity data to conclude whether OME₃₋₅ is overall a greener option than 1,4-dioxane, the OME mixture does present an improvement

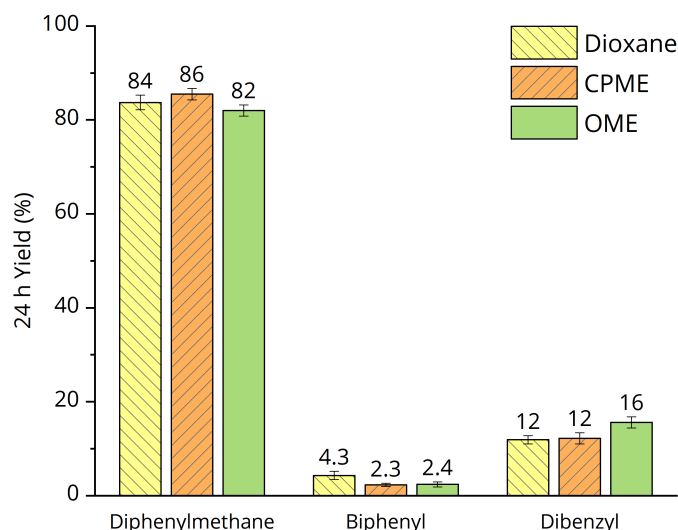


Figure 5.5: Suzuki-Miyaura reaction yields of diphenylmethane cross-coupling product as well as biphenyl and dibenzyl homocoupling products for reaction 5.4b. Yields were calculated by GC-FID. Results are presented as the average of three independent trials \pm standard deviation.

in some categories where data is available. While dioxane is classified as a highly flammable liquid and vapour under GHS criteria due to its low flash point of 12°C, the 70°C flash point of the OME mixture should put it in the less hazardous combustible liquid category.²⁴⁶ Additionally, the higher boiling point of OME₃₋₅ should reduce its concentration in the air, minimising worker exposure to a potentially hazardous vapour. As for renewable origin, 1,4-dioxane could hypothetically be derived from cellulose in a bio-refinery, though it is currently derived from petroleum.²⁹¹ In short, it appears that OME₃₋₅ could be considerably greener than dioxane (if it is shown to be non-toxic and non-mutagenic), slightly greener (if it is found to be mutagenic), or less green (if it is found to be toxic). More data is needed for a full assessment.

5.3.2 Enzymatic Polymerisation

Research in this section was carried out in collaboration with Alessandro Pellis.

Greener solvents are also in demand for biocatalytic (enzymatic) reactions, which are growing in popularity for industrial processes. Enzymatic catalysts offer many advantages over their conventional chemical counterparts, including mild reaction conditions, reduced toxicity, and high selectivity for the preferred product.²⁹² However, green solvents are still a new area with respect to enzymatic reactions. Recent studies have compared the performance of greener solvents such as tetramethyloxolane (TMO) and

2-MeTHF against more traditional choices such as toluene and THF in simple esterification reactions between 1-hexanol and dodecanoic acid,²⁹³ as well as between the bulkier 2-phenylpropionic acid and ethanol.²⁹⁴

For enzymatic polycondensations with the industrially popular enzyme *Candida antarctica* lipase B (CaLB), the preferred solvent is diphenyl ether (DPE), due to its hydrophobicity, low volatility, ability to dissolve a variety of substrates, and ability to promote formation of long-chain polyesters.^{295,296} Replacing DPE in this application is a challenging endeavor, as catalytic activity can depend on solvent hydrophobicity, boiling point, geometry, polarity, and substrate solubility, as well as other solvent properties.²⁹² As OME₃₋₅ is close to DPE in the KAT space (particularly in the important polarity parameter, π^*) and has a similarly high boiling point, it was tested as a bio-based solvent in an enzymatic polymerisation reaction. CaLB was chosen as the enzyme due to its versatility and popularity in industry.

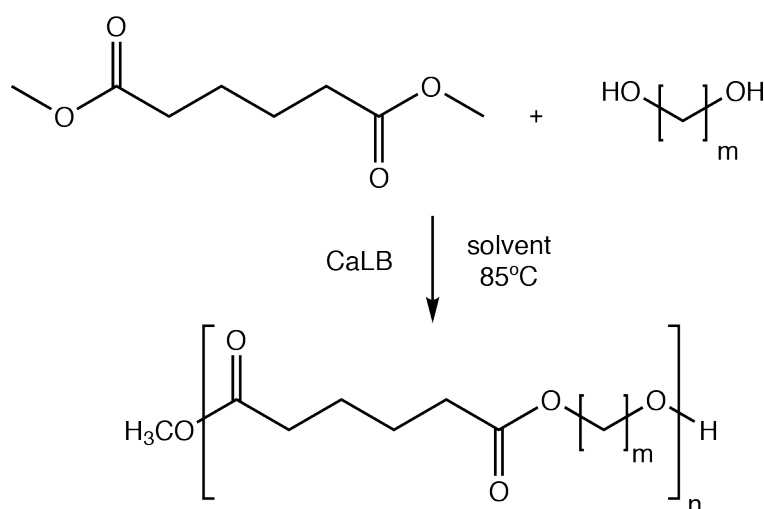


Figure 5.6: Enzymatic polycondensation reaction was performed using dimethyl adipate and diols with chain length $m = 4, 6,$ and 8 . Immobilised *Candida antarctica* lipase B (Novozyme 435) was used as the enzyme catalyst.

A polycondensation/transesterification reaction was performed, combining bio-based ester dimethyl adipate with an aliphatic diol (Figure 5.6). Three different diols were chosen, with carbon chain lengths of 4, 6, and 8 atoms, in order to investigate the impact of diol chain length on enzymatic performance. Control reactions were performed in DPE to observe performance differences between the traditional solvent and OME₃₋₅, and a previous study of the same reaction in solventless conditions was referenced as a third point of comparison.^{297,298} Results indicate the purified products of each reaction

were largely similar by $^1\text{H-NMR}$ spectra (Fig. A.11). All monomer conversions reached $>95\%$ (Fig. 5.7a). The solventless reactions gave similarly high conversions.

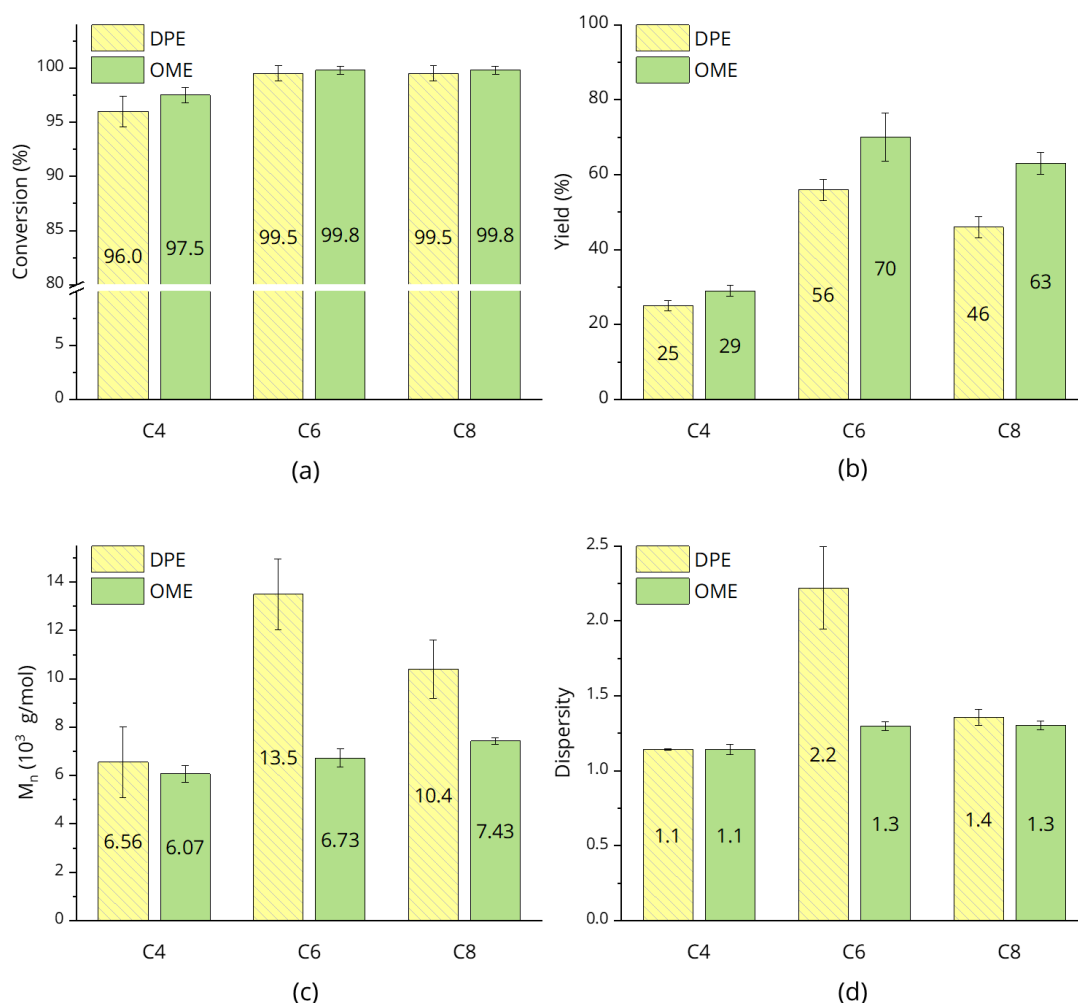


Figure 5.7: Results of enzymatic polycondensation reactions with C4, C6, and C8 diols in traditional solvent DPE and OME_{3-5} . (a) Monomer conversion, (b) Isolated yield, (c) Number-average molecular weight, and (d) Dispersity. In each case, results are presented as the average of two independent trials \pm standard deviation.

Solvent-related differences begin to appear when examining the isolated yield of each reaction (Fig. 5.7b). In a solventless reaction, a simple one-step work-up with THF is used to recover the polymer, and the yields are not calculated,^{299,300} but organic reaction media necessitates a multi-step recovery procedure, resulting in product loss. Figure 5.7b compares isolated yields for reactions with the various diols in DPE as well as OME_{3-5} . The monomer with the shortest chain length—C4, or 1,4-butanediol—gave the lowest yield. This is possibly due to the formation of shorter-chain polymer products, some of which are partially methanol-soluble and could have been removed during work-up. Alternatively, it could be that the enzyme is more reactive with the more hydrophobic C6

and C8 diols, though in that case, differences in monomer conversion would be expected. In reactions with longer-chain diols (C6 or 1,6-hexanediol, and C8 or 1,8-octanediol), the isolated yield was more than double that of the C4 reaction. Regardless, in all cases, the isolated yields from reactions performed in OME₃₋₅ were significantly higher than those performed in DPE.

In solventless polymerisation reactions, Pellis *et al.* reported number-average molecular weights (M_n) in the range of 6500-7500 g/mol, depending on the diol used.²⁹⁷ OME₃₋₅ reactions yielded comparable M_n , while DPE reactions resulted in significantly higher M_n for the C6 and C8 diols (Fig. 5.7c). This indicates that that DPE is promoting higher degrees of polymerisation, particularly for C6 diols, where DPE gives double the M_n of solventless or OME₃₋₅ reaction. However, the polymer products from OME₃₋₅ reactions have a much narrower dispersity (\mathcal{D} , variance in chain lengths) compared to either solventless or DPE reactions (Fig. 5.7d, Table 5.4).

Table 5.4: Enzymatic polycondensation in solventless conditions, DPE, and OME₃₋₅

Diol	M_0 (g/mol)		Solventless ^a	DPE	OME ₃₋₅
C4	200.13	M_n (g/mol) ^b	6630	6560	6070
		\mathcal{D} ^b	1.706	1.141	1.142
		DP ^c	33	30	30
C6	228.18	M_n (g/mol) ^b	6710	13500	6730
		\mathcal{D} ^b	2.045	2.220	1.297
		DP ^c	29	59	29
C8	256.23	M_n (g/mol) ^b	7140	10400	7430
		\mathcal{D} ^b	1.760	1.356	1.301
		DP ^c	28	41	29

^aPellis *et al.*²⁹⁷ ^bCalculated via GPC, calibrated with polystyrene standard and using toluene as a reference. ^cCalculated by dividing M_n by M_0 .

It is also worth noting that with the OME₃₋₅ mixture, a 5-10% w/w reduction in solvent was observed over the course of the reaction, while in DPE, <5% w/w solvent was lost. This difference is easily explained by removal of some of the more volatile OMEs, along with the methanol byproduct, when vacuum is applied.

The complexity of the biocatalytic system makes it very difficult to determine the cause of the significant differences between reactions performed in DPE and OME₃₋₅. Most likely, the differences are due to a combination of factors, including enzyme selectivity, solvent and reactant hydrophobicity, solvent geometry, and other solvent properties.

Detailed molecular modelling studies would be necessary to isolate the individual effects in such a dynamic system.

In short, enzymatic polymerisations in OME₃₋₅ are possible, and while the average molecular weights of the polymers produced here tend to be lower than in the traditional solvent DPE, the yields are considerably higher. Compared to solventless reactions in other studies, OME₃₋₅ gives similar molecular weight and degree of polymerisation, but also yields a marked reduction in dispersity, producing much more consistent polymers. Thus, this solvent could be very useful in synthesising polyesters with moderately high molecular weights and narrow dispersity.

5.3.3 Solvent Miscibility

The miscibility of OME₃₋₅ with a broad range of organic solvents was tested in order to assess the mixture's suitability for use in extractions and separations following organic reactions (Table A.3). The solvents were considered miscible if they could be mixed in equal proportions without any separation being observed. OME₃₋₅ is miscible with most organic solvents, the only exceptions being ethanolamine and ethylene glycol. It is, however, immiscible with water, opening potential application possibilities in aqueous extractions and separations.

5.4 Dissolution of Polymers and Coatings

Research in this section was carried out in collaboration with Roxana Milescu.

Polymer dissolution and processing with green solvents is also a growing field of interest, with the goal being to reduce the polymer industry's environmental impact and create healthier, less-damaging polymers.³⁰¹ A vast diversity of polymers are used in industry to achieve different effects, ranging from simple linear aliphatic backbones to complex arrangements involving branching, aromatic groups, and heteroatoms. To test applicability of OME₃₋₅ in polymer dissolution, a variety of polymers commonly used in industry were selected, based on their ready availability for purchase (Fig. 5.8). It should be noted that molecular weight of a polymer can impact its solubility; the samples used here were common industrial variants (see Experimental for more details).

Each polymer was combined with OME₃₋₅ at 5% w/v, then heated to 60°C and stirred overnight in order to overcome kinetic barriers. The results are pictured in Figure 5.9. OME₃₋₅ appears to have no effect on polypropylene (PP), polyethersulfone (PES), or

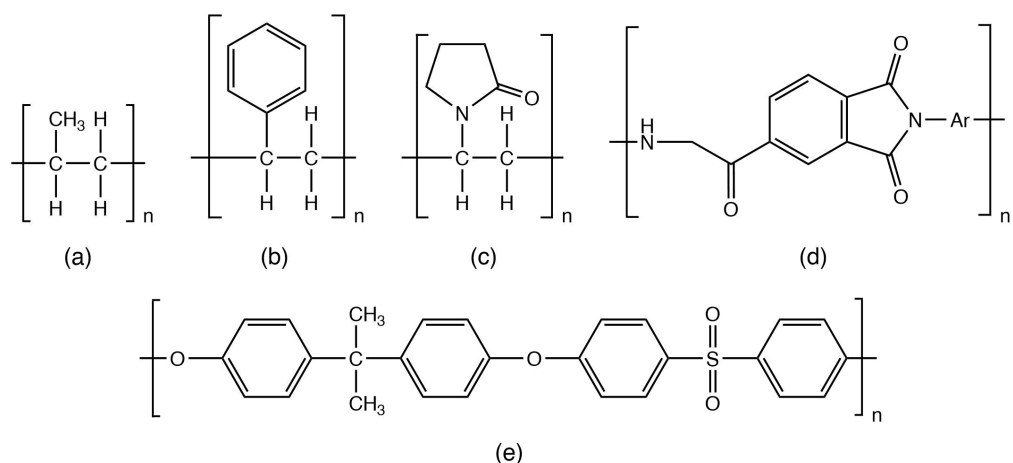


Figure 5.8: Structures of polymers tested with OME₃₋₅. (a) Polypropylene (PP), (b) polystyrene (PS), (c) polyvinylpyrrolidone (PVP), (d) polyamide-imide (PAI), and (e) polyethersulfone (PES).

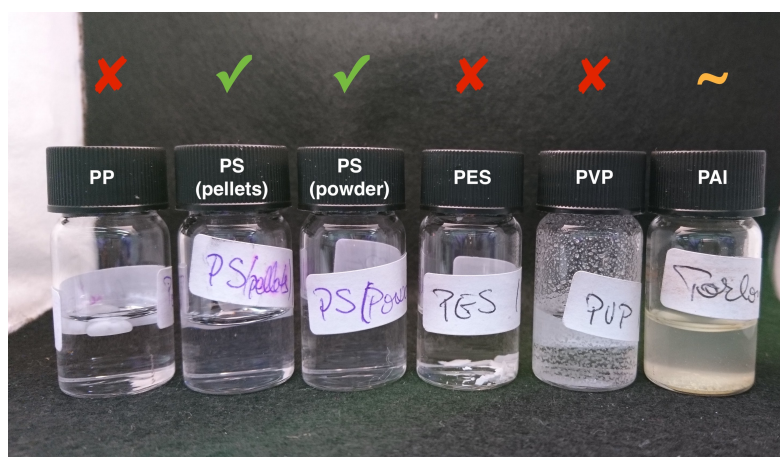


Figure 5.9: Performance of OME₃₋₅ in dissolving a variety of polymers. From left to right: polypropylene (PP), polystyrene (PS, pellets), polystyrene (PS, powder), polyethersulfone (PES), polyvinylpyrrolidone (PVP), and polyamide-imide (PAI).

polyvinylpyrrolidone (PVP). There is some slight interaction evident with polyamide-imide (PAI), but the only polymer that dissolved fully was polystyrene (PS).

While it may not seem intuitive that an aromatic non-polar polymer dissolves readily in an ether solvent, Hansen parameters can help explain this discrepancy. HSP values for the five polymers tested were drawn from the HSPiP polymer database, which is composed of empirical data from a range of sources (Table 5.5). As discussed in Chapter 1, the relative energy difference, or RED, is a ratio that provides a simple predictor of whether a polymer will dissolve in a given solvent. For RED < 1, the solvent is within the polymer's sphere of solubility, and will likely dissolve it. For RED > 1, the opposite is true, and RED values close to unity are borderline cases which are less predictive.

All of these predictions are thermodynamic, meaning that despite a positive prediction, unfavorable kinetics may prevent the observation of dissolution on a short timescale.

Table 5.5: Hansen Solubility Parameters of tested polymers

	δ_D	δ_P	δ_H	R_0	RED
OME ₃₋₅	15.6	7.1	6.1	-	-
PP	18.0	0.0	1.0	8.0	1.25
PS	18.0	5.0	5.0	10	0.54
PES	19.6	10.8	9.2	6.2	1.51
PVP	18.1	10.0	18.0	8.0	1.65
PAI	18.5	5.7	8.7	4.2	1.55

Values in units of MPa^{1/2}, drawn from HSPiP database.⁵⁰

In Table 5.5, only PS is predicted to be soluble in OME₃₋₅. This is consistent with the experimental results, giving an initial indication that the model is valid for this solvent. However, this cannot be firmly concluded using only these five data points. More tests should be performed, identifying polymers with both positive and negative predicted results, in order to confirm the validity of the OME₃₋₅ solubility model.

Looking more closely at the polymer HSP data, there are large variations in both δ_P and δ_H across polymers, while δ_D stays within a small range. The long chain length of polymers gives them uniformly high dispersion forces regardless of structure, though the numerous aromatic rings in the PES backbone (Fig. 5.8e) do appear to increase its δ_D slightly. The real differences arising from the polymer chemical structures are apparent in their polarities and hydrogen-bonding abilities.

The δ_P values depend on the polymer having localised regions of high electron density, which are present primarily in PVP and PES. PVP (Fig. 5.8c) contains a single pyrrolidone moiety in its repeating subunit, which withdraws electrons from the nearby methylene bridge. This creates a highly polar polymer backbone, with the pyrrolidone being more electronegative than its surroundings. Similarly, PES (Fig. 5.8e) has isolated ether oxygens and a sulfonyl moiety in its repeating subunit, creating localised regions of high electronegativity. The phenylene and dimethyl methylene structural units provide contrasting regions of low electronegativity, creating polarity in the backbone. PP, PS, and PAI, on the other hand, do not have clearly separated electronegative regions, resulting in their reduced δ_P values. The phenyl ring in PS (Fig. 5.8b) makes it slightly more polar than PP due to the higher electronegativity of sp² carbon atoms, which in turn gives it a

δ_P value similar to that of OME₃₋₅.

δ_H values are highest in PVP, PES, and PAI, making them less soluble in OME₃₋₅, which has a moderate δ_H value. All three of these have traditional acceptors of hydrogen bonds (O and N), which are lacking in PP (Fig. 5.8a) and PS (Fig. 5.8b). However, PS does contain an aromatic ring, allowing it to serve as a weak H-bond acceptor.³⁰² This brings its δ_H up to 5.0, quite close to OME₃₋₅.

The easy dissolution of PS in OME₃₋₅ suggests potential application as a safer, less volatile replacement for dichloromethane in plastic welding and polystyrene extraction applications. A higher-volume application could be polystyrene dissolution for recycling, as green solvent systems for this are not yet well developed.³⁰³

As the data here suggest that the HSP of OME₃₋₅ are reasonably good predictors of its ability to dissolve a polymer, further polymer targets could be chosen by using HSPiP. Polymers with mid-range δ_P and δ_H are good targets for dissolution in OME₃₋₅. A selection of common industrial polymers with these characteristics is shown in Table 5.6, presenting many possible directions for future work in this area.

Table 5.6: Polymers predicted to dissolve in OME₃₋₅

	δ_D	δ_P	δ_H	R_0	RED
OME ₃₋₅	15.6	7.1	6.1	-	-
Polysulfone	16.0	6.0	6.6	8.0	0.18
Natural rubber	14.5	7.3	4.5	11.0	0.25
Nitrile	16.6	9.1	4.4	10.0	0.33
Poly(butyl acrylate)	16.2	9.0	3.0	10.1	0.38
Viton	16.5	8.1	8.3	6.6	0.46
Polyvinyl chloride	17.6	7.8	3.4	8.2	0.59
Poly(methyl methacrylate)	18.1	10.5	5.1	9.5	0.65
Polycarbonate	19.1	10.9	5.1	12.1	0.66
Polyethylene terephthalate	18.2	6.4	6.6	8.0	0.66
Cellulose acetate	16.9	16.3	3.7	13.7	0.72
Epoxy	17.4	10.5	9.0	8.0	0.72
Lard (23°C)	17.7	2.7	4.4	8.0	0.79

Values in units of MPa^{1/2}, drawn from HSPiP database.⁵⁰

OME₃₋₅ was also tested for efficacy in removing polymer-based paints from porous ceramic material, simulating its behavior in graffiti removal. For acrylic paint, it performed quite well, showing performance similar to that of traditional paint remover *N*-methyl-2-pyrrolidinone (NMP) but leaving a small amount of colour behind (Fig.

5.10). For cellulose paint, OME₃₋₅ performed moderately well, removing the coating but leaving a fair amount of colour behind.

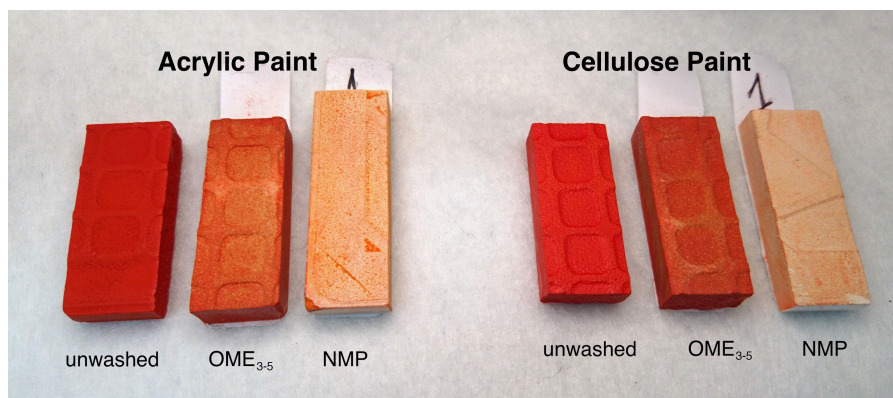


Figure 5.10: Performance of OME₃₋₅ in removing graffiti-like paint. OME₃₋₅-cleaned tiles are shown between uncleaned tiles and tiles cleaned with traditional solvent NMP.

The components of commercial paint are typically not disclosed, making it difficult to determine why one solvent is more effective than another. Generally speaking, cellulose paints contain a nitrocellulose polymer binder, while acrylic paints contain an acrylate-based polymer or copolymer.³⁰⁴ Some examples of these polymers were found in the HSP database and compared with OME₃₋₅ (Table 5.7). While nitrocellulose has a consistent structure and reliable set of HSP values, the term “acrylic” covers an entire class of polymers and therefore spans a wide range of values. It can be concluded that while the polymer component of cellulose-based paints will reliably dissolve in OME₃₋₅, acrylic paint binders may or may not, depending on what specific polymer is used. To investigate these paints further, FT-IR or Raman spectroscopy could help to identify the polymer binder(s) being used.

Table 5.7: Polymers used in paint formulations

	δ_D	δ_P	δ_H	R_0	RED
OME ₃₋₅	15.6	7.1	6.1	-	-
Nitrocellulose	15.4	14.7	8.8	11.5	0.71
Poly(methyl methacrylate)	18.1	10.5	5.1	9.5	0.65
Polyacrylonitrile	21.7	14.1	9.1	10.9	1.95
Poly(ethyl methacrylate)	17.6	9.7	4.0	10.6	0.65
Polymethacrylonitrile	17.2	14.4	7.6	3.8	2.13

Values in units of MPa^{1/2}, drawn from HSPiP database.⁵⁰

The performance of OME₃₋₅ in this test is not perfect, as colour obviously remains

behind in both cases, while NMP largely removes the colour, leaving a clean tile behind. This suggests that while the polymer component of the paints can be removed by either solvent, the solubility of the coloured component varies. The colour in paints is provided by a pigment that, again, is typically not disclosed by the manufacturer. While OME₃₋₅ appears to remove the polymer, potentially opening up the pigment for removal by a different solvent, such a two-step process would create difficulties in commercial application, as competing products can remove both polymer and pigment in one step. It is therefore worthwhile to investigate, in future work, the origin of the pigment solubility differences between NMP and OME₃₋₅.

The pigments present here could be either organic or inorganic, spanning options like metal oxides and azo compounds.³⁰⁴ These could be difficult to identify spectroscopically due to the diverse components of the paint and likely presence of multiple pigments that are chemically similar. GC-MS analysis could yield helpful results, but the most time-effective route for further investigation might be to find a paint manufacturer willing to partially disclose their ingredients. Additionally, comparing the efficacy of OME₃₋₅ in removing different colours of paint (or dissolving isolated pigments) would give a better overall idea of its performance in this area, as the chemical composition of the paint varies greatly with the colour.

5.5 Safety and Stability

In developing new green solvents, safety testing is critical. Green solvents must be innocuous, presenting minimal hazards to humans and the environment. OME₃₋₅ has been shown to have some characteristics that make it safer and greener than other ethers—namely, low volatility, high auto-ignition temperature, low water solubility, and a cost-efficient route from sustainable feedstocks. However, its toxicological properties, environmental persistence, and peroxide formation capability are currently unevaluated, leaving many data gaps. This data must be obtained if the mixture is to be registered under REACH, including information on:

- skin/eye irritation/corrosion
- skin sensitisation
- mutagenicity/cytogenicity/carcinogenicity
- toxicity, acute and chronic
- reprotoxicity and developmental toxicity

- aquatic toxicity and growth inhibition

Studies must also be conducted to assess the behaviour of the substance in soil and water, including identification of degradation products, adsorption/desorption behaviour, and long-term environmental effects.³⁰⁵

Currently, neither the individual components nor the mixture OME₃₋₅ are registered under REACH. No data is available to fulfill the safety testing requirements, with the exception of some information on mutagenicity/genotoxicity of a related mixture. A great deal of testing needs to be done before these solvents can be considered safe for humans or the environment.

5.5.1 Mutagenicity and Genotoxicity

A number of tests have been performed by ChemCom Industries for OME₂₋₈, which is closely related to OME₃₋₅ and is likely to have similar toxicological properties. The tests performed were OECD 471 (bacterial mutation), OECD 473 (mammalian mutation *in vitro*), and OECD 474 (mammalian mutation *in vivo*).³⁰⁶ The data is restricted by confidentiality agreements and cannot be provided in full, but the tests and their outcomes are summarised below.

OECD 471, more commonly known as the Ames test, is an early *in vitro* assessment of the mutagenic potential of a compound. Multiple bacterial strains are exposed to the test compound, then compared to a control sample to check whether their genetic ability to synthesize an essential amino acid has been affected. A positive result confirms that the test compound readily induces mutations in DNA, suggesting that it will likely be mutagenic to more complex organisms as well. A negative result suggests low mutagenic potential.³⁰⁷ However, as the Ames test is a relatively simple screening, a negative result does not guarantee that the test compound is not mutagenic, and should be followed by more detailed *in vitro* testing for chemicals to be manufactured at a scale greater than 10 tonnes.³⁰⁵ OME₃₋₅ gave a negative result on this test, suggesting that it does not have high mutagenic potential.

OECD 473 is a more detailed *in vitro* assessment of mutagenic potential towards mammalian cells. By exposing mammalian cell cultures to the test compound and then examining their chromosomes under a microscope, it is possible to detect chromosomal aberrations, which are linked with genetic disease and tumor formation in humans.³⁰⁸ In this test, OME₃₋₅ gave a negative result, giving further evidence that it is not likely to

be mutagenic. By REACH regulations, a negative result from OECD 473 coupled with an *in vitro* test of cytogenicity (which has not yet been performed for OME₃₋₅) provides sufficient evidence of mutagenic safety to manufacture a substance at volumes up to 100 tonnes, but higher volumes require more advanced reprotoxicity testing.

OECD 474, also known as the mammalian erythrocyte micronucleus test, tests genotoxicity *in vivo*. Animals, typically mice or rats, are exposed to the test substance via direct injection, after which their blood or bone marrow cells are analysed for the presence of micronuclei. Formation of micronuclei indicate chromosomal damage has occurred, indicating that the substance is genotoxic.³⁰⁹ Under REACH, this test can be used to supplement genotoxicity data for substances at volumes up to 100 tonnes. OME₃₋₅ gave a negative result on this test, supporting its lack of genotoxic effects.

Overall, these results indicate that the OME₂₋₈ mixture is neither genotoxic nor mutagenic, implying that OME₃₋₅ (a subset of OME₂₋₈) is similarly safe on these endpoints. The combination of tests is sufficient to establish that OME₂₋₈ is not genotoxic nor mutagenic under the EU classification, labelling, and packaging (CLP) criteria.³¹⁰ Further testing will be required going forward to establish the overall safety of OME mixtures under REACH, particularly with respect to toxicity, developmental toxicity, and aquatic toxicity. At this point, there is not enough data to call these solvents truly green.

5.5.2 Peroxide Formation Potential

One of the key safety issues relating to the use of ether solvents is their gradual autoxidation to unstable peroxides, creating an explosion hazard when the solvent evaporates or is otherwise concentrated.³¹¹ While the high boiling point of OME₃₋₅ reduces evaporation, making peroxide concentration less likely, it is still important to know how quickly peroxides form in the solvent. To this end, the peroxide formation potentials of the individual OMEs and the OME₃₋₅ mixture were assessed and compared with other ether solvents. THF was used as an example of a conventional ether, and CPME as a “safer” ether solvent which ostensibly forms no peroxides.²⁵⁷

In order to assess peroxide formation potential, the solvents were exposed to conditions that promote peroxide formation, comprising strong UV radiation and a bubbling stream of air.²⁸³ The peroxide concentration was measured at intervals and compared against control samples stored in the dark, and these measurements used to estimate rates of peroxide formation in each solvent (Table 5.8). The volume of solvent lost to

evaporation was <10% for each sample and did not significantly impact the peroxide concentration. Based on these results, it is clear that the OME₃₋₅ mixture forms peroxides far more slowly than THF; indeed, the rate of formation is similar to that of CPME. The bulk of peroxide formation in the OME mixture is likely due to the presence of short-chain OME_{≤3}, as the longer-chain OMEs form peroxides even more slowly.

Table 5.8: Peroxide formation test results (mg peroxide/L solvent)

Solvent	Sample	Peroxide Conc.			Rate (mg/L/h)	Vol. Lost (%)
		0 h	2 h	4 h		
THF	Control	10	10	10	0	-
	Test	10	30	30-100	14	10
CPME	Control	3	3	3	0	-
	Test	3	10	10	2	2
OME ₃₋₅	Control	10	10	10	0	-
	Test	10	10	10-30	3	2
OME ₃	Control	3	3	3	0	-
	Test	3	3-10	10	2	8
OME ₄	Control	1-3	1-3	1-3	0	-
	Test	1-3	3	3-10	1	0
OME ₅	Control	<1	<1	<1	0	-
	Test	<1	1-3	3	1	2

The slower rate of peroxide formation makes OME₃₋₅ somewhat safer than conventional ethers like THF, but as it is still capable of forming peroxides, this solvent will have to be stabilised for storage.

5.5.3 Acid Stability

The acid stability of the OMEs presented a concern, due to their highly oxygenated structures and previous reports of the decomposition of OME₅ in the presence of hydrochloric or phosphoric acid.³¹² To assess the acid stability of the OMEs, the OME₃₋₅ mixture was exposed to a selection of Brønsted and Lewis acids in low concentrations (1.0 mol%) and stirred at 50°C. In most cases, the mixture formed a cloudy mixture or solid mass either immediately or over the course of 72 hours stirring (Fig. 5.11). Hydrochloric acid caused no obvious reaction at this low concentration, but at a higher concentration of 20 mol%, it also effected solidification. OMEs are known to produce formaldehyde in the presence of acid, and under these conditions could be reacting further to produce

trioxane or polymerising to form paraformaldehyde.¹⁰⁵ These results suggest that the various OMEs are acid-labile and are not suitable solvent candidates for acid-catalysed reactions.

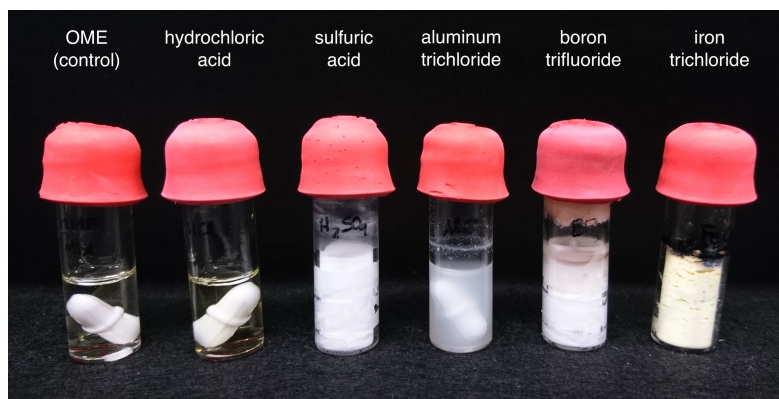


Figure 5.11: Samples of OME₃₋₅ mixture treated with 1.0 mol% of selected Brønsted and Lewis acids.

5.6 Summary and Future Work

In conclusion, a new field of application has been opened for OME₃₋₅ to serve as an alternative ether solvent, complementing its current application as a diesel fuel additive. The OME compounds can be sourced from sustainable feedstocks in a cost-effective way, but further safety testing is required to confirm whether they can be considered green. While their low flammability, volatility, and peroxide formation rate make these mixtures safer than many ethers, their toxicological properties and environmental persistence are largely unexplored. Initial tests indicate no mutagenicity or genotoxicity, but there is no toxicity data available.

While some applications of OME₃₋₅ may be limited by instability in the presence of acids, many solvent applications remain open, particularly in high-volume industrial sectors. The immiscibility of OME₃₋₅ with water could allow its use as a solvent for aqueous separations and purifications. As a demonstration of applicability in pharmaceutical and fine chemical synthesis, this solvent has been shown to satisfactorily promote the Suzuki-Miyaura reaction, performing comparably to 1,4-dioxane and CPME in two examples of this popular cross-coupling. OME₃₋₅ can also facilitate biocatalytic polymerisation using the CaLB enzyme, making it a potential replacement for diphenyl ether in reactions where hydrophobicity is important. Finally, this solvent has been shown to dissolve polystyrene as well as nitrocellulose and an acrylic resin, suggesting applications in

industrial polymer processing and paint removal. Further investigation is needed to confirm whether the HSP model of polymer solubility in OME₃₋₅ is valid, which would allow reliable prediction of polymer targets for dissolution. In paint removal, OME₃₋₅ is not fully effective in removing red paint pigment from porous surfaces, which could be studied in more detail by investigating its dissolution of different pigments.

This work has shown that OME₃₋₅ can be considered as a novel ether solvent for a range of products and processes. While extensive safety testing must be performed before it can be called green, OME₃₋₅ can expand the palette of renewably-sourced ether solvents, providing more options for chemists in a bio-economy.

CHAPTER 6

CONCLUSION

Though barriers to use of conventional solvents in polymer dissolution are rising, the adoption of alternatives by academia and industry has been slow. This can be attributed to a shortage of suitable solvent options as well as a lack of knowledge about their polymer dissolution applications. The work in this thesis was intended to open new avenues for green solvents in polymer dissolution, using computational and solvatochromic solubility parameters to quickly identify suitable applications.

Solvents used in this work were selected from a variety of academic and commercial lists of green solvents. The solvent studied most extensively was Cyrene, a green solvent discovered at the Green Chemistry Centre of Excellence in 2014. While it had previously been investigated as a traditional solvent—that is, as a reaction medium for organic synthesis—and in graphene dispersion, Cyrene had not been tested in any polymer-related use when this thesis was begun.^{100,110} A selection of other green dipolar aprotics (γ -valerolactone (GVL), dimethylsulfoxide (DMSO), cyclopentanone (CP)) were tested for comparison. A new type of bio-derived ether (poly(oxymethylene) dimethyl ether, or oxymethylene ether (OME)) was investigated for its solvent properties, adding another class of solvents to broaden the scope of the work.

The results of each project, as well as directions for future work, were discussed in detail in the relevant chapters. Brief summaries are given below, followed by an examination of the utility of solubility parameters in this type of research.

6.1 Summary of Research

6.1.1 Green Solvents for Dissolution of Polyvinylidene Difluoride

Dissolution of high molecular weight polyvinylidene difluoride (PVDF) is critical for manufacture and recycling of lithium-ion batteries, which is a growing field as electric vehicles come closer to widespread adoption. The traditional solvent for this application is NMP, which is reprotoxic, yet lacks obvious replacements. This research identified four potential replacement solvents, each of which is bio-derived, lacks serious hazards, and presents intriguing properties that could be industrially useful.

DMSO was found to be the best candidate for a drop-in replacement, as it can dissolve PVDF at room temperature and the solution acts as a viscous liquid. The other three candidates (GVL, Cyrene, and CP) present a processing challenge, as they require heating for dissolution and gel when cooled. However, these gelling solvents actually improve the rate of dissolution, as they disperse PVDF at room temperature instead of forming clumps like NMP and DMSO. When casting membranes with these solvents, DMSO behaves similarly to NMP, while GVL produces a more regular morphology with smaller pores. Cyrene and CP form non-porous, glassy films that are not suitable as membranes, but could be useful in applications where transparency is required.

This research has laid the groundwork for selecting an effective green solvent for PVDF manufacturing and recycling, identifying solvent candidates that are bio-derived, non-toxic, and non-mutagenic.

6.1.2 Cellulose Dissolution in Cellulose-Based Solvent

Cellulose is one of the highest-potential renewable feedstocks, and is already spun into textiles on an industrial scale. However, cellulose dissolution is primarily performed in carbon disulfide, which is a volatile, flammable neurotoxin. A green, economical system for dissolution could replace this highly hazardous solvent. This research discovered that Cyrene, a cellulose-based solvent, has some potential in dissolving cellulose.

With a mixture of tetrabutylammonium chloride (TBAC) and Cyrene, almost 0.5% w/v cellulose was dissolved. The cellulose regenerated from solution was shown by XRD to be a mixture of phases I and II, suggesting that the actual behaviour is a combination of dissolution and dispersion. However, the stability and optical clarity of the cellulose solution is excellent, suggesting that Cyrene/TBAC could be suitable for processing cellulose if the amount of dissolution could be increased. Sonication, mechanical mixing, and even simple freezing were shown to be effective processing methods for this solvent system. With further work, this solvent system could prove useful in industry.

6.1.3 Blending Solvents for Novel Properties

Derivatives of Cyrene, known as Cygnets, can be synthesised in one step using an acidic catalyst. The synthesis of Cygnet 0.0 from ethylene glycol and Cyrene was improved in several green metrics, including waste reduction, reaction time, and recrystallisation procedure. Cygnet was then blended with Cyrene in varying ratios, and the solubility

parameters of the blends shown to diverge from ideal predictions.

A 50% w/w solution of Cygnet in Cyrene was shown to be effective in casting water filtration membranes from polyimide (PI), polysulfone (PSU), and polyethersulfone (PES). The Cygnet blends behaved differently than unblended Cyrene, changing the morphology of the membranes in various ways. However, the degree of difference may not be sufficient to justify the additional difficulty and expense of synthesising Cygnet.

6.1.4 Applications of Oxymethylene Dimethyl Ethers as Novel Solvents

Oxymethylene ethers, or OMEs, are heavily researched as fuel additives, but prior to this work were never used as solvents, though renewably sourced OME mixtures could be cost-competitive in this application. Here, a commercial mixture (OME_{3.5}) was found to function as a potentially safer ether alternative, forming peroxides much more slowly than conventional solvent tetrahydrofuran (THF). Conclusions about their overall safety cannot be drawn, as there is no available data on toxicity and aquatic toxicity.

A mixture of OME_{3.5} was shown to work as a traditional reaction medium in organic reactions as well as biocatalytic polymerisations, though instability to acids may limit its applications in certain chemical syntheses. In addition, this mixture was proven to be effective in dissolution of polystyrene, and partially effective in removal of paints and coatings. The insolubility of OME_{3.5} with water suggests potential applications in aqueous extraction. Pending further safety testing, this new bio-based ether could be considered a candidate for a number of industrial products and processes, with the option of tuning the synthesis and composition of the mixture to capture desired properties.

6.2 Solubility Parameters

In this work, Hansen Solubility Parameters (HSP) and Kamlet-Abboud-Taft (KAT) parameters were used to inform choice of solvent, polymer, and application. While they can be useful shortcuts in solvent screening, their applications are limited, sometimes in unexpected ways.

As HSP can be quickly predicted, they were used in most chapters of this thesis as an initial screening step. Generally speaking, they serve two purposes: to identify potential replacement solvent candidates for a specific application, or to narrow down possible applications of a new solvent. In identifying solvent candidates, HSP were most helpful in Chapter 2. The use of HSP narrowed a candidate list from 224 solvents to six that required

testing. This process expanded the number of candidates under consideration, while reducing the cost of testing. However, in the same project, an unexpected shortcoming of HSP was discovered. HSP are commonly used in polymer swelling and dissolution, with a particular strength being their ability to predict blends of non-solvents that can be combined to make a polymer solvent.⁵⁰ Despite this, the solubility model constructed for PVDF proved to only be functional for single solvents, and blends of non-solvents did not work. The inability to predict effective blended solvents in this specific application has not been previously reported, and is unfortunately limiting, as blending solvents can be a cost-effective approach that complies with existing regulations. Additionally, this project highlighted the fundamental limitations of HSP—while they can predict a yes/no for thermodynamic dissolution, kinetics and more complex effects such as gelation are not predicted, requiring testing to confirm whether the identified solvents are actually suited for purpose.

Certain applications, such as cellulose dissolution, resist the use of HSP for solvent selection. When constructing a polymer solubility model, it is critical to have several compatible solvents with known HSP to generate the solubility sphere. In the case of cellulose, no single-component systems have been discovered, and most of the known solvent systems involve complex ionic interactions that are not yet predictable using HSPiP.⁵¹ This prevents the generation of a solubility model. Though HSP was used in Chapter 3 to attempt comparison of Cyrene with known solvents, this did not prove very useful, as the behaviour of ionic additives could not be included. For the time being, it appears that HSP are not very useful for polymers with few known solvents, or polymers that require complex solvent/additive combinations.

The study of a new solvent candidate, Cygnet 0.0, in blends with Cyrene (Chapter 4) utilised both HSP and KAT parameters. HSP initially identified Cygnet 0.0 as a promising candidate that is quite close to dichloromethane (DCM) in the solvent space, and blending it in equal proportion with Cyrene was predicted to create a mixture with an intermediate dipolarity. However, when this mixture was assessed with solvatochromic dyes, the KAT parameters were non-linear, and diverged only slightly from those of Cyrene. This highlights a fundamental difference between HSP and KAT parameters, particularly relevant in the case of mixed solvents. The HSP of blends are predicted by treating the mixture as a linear combination, with the relative influence of each solvent based on its proportion in the mixture. This is a simplified view that assumes an even

distribution of solvents in the bulk mixture, with no clustering or preferential solvation, and therefore is not always accurate. With KAT parameters, the measurement of the absorbance wavelength reflects the real local environment encountered by the solute dye. While this is in some respects an improvement, as inhomogeneity of the solvent mixture may be better represented, the solute dye can itself undergo preferential solvation and demonstrate solvent behaviour that is not experienced by all solutes.^{60,61}

In Chapter 5, HSP were used for the purpose of identifying potential applications for a new solvent candidate. In this case, the predicted parameters of OME₃₋₅ were compared to known values for traditional solvents, determining which solvents were closest in Hansen space, and therefore which applications could be appropriate for this OME mixture. The KAT parameters of the mixture were also measured and compared with those of traditional solvents. While both sets of parameters put OME₃₋₅ close to the conventional ether space, HSP predicted the closest solvent to be THF, while KAT parameters predicted this to be 1,4-dioxane. Again, this demonstrates the difference between HSP and KAT parameters in studying solvent mixtures—HSP assume a homogeneous bulk mixture and ignore complex behaviours, while KAT parameters reflect the local environment of each dye molecule and may be affected by preferential solvation. Neither system gives a perfect representation of solvent behaviour, but their combination can give a clearer picture. Ultimately, application testing is key in confirming predictions with any solubility parameters.

6.3 Green Solvent Outlook

Research that explores green solvent options for large-scale industrial applications is essential for the transition to the bioeconomy. Since the start of this work, there has been progress in this direction. The ReSolve project, led by the University of York, has received €4 million of EU funding towards finding new bio-based alternatives for NMP and toluene.³¹³ Circa Group have successfully scaled up their pilot plant, achieved Annex VIII REACH registration, and begun distributing Cyrene through Sigma-Aldrich, enabling more researchers to explore the possibilities of Cyrene for industry.^{99,102} The UK government is funding the Faraday Challenge to put £246 million toward development of holistically safe electric batteries, including solvents for their manufacture and recycling. The establishment of the International Sustainable Chemistry Collaborative Centre (ISC3) reflects Europe's interest in moving green and sustainable chemistry forward through

policy, research, and education.³¹⁴

More work remains to be done, but researchers and funders are beginning to move in the right direction. The exploratory work in this thesis will be continued as a start-up company called Green Rose Chemistry, working with industry to target solvents of high priority and identify or develop replacements. Through a combination of industrial funding, academic collaborations, and research grants, Green Rose Chemistry will work to make all solvents safe and bio-based.

CHAPTER 7

EXPERIMENTAL

7.1 Instrumentation and Analysis

Ultraviolet-visible Spectroscopy For ambient temperature UV-Vis analysis, spectra were obtained with a Jasco V-550 UV-Vis spectrophotometer using 1 cm quartz cells at ambient temperature (roughly 18°C). For high-temperature analysis, UV-Vis spectra were obtained with a Shimadzu UV-1800 equipped with a Shimadzu CPS-100 Peltier cell holder, scanning from 600–350 nm for KAT measurements. Data was collected using a slit width of 0.1, accumulation time of 0.1 sec, sampling interval of 0.2, and fast scan speed. Data collection and analysis was performed with Shimadzu UV Probe (Version 2.70).

Scanning Electron Microscopy (SEM) Scanning electron microscopy was performed with a Jeol JSM-6490LV instrument.

Rheometry Rheometry tests were performed using a Malvern Kinexus Pro rheometer equipped with a Peltier plate cartridge for temperature control. For gel tests (amplitude sweeps), rheometer was equipped with a 20 mm parallel plate geometry (PU 20 SR1910 SS), while viscosity measurements for fluids were performed with a 40 mm cone-plate geometry (CP4/40 SR2013 SS). Data was collected using Kinexus rSpace version 1.60.1731, and analysed with OriginPro version b9.5.1.195.

FT-IR Spectroscopy ATR FT-IR spectra were performed on a Perkin Elmer Spectrum 2 instrument with diamond window ATR accessory. Force gauge on pressure arm was kept at 105. Spectra were collected from 4000–450 cm⁻¹, with a resolution of 4 cm⁻¹. Data was collected and analysed with Perkin Elmer Spectrum software (Version 10.5.4).

X-Ray Diffraction Small-scale cellulose samples were analysed with a Rigaku Micro Max 007HF, scanning from 5-50° 2 θ .

Large-scale cellulose samples were analysed via powder XRD using a Bruker-AXS D8 Avance with a Lynx eye detector. Patterns were recorded using Cu K α radiation ($\lambda =$

1.5406 Å) scanning from 5-50° 2θ, with a step size of 0.05° and data points collected for 0.1 sec each. Data was collected with Bruker DIFFRAC plus XRD Commander version 2.6.1 and analysed with OriginPro version b9.5.1.195.

The diffraction intensity of all spectra was normalized by the peak area between 2θ = 5 and 50 degree.

Centrifugation Small-scale centrifugation was performed using a SciSpin Mini Microfuge with a fixed speed of 7,000 rpm, or relative centrifugal force (RCF) of 2,680×g, at ambient temperature. Large-scale centrifugation was performed with a Thermo Scientific Megafuge Heraeus Megafuge 40R at 3,500 rpm, or RCF of 1,372×g.

Ultrasonication Probe Ultrasound treatment was performed with a VCX-130 ultrasonic processor (130W max power output) equipped with a 2-mm stepped titanium alloy microtip.

HSPiP Software Hansen solubility parameters were determined and analysed using HSPiP software 5.0.10. Database values were used when available. Otherwise, SMILES codes were used to predict HSP using native Y-MB algorithm. For solvent mixtures, values were predicted for each component, then linearly combined according to mixture ratio.

GC-FID GC-FID chromatograms were obtained with an Agilent 6890N gas chromatograph equipped with an HP autosampler. The column used was a Restek Rxi-5HT fused silica column (30m length x 0.25mm x 0.25µm) for low-polarity mixtures, or a Restek Stabilwax fused silica column (30m length x 0.25mm x 0.25µm) for high-polarity mixtures. Helium was used as the carrier gas at a flow rate of 2.7 mL/min. Sample injection volume was 0.4µL with a split ratio of 30:1 into a 300°C inlet (240°C for Stabilwax columns). The oven temperature was initially set to 50°C, then immediately increased by 30°C/min to a final temperature of 300°C. The final temperature was held for 5 minutes. The flame ionisation detector was maintained at a temperature of 340°C.

GPC Gel permeation chromatography (GPC) was carried out using a PSS SDV High set of 3 analytical columns (300 × 8 mm, particle diameter 5 µm) of 1000, 10⁵, and 10⁶ Å pore sizes, plus guard column (PSS GmbH) installed in a PSS SECcurity SEC system. THF was used as the mobile phase (1 mL/min) with a column temperature of 23°C

and detection by refractive index. For each measurement, 20 μL of a roughly 2 mg/mL sample in THF was injected and eluted for 50 min. Calibration was carried out in the molecular weight range 370– 2.52×10^6 Da using ReadyCal polystyrene standards from Sigma Aldrich. Toluene was used as internal standard.

GC-MS Gas chromatograph-mass spectrometry was performed using a Perkin-Elmer Clarus 560 S mass spectrometer coupled to a Perkin-Elmer Clarus 500 gas chromatograph. The GC column used was a Restek Rxi-5HT fused silica column (30m \times 0.25 mm \times 0.25 μm), with helium as a carrier gas at a flow rate of 2 mL/min. Sample injection volume was 0.5 μL with a split ratio of 10:1 into a 300°C inlet. The oven temperature was initially set to 50°C, then immediately increased by 30°C/min to a final temperature of 300°C. The final temperature was held for 5 minutes. Clarus 500 quadrupole mass spectra were performed in electron ionisation (EI) mode at 70 eV with the source and quadrupole temperature both at 300°C. The mass scan was conducted from 40 to 640 m/z. GC-MS data was collected and analysed with PerkinElmer enhanced TurboMass software (Version 5.4.2). GC-MS samples were prepared by dissolving 10-50 mg product in 1.5 mL acetone.

NMR Spectroscopy NMR samples were prepared by dissolving 5-20 mg product in CDCl_3 . NMR spectra were recorded by a Jeol JNM-ECS 400 MHz spectrometer. For ^1H NMR, 16 scans were used, while for ^{13}C NMR, 256 scans were used. NMR data was analysed using iNMR version 6.1.5 from Mestrelab Research. Signals were calibrated against the residual solvent peak.

ArgusLab Software To calculate surface electrostatic potential of molecules, ArgusLab modelling software (Version 4.0.1) was used. Molecular geometry was optimised using the Austin Model 1 (AM1) parameterisation of the Modified Neglect of Diatomic Differential Overlap (MNDO) method and a restricted Hartree-Fock (RHF) calculation.

7.2 Green Solvents for Dissolution of Polyvinylidene Difluoride

7.2.1 Materials

N-methylpyrrolidinone ($\geq 99\%$) was purchased from Alfa Aesar. Dimethylsulfoxide ($>99\%$) was purchased from Fisher Scientific. γ -valerolactone ($\geq 99\%$) and cyclopent-

tanone ($\geq 99\%$) were purchased from Sigma-Aldrich. Cyrene (99%) was received from Circa Ltd. Solvents were dried over activated 4Å molecular sieves for at least 48h prior to use, with the exception of Cyrene, which is not stable to molecular sieves and was used as received. Water content of all solvents was found to be $<0.25\%$. Solef® 5130 PVDF was obtained from Solvay, dried under vacuum overnight, and stored in dessicator.

7.2.2 Experimental

Initial Dissolution Trials Acetonitrile (99.8%), benzyl alcohol (99.8%), benzyl benzoate ($\geq 99.0\%$), cyclohexane (99.5%), dimethylacetamide (DMAc, 99.8%), *N,N*-dimethyl formamide (DMF, 99.8%), ethylene carbonate (98%), glycerol (99%), isobutanol ($\geq 99\%$), methanol ($\geq 99.9\%$), *p*-Cymene (99%), and propylene carbonate (99.7%) were purchased from Sigma-Aldrich. γ -butyrolactone ($>99.0\%$) and glycerol 1,2-carbonate ($>90\%$) were purchased from Tokyo Chemical Industry UK. Acetic acid ($\geq 99.7\%$), ethylene glycol ($\geq 99\%$) and 5-hydroxymethylfurfural (5-HMF, 98%) were purchased from Acros Organics. Acetic anhydride ($\geq 97\%$) was purchased from Alfa Aesar. For each dissolution trial, 100 mg PVDF were weighed into a glass sample vial, and 1 mL solvent added with a micropipette. The sample vial was sealed with a rubber septum and briefly shaken to mix, then either rolled at room temperature (20°C) overnight, or equipped with magnetic stirbar and heated to 60°C, stirring at 600 rpm, for 24 h. For binary gradient sphere determination, NMP was used as the primary solvent, with benzyl benzoate, ethylene carbonate, and methanol as non-solvents. Each non-solvent was combined with the primary solvent in 10% v/v ratios (e.g. 90% NMP with 10% methanol, etc.) and shaken to mix, then used as a solvent in dissolution trials. For other solvent blend dissolution trials, each component solvent was measured individually with a micropipette into the sample vial.

PVDF Dissolution To prepare 10% w/v PVDF solution, 2 mL solvent was measured via syringe into a glass sample vial equipped with a magnetic stirbar. While stirring, 200 mg PVDF powder was added slowly to reduce clumping. The vial was sealed with a screw cap and Parafilm, and the mixture was magnetically stirred and heated to 60°C (for cyclopentanone) or 100°C (for all other solvents) in an aluminium heating block on a hot-plate. PVDF was considered fully dissolved when solution was completely transparent, with no remaining powder or clumps. Dissolution typically took from 1 to 6

hours, depending on solvent.

Minimum Gelator Concentrations To measure the minimum gelator concentration of PVDF in each solvent, 1% w/v PVDF solutions were prepared by adding 10 mg PVDF to 1 mL solvent, stirring and heating as above. When the PVDF was fully dissolved, the solutions were allowed to cool to room temperature. After 24h, each sample vial was inverted to check for gelation. If the solution was not fully gelled, the process was repeated with a new solution, increasing PVDF concentration by 1% w/v each time. The minimum gelator concentration was considered achieved once the solution was fully gelled after 24h at room temperature.

Rheometry Solutions of 10% w/v PVDF were prepared as described above. Roughly 2 mL of sample was used for each viscosity test, with liquid samples being prepared in bulk and poured onto the rheometer plate. Viscosity trials were conducted at a constant temperature (either 25°C or 100°C) with an incrementally increasing shear rate, ranging from 0.1 s⁻¹ to 10.0 s⁻¹. 7 samples per decade were taken in a logarithmic progression, with a maximum sampling interval of 3 min.

Gel samples were prepared individually, using bottomless glass sample vials to ensure a uniform and undisturbed gel network. Samples were 1.5-2.5 mm thick, and gap was set to 0.2 mm less than gel thickness to prevent slippage. With the exception of GVL gel samples, each sample was analysed within four hours of being prepared. GVL gel samples were analysed either 17h or 72h after preparation, to allow time for gelation. GVL viscosity measurements were performed within four hours of making the sample, before gelation had occurred. Amplitude sweeps were conducted at a fixed temperature of 25°C, with shear strain ranging from 0.1% to 100.0%. 10 samples per decade were taken in a logarithmic progression.

Gelation in Bottomless Vials Standard glass sample vials were cut to remove their bottoms. Each bottomless vial was attached to a glass microscope slide using silicone sealant, which was allowed to cure overnight. Once the sealant had cured, the bottomless vial and slide were placed on a hot plate at 60-100°C. 10% w/v samples of PVDF in solvent were prepared as above, then poured while hot into the vial to a height of roughly 2 mm. The vial was capped and allowed to cool to room temperature. For CP and Cyrene, this was sufficient to set the gel. For GVL, 24h standing at room temperature was required

to fully set the gel. To transfer the gels to the rheometer plate, the silicone sealant was cut with a scalpel and the bottomless vial detached from the microscope slide. The gel was then gently pushed out of the vial using a metal spatula.

Film Casting Solutions of 10% w/v PVDF were prepared as described above. For NMP, DMSO, and GVL, solutions were allowed to cool to roughly room temperature before casting. CP and Cyrene solutions were cast at 60°C and 100°C, respectively. Each solution was poured onto a glass plate and a stainless steel casting blade set to 500 microns was used to quickly spread the solution. The glass plate was then immediately transferred to a phase inversion bath of room-temperature deionised water, where it was kept until the film was fully solidified. Films were stored in glass powder bottles filled with deionised water.

Sample Preparation for FT-IR To prepare samples for analysis, the membranes were removed from the water, cut to size using scissors, and sandwiched gently between two pieces of membrane fabric support placed atop a glass microscope slide. The fabric was held in place with adhesive tape to ensure membranes remained flat during drying. Membranes were dried under vacuum overnight, then gently removed from their fabric supports prior to IR analysis.

Sample Preparation for SEM Films were dried as above, then soaked in ethanol for several minutes. Each sample was transferred directly from the ethanol bath to liquid nitrogen, where it was kept using tweezers until thermal equilibration had occurred, as indicated by cessation of bubbling. The film was then fractured and removed from the liquid nitrogen. Remaining ethanol was allowed to evaporate at room temperature, and each sample was mounted on a sticky carbon tab and sputter coated with 7 nm of gold/palladium for imaging. The top of each film, defined as the surface contacting the water bath during coagulation, was oriented upwards for cross-sectional images.

7.3 Cellulose Dissolution in Cellulose-Based Solvent

7.3.1 Materials

Microcrystalline cellulose from cotton linters (Avicel PH-101, 50 µm particle size) was purchased from Sigma-Aldrich. Glycerol 1,2-carbonate (>90.0%) was purchased from Tokyo

Chemical Industry. Lithium bromide ($\geq 99\%$), lithium chloride ($\geq 99\%$), lithium fluoride ($\geq 99.99\%$), zinc bromide (99.999%), zinc chloride (99.999%), zinc fluoride ($\geq 99.99\%$), tetrabutylammonium fluoride hydrate (98%), tetrabutylammonium chloride ($\geq 97\%$), tetrabutylammonium tribromide (98%), tetrabutylammonium iodide (98%), tetrabutylammonium acetate (97%), tetrabutylammonium hydrogen sulfate ($\geq 99\%$), tetramethylammonium fluoride tetrahydrate (98%), tributylmethylammonium chloride ($\geq 98\%$), trimethyloctylammonium chloride ($\geq 97\%$), tetraoctylammonium bromide (98%), and propylene carbonate (99.7%) were purchased from Sigma-Aldrich. All reagents were used without further purification.

7.3.2 Experimental

Preparation of Additive Solvent Systems Water was added to Cyrene on a v/v basis, shaking each sample vigorously to ensure mixing. For solvent systems involving additives, the additive was weighed into a glass vial, solvent added on a w/v basis, and the sample heated to 60°C for 20 min to aid dissolution. These samples were stored at room temperature for up to 6 weeks. Samples that were immiscible or obviously degraded (strong color change plus formation of solid) were considered unsuitable for use.

Small-Scale Cellulose Pre-treatment Cellulose (10 mg) was placed in a 1-mL plastic Eppendorf tube. Deionised water (1 mL) was added and shaken to mix, then sample was centrifuged for 10 min and water gently removed via glass pipette. Process was repeated once with ethanol, then three times with test solvent (e.g. Cyrene).

Large-Scale Cellulose Pre-treatment Cellulose was placed in a sintered glass Buchner funnel, and deionised water added to twice the height of the cellulose. Cellulose was allowed to soak for roughly five minutes, then vacuum was briefly applied to remove water. Process was repeated once with ethanol, then three times with test solvent (e.g. Cyrene).

Cellulose Dissolution via Freezing Solvent system (e.g. Cyrene/TBAC, 1 mL) was added to Eppendorf tube with pretreated cellulose (10 mg). Sample was either vortexed (for low-viscosity solvent systems) or inverted and forcefully tapped repeatedly (for high-viscosity solvent systems) until solid appeared evenly dispersed, then placed upright in freezer (-25°C) for 24 h.

Cellulose Dissolution via Sonication Solvent system (e.g. Cyrene/TBAC, 1 mL) was added to Eppendorf tube with pretreated cellulose (10 mg). Sample was sonicated for 5 sec, then transferred to 2-mL glass sample vial, using thin metal spatula to maximise volume transferred. Sample vial was placed in centre of 100-mL beaker, kept upright by custom-made acrylic disc. For room-temperature processing, roughly 10 mL water was added to beaker, covering bottom of sample vial. For ice-bath processing, beaker was packed to rim of sample vial with ice and water. Sample was then sonicated at 60% amplitude (max power delivery of 78W), pulsing for 1 sec on, 2 sec off to allow sample cooling.

Small-Scale Cellulose Dissolution Check Cellulose sample was treated by one of the methods above, then centrifuged for 10-60 min, depending on strength of dispersion, to remove undissolved solid. Clear supernatant was gently transferred to fresh Eppendorf tube via glass pipette. Ethanol (0.3 mL) was added as anti-solvent to force precipitation of any dissolved cellulose, and sample centrifuged to force precipitate to bottom. Supernatant was gently removed via pipette, and any solid remaining was washed with water (1 mL) three times, then ethanol (1 mL) three times. Sample was allowed to stand uncapped at room temperature overnight to remove any residual ethanol.

Small-Scale Cellulose XRD Regenerated cellulose was washed and dried as above, then charged into quartz capillary tube. XRD was measured directly and compared with untreated cellulose (Cellulose I) and cellulose regenerated from lithium bromide solution (Cellulose II). Cellulose I and II diffractograms were superimposed in a 1:1 ratio to model sample of Cellulose I + II.

Large-Scale Cellulose XRD Regenerated cellulose was washed and dried as above, and the resulting pellet was crushed with mortar and pestle. The regenerated cellulose powder was then suspended in a small amount of ethanol and transferred to a transparent glass disc, where ethanol was allowed to evaporate in order to deposit powdered cellulose. The sample disc was mounted in a transparent plastic specimen holder, allowing measurement of powder XRD without background interference. Procedure was repeated with microcrystalline cellulose for comparison.

7.4 Blending Solvents for Novel Properties

7.4.1 Materials

Dihydrolevoglucosenone (Cyrene) was obtained free of charge from Circa Group and used without further purification. Reagents were obtained as indicated below and used as received.

7.4.2 Experimental

Synthesis of 7,8-dioxaspiro[bicyclo[3.2.1]octane-2,2'-[1,3]dioxolane (Cygnnet 0.0) Ethylene glycol (>99%) was purchased from Fisher Scientific. Montmorillonite KSF (surface area 20-40 m²/g) was purchased from Sigma-Aldrich and heated to 200°C for 1 h in furnace to activate. Ethanol ≥99.8% was purchased from Sigma-Aldrich. Dihydrolevoglucosenone (40 mmol) was combined with an excess of ethylene glycol (73 mmol) and acidic heterogeneous catalyst KSF-200 (0.25 g) in a 25-mL round-bottomed flask equipped with a magnetic stirbar. The flask was covered with a vented septum and heated under stirring to 373K for 1 hour, during which the reaction mixture gradually turned dark purple. The catalyst was removed by vacuum filtration on a sintered glass fritted funnel, rinsing with minimal ethanol, and the reaction mixture briefly heated with a heat gun to facilitate transfer to a glass powder bottle. This was refrigerated at 5°C until crystallisation occurred. The resulting pinkish solid was collected via vacuum filtration, rinsed with minimal cold ethanol, then dissolved in minimal ethanol at 60°C. The resulting solution was treated by hot vacuum filtration to remove any remaining solids, and refrigerated overnight. This recrystallisation process was repeated twice more, for a total of three recrystallisations from ethanol. Fine, needle-like white crystals were collected by vacuum filtration on a sintered glass fritted funnel and dried under vacuum overnight.

Cygnnet/Cyrene Blends Cygnnet/Cyrene blends were prepared on a w/w basis by first measuring Cygnnet into a sample vial, then adding Cyrene. Samples were heated to 60-70°C, occasionally shaking, to dissolve. Dissolution was considered complete when no solid was visible at elevated temperature. Samples were stored at room temperature and reheated as needed for use.

KAT Parameters 4-nitroaniline ($\geq 99\%$) was purchased from Sigma-Aldrich, and N,N-diethyl-4-nitroaniline (97%) was purchased from Fluorochem. Acetone ($\geq 99.5\%$) was purchased from Sigma-Aldrich. Roughly 1-3 mg of each dye was dissolved in 2 mL acetone. To prepare a vial for UV-Vis spectroscopy, a single drop of dye solution was transferred to a glass sample vial and dried, then 1 mL test solvent was added to the vial. The UV-Vis absorbance was measured and the concentration of dye was tweaked, either diluting or transferring to a second glass vial with more dried dye, until the absorbance of the maximum peak was between 0.3 and 0.9.

Membrane Casting Polyimide P84 (PI) was obtained from Ensinger Sintimid. Polysulfone (PSU, M_w 35,000, M_n 16,000) was purchased from Sigma-Aldrich. Polyethersulfone (Ultrason E3020, PES) was obtained from INGE. Solutions of PI (15% w/v), PSU (20% w/v), or PES (20% w/v) were prepared by adding solvent to polymer, then stirring and heating to 80°C until dissolved. Each solution was allowed to cool to room temperature, then poured onto a glass plate. A stainless steel casting blade set to 500 microns was used to quickly spread the solution. The glass plate was then immediately transferred to a phase inversion bath of room-temperature deionised water, where it was kept until the film was fully solidified. Membranes were stored in glass powder bottles filled with deionised water.

Sample Preparation for SEM Membranes were dried under vacuum. Each sample was placed in liquid nitrogen, where it was kept using tweezers until thermal equilibration had occurred, as indicated by cessation of bubbling. The membrane was then fractured and removed from the liquid nitrogen. Each sample was mounted on a sticky carbon tab and sputter coated with 7 nm of gold/palladium for imaging. The top of each membrane, defined as the surface contacting the water bath during coagulation, was oriented upwards for cross-sectional images.

7.5 Applications of Oxymethylene Dimethyl Ethers as Novel Solvents

7.5.1 Materials

OME₃₋₅ mixture was supplied free of charge by ChemCom Industries B.V., Netherlands. Individual OME₃, OME₄, and OME₅ samples (all $>99\%$) were purchased from ASG Analytik-Service GmbH, Germany. Reagents were obtained as indicated below and used

as received.

7.5.2 Experimental

Solvent Miscibility Acetone ($\geq 99.5\%$), acetonitrile (99.8%), benzyl benzoate ($\geq 99.0\%$), diethylamine ($\geq 99.5\%$), diethyl ether ($\geq 99.7\%$, stabilised with 1 ppm BHT), *N,N*-dimethyl formamide (99.8%), 1,4-dioxane (99.8%), dipropylamine (99%), ethanol ($\geq 99.8\%$), ethanol amine ($\geq 99.5\%$), ethyl acetate (99.8%), ethyl lactate ($\geq 98\%$), ethylene carbonate (99%), formic acid ($\geq 95\%$), *N*-methyl-2-pyrrolidinone (99%), propylene carbonate (99.7%), propylene glycol ($\geq 99.5\%$), tetrahydrofurfuryl alcohol (99%), and toluene (99.8%) were purchased from Sigma-Aldrich. *tert*-butyl alcohol ($>99\%$) was purchased from Fluorochem. Carbon tetrachloride ($>99.9\%$) was obtained from Fluka. Cyclohexanol ($>99\%$) was purchased from Avocado Research Chemicals. Dichloromethane ($\geq 99.8\%$, stabilised with amylene), dimethyl sulfoxide ($>99\%$), and *n*-propanol ($\geq 99\%$) were purchased from Fisher Scientific. Ethylene glycol ($\geq 99\%$) and *n*-heptane ($\geq 99\%$) were purchased from Acros Organics. Water was obtained from lab supply of deionised water. Each test solvent was combined with the OME₃₋₅ mixture in a 1:1 ratio by volume, and this sample shaken vigorously at ambient temperature for several seconds. The sample was then allowed to stand at room temperature for one hour. If any turbidity or separation of layers occurred, the solvent was considered immiscible with OME₃₋₅. Samples that remained fully homogeneous and transparent were considered miscible.

KAT Parameters 4-nitroaniline ($\geq 99\%$) was purchased from Sigma-Aldrich, and *N,N*-diethyl-4-nitroaniline (97%) was purchased from Fluorochem. Acetone ($\geq 99.5\%$) was purchased from Sigma-Aldrich. Roughly 1-3 mg of each dye was dissolved in 2 mL acetone. To prepare a vial for UV-Vis spectroscopy, a single drop of dye solution was transferred to a glass sample vial and dried, then 1 mL test solvent was added to the vial. The UV-Vis absorbance was measured and the concentration of dye was tweaked, either diluting or transferring to a second glass vial with more dried dye, until the absorbance of the maximum peak was between 0.3 and 0.9.

Acid Stability Hydrochloric acid ($>37\%$), sulfuric acid ($>95\%$), and aluminum chloride (99%) were purchased from Fluka. Boron trifluoride (14% in methanol) and iron (III) trichloride (97%) were purchased from Sigma-Aldrich. Each acid was combined with the OME₃₋₅ mixture at a concentration of 1 mmol acid/mL solvent. The samples were

sealed in glass vials and magnetically stirred while heating to 50°C for 72h. In the case of hydrochloric acid, an additional sample with 20 mol% acid was prepared and treated in the same way.

Peroxide Formation Peroxide concentrations were measured using Quantofix[®] peroxide test sticks, purchased from Macherey-Nagel. For each sample, a test stick was dipped into the solvent for 1 second, then removed and shaken to remove excess solvent. A drop of water was added to the test strip, the strip shaken to dry, and the color recorded after five seconds. To test peroxide formation potential, 10 mL of solvent was transferred to a wide-necked round-bottomed flask, and a stream of air (from compressed source) bubbled through via a needle while stirring under UV radiation. UV radiation was achieved via a UVP UVGL-58 handheld UV lamp that was mounted directly above the neck of the flask and set to 254 nm. Peroxide concentration was measured after 2 hours and 4 hours. After 4 hours, the stirbar was removed and the solvent decanted into a measuring cylinder to measure solvent evaporation.

When calculating the peroxide formation rate, any ranges reported were treated as the midpoint of the range (e.g. 1-3 was treated as 2). Values below 1 were treated as 0. The rate of formation was calculated for each 2-hour time interval, and the results averaged across the intervals for each solvent. Values were rounded to the nearest integer.

Polymer Dissolution Polypropylene pellets (PP, weight-averaged molecular weight (M_w) 12,000 Da), polystyrene pellets (PS, M_w 192,000 Da), and polystyrene powder (PS, M_w unknown) were purchased from Sigma-Aldrich. Ultrason[®] E3020 P Polyarylethersulfone (PES, M_w 55,000 Da) and PVP Luvitek[®] K-90 Pulver (1,500,000 Da) were obtained from BASF Inge GmbH. Torlon AI-10 was provided by Solvay, containing 90-99.9% PAI with 3-6% NMP. A small amount of each polymer was placed in a sample vial, and OME mixture added (3-4 mL). The samples were agitated on a Stuart tube roller at room temperature for 3 days, after which the samples were visually inspected for signs of polymer swelling or dissolution. The effect of heating was tested by heating each sample to 60°C while stirring at 600 rpm on a magnetic hotplate for 24 h, followed by visual inspection.

Paint Removal *N*-methyl-2-pyrrolidinone (99%) was obtained from Sigma-Aldrich. Commercial spray paints were obtained from Clostermann Coatings (cellulose paint)

and Kobra Paint (acrylic paint). Glazed ceramic tiles were purchased from B&Q. Tiles were broken into rectangular fragments for testing. Tile fragments were sprayed with paint and allowed to cure for at least 48 hours. After curing, painted fragments were placed in vials containing 15 mL of solvent and agitated on a Stuart tube roller for 3 days. The tiles were then removed from the vials, wiped with a tissue, and left to dry.

Suzuki Reaction Tris(dibenzylideneacetone)dipalladium(0) (97%), triphenylphosphine (99%), iodobenzene (98%), and phenylboronic acid ($\geq 97\%$) were purchased from Sigma-Aldrich. Potassium carbonate ($\geq 99\%$) was purchased from Alfa Aesar. Tris(dibenzylidene acetone)dipalladium(0) (2.5 mol%, .062 mmol, 57 mg) and triphenylphosphine (15 mol%, .375 mmol, 98 mg) were combined with 3M aqueous potassium carbonate (5 mmol, 1.67 mL) and 5 mL solvent in 2-necked round-bottomed flask equipped with reflux condenser. Nitrogen was bubbled through, stirring, at 50°C for several minutes, then iodobenzene (2.5 mmol, 280 μ L) and phenylboronic acid (2.75 mmol, 335 mg) were added. Reaction mixture was heated to 100°C and stirred under nitrogen for 24 hours, taking samples for GC-FID analysis 1 hour and 24 hours after reaching temperature.

Enzymatic Polymerisation Dimethyl adipate (DMA, $\geq 99\%$), 1,4-butanediol (BDO, 99%), 1,6-hexanediol (HDO, 99%), 1,8-octanediol (ODO, 98%), and diphenyl ether (DPE, 99%), and *Candida antarctica* lipase B immobilised on acrylic resin code L4777 (CaLB, Novozyme 435[®]) were obtained from Sigma-Aldrich. DMA (0.1394 g, 8.0×10^{-4} mol, 0.2 M) was combined with an equimolar amount (8.0×10^{-4} mol, 0.2 M) of diol (BDO, HDO, or ODO) and 4 mL organic solvent (DPE or OME₃₋₅) in a 25-mL round-bottomed flask. The mixture was stirred, heating to 85°C on a magnetic hotplate, until the monomers were completely dissolved. Then, 10% w/w (based on total weight of monomers) immobilised CaLB was added. The reaction was run for 6 hours at 1000 mbar, then a 20 mbar vacuum was applied for the next 18 hours, maintaining the 85°C reaction temperature. Reaction work-up was performed by adding roughly 5 mL warm dichloromethane to the reaction mixture and stirring for 10 min at 50°C before using a cotton filter to remove the biocatalyst. Dichloromethane was removed under vacuum. The remaining mixture was added to ice-cold methanol to precipitate the polymer, and then washed three times with methanol to remove the non-volatile solvent residues. The precipitated, purified polymers were dried under vacuum for 24 hours to reach a constant weight, and appeared as a white powder. Reactions were performed in duplicate.

Appendices

APPENDIX A
SUPPLEMENTARY DATA

A.1 Green Solvents for Dissolution of Polyvinylidene Difluoride

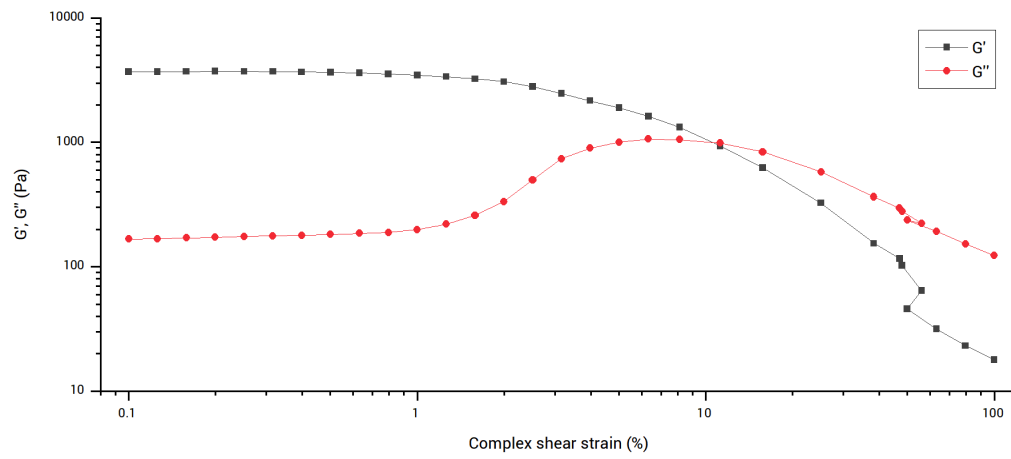


Figure A.1: Amplitude sweep of 10% w/v PVDF in GVL at 25°C.

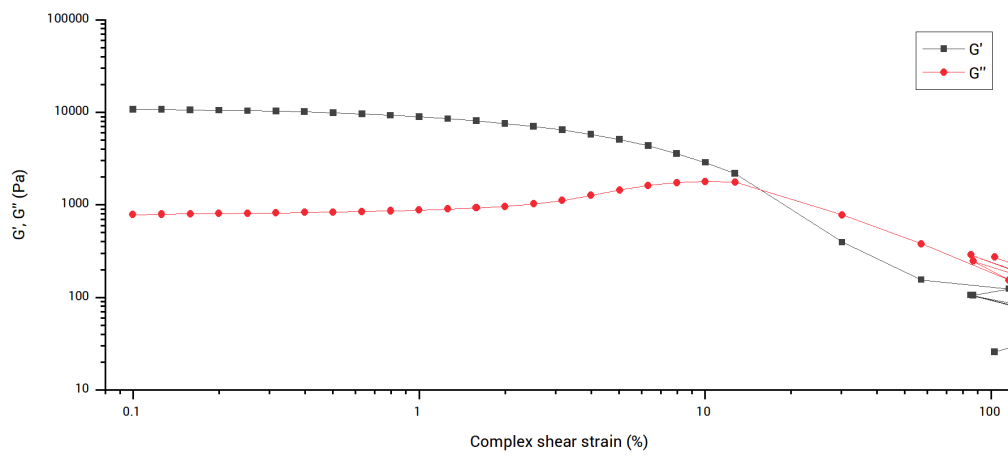


Figure A.2: Amplitude sweep of 10% w/v PVDF in Cyrene at 25°C.

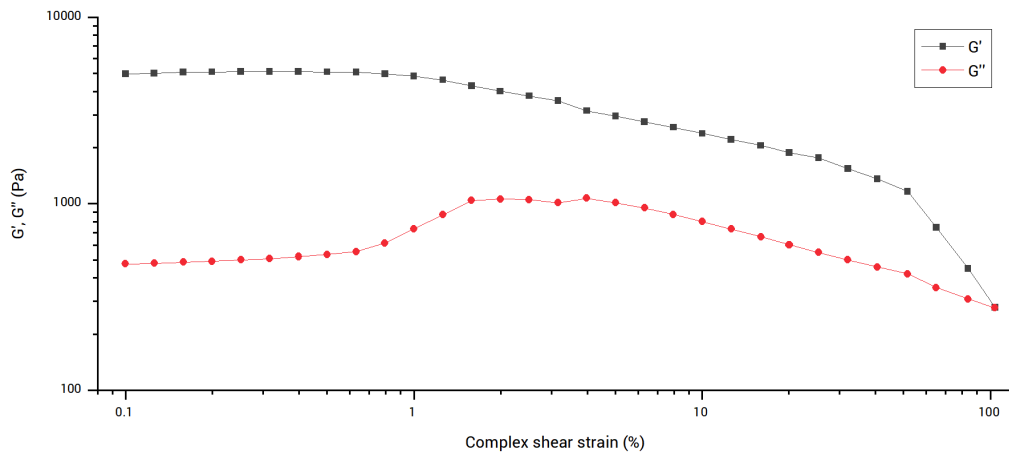


Figure A.3: Amplitude sweep of 10% w/v PVDF in CP at 25°C.

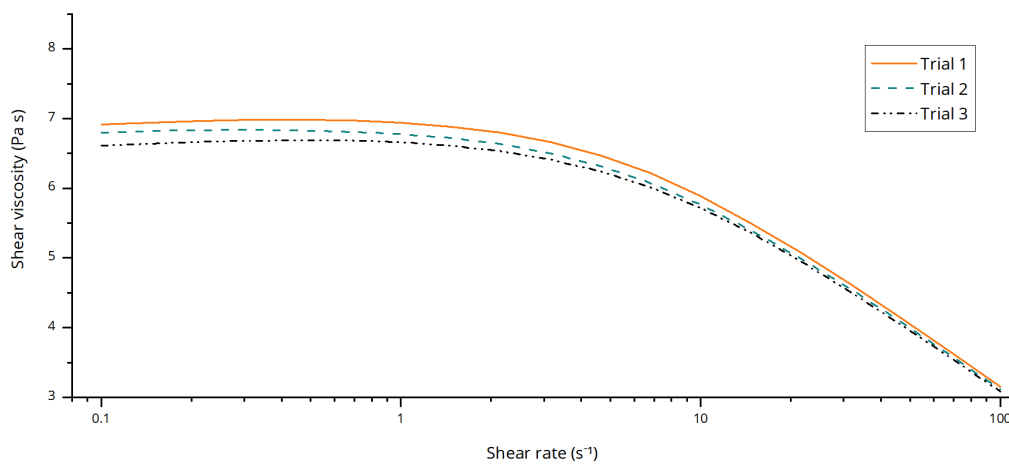


Figure A.4: Viscosity of 10% w/v PVDF in NMP at 25°C. Results of three independent trials.

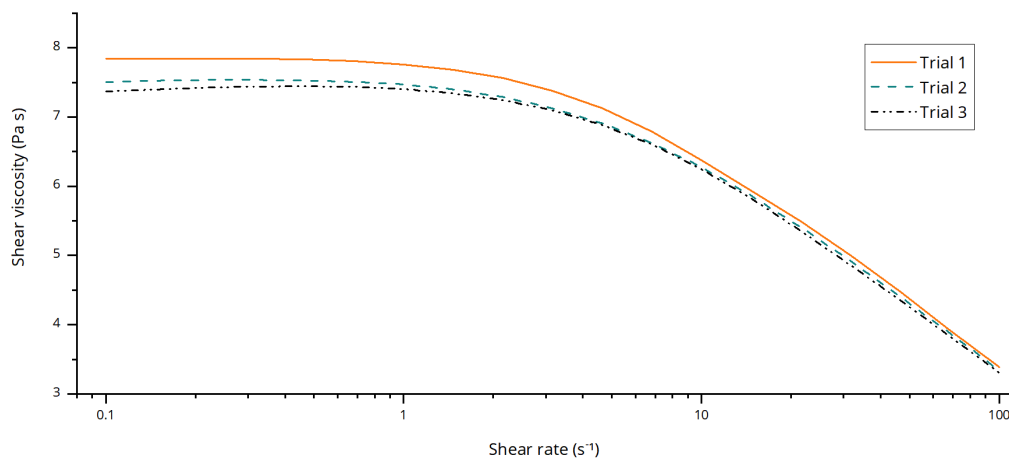


Figure A.5: Viscosity of 10% w/v PVDF in DMSO at 25°C. Results of three independent trials.

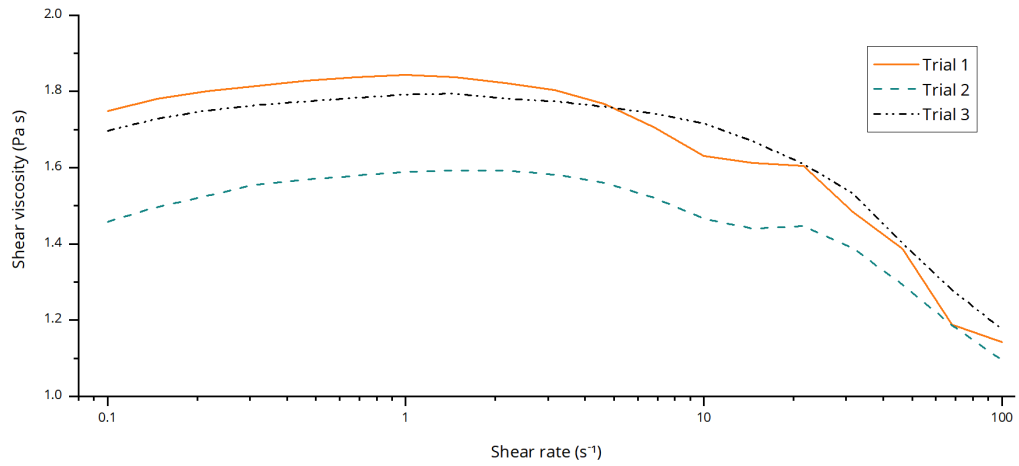


Figure A.6: Viscosity of 10% w/v PVDF in NMP at 100°C. Results of three independent trials.

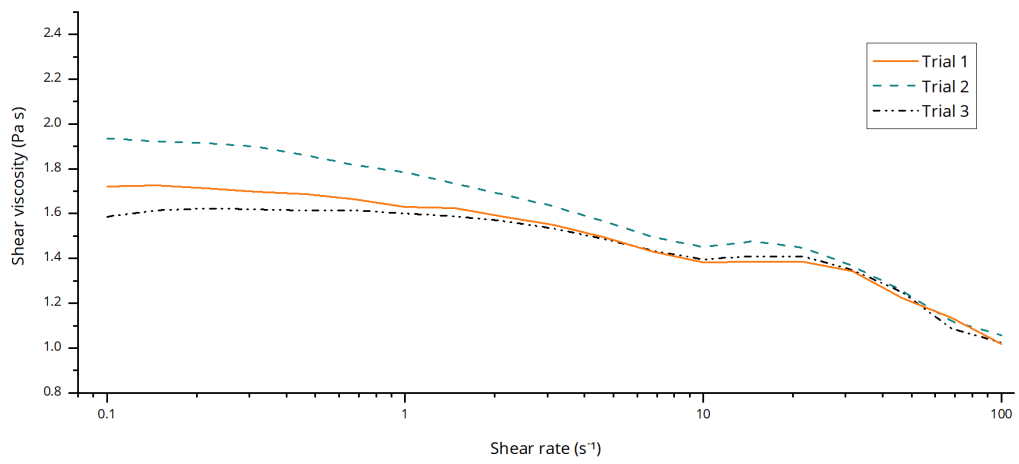


Figure A.7: Viscosity of 10% w/v PVDF in DMSO at 100°C. Results of three independent trials.

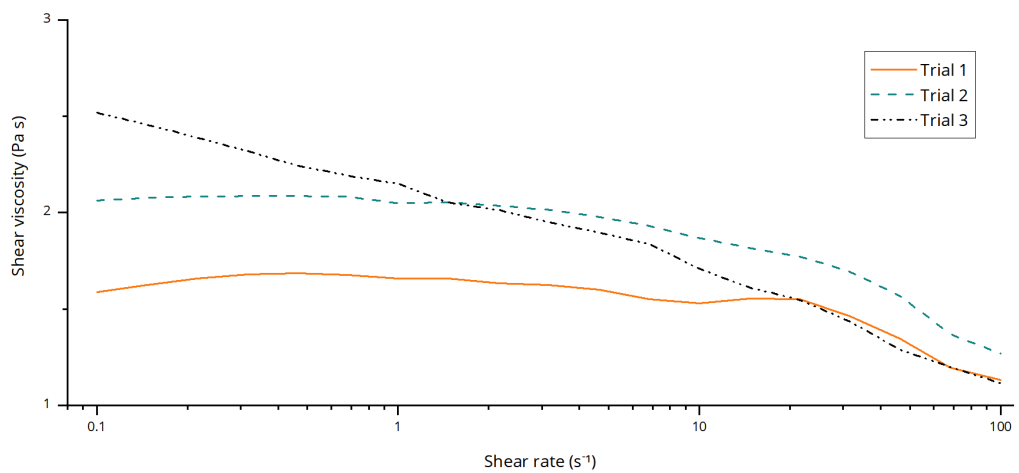


Figure A.8: Viscosity of 10% w/v PVDF in GVL at 100°C. Results of three independent trials.

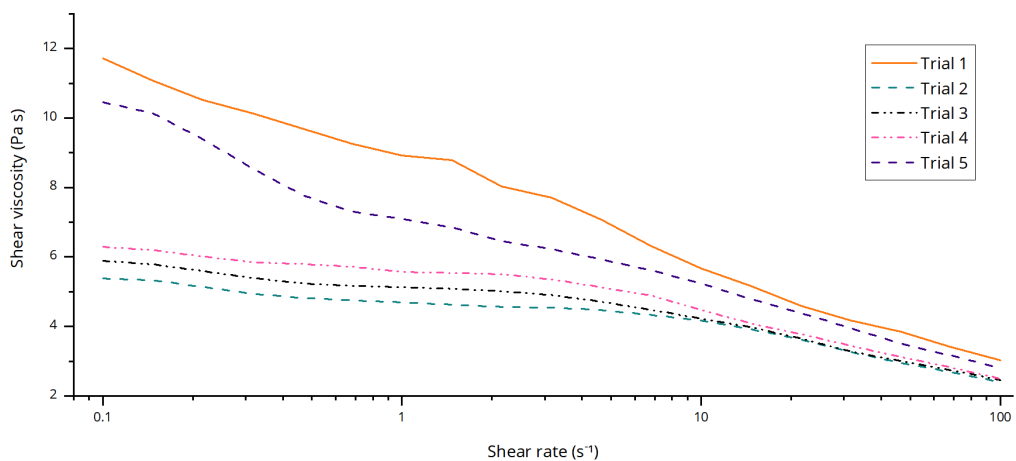


Figure A.9: Viscosity of 10% w/v PVDF in Cyrene at 100°C. Results of three independent trials.

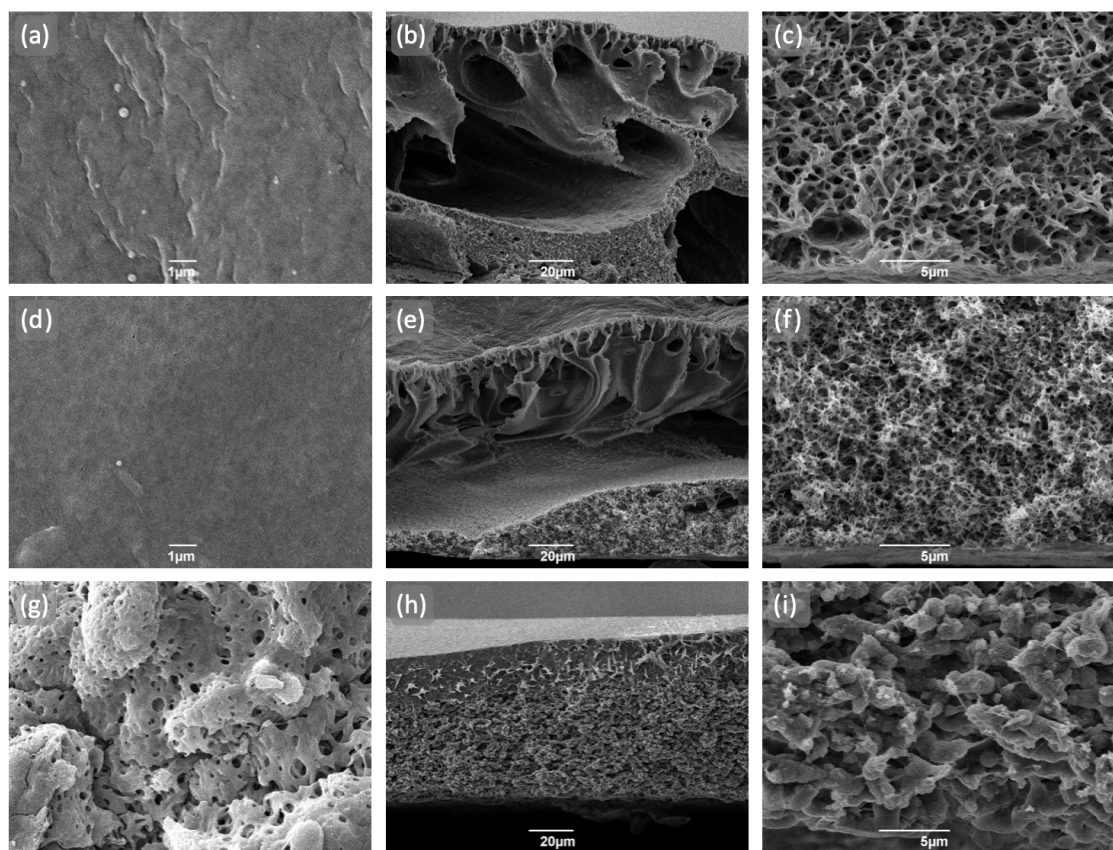


Figure A.10: SEM micrographs of films prepared with 10% w/v PVDF in NMP (a-c), DMSO (d-f), and GVL (g-i) at room temperature, showing surfaces at 10,000x (a, d, g), cross-sections at 800x (b, e, h), and cross-sections at 5,000x (c, f, i)

A.2 Cellulose Dissolution in Cellulose-Based Solvent

Table A.1: Additive concentrations used in trials of cellulose dissolution systems

Additive	% w/v
lithium fluoride	8
lithium chloride	8
lithium bromide	8
zinc fluoride	15
zinc chloride	15
zinc bromide	15
tetrabutylammonium fluoride hydrate	20
tetrabutylammonium chloride	50
tetrabutylammonium tribromide	20
tetrabutylammonium iodide	20
tetrabutylammonium acetate	15
tetrabutylammonium hydrogen sulfate	20
tributylmethylammonium chloride	50
tetramethylammonium fluoride tetrahydrate	20
trimethyloctylammonium chloride	20
tetraoctylammonium bromide	20
propylene carbonate	60
glycerol carbonate	40

A.3 Applications of Oxymethylene Dimethyl Ethers as Novel Solvents

Table 112. GC-MS Analysis of OME₃

Compound	Area Percent	CAS
OME ₃	42.8	13353-03-2
OME ₄	23.8	13352-75-5
D-OME ₁	9.6	-
OME ₅	10.2	13352-76-6
D-OME ₂	3.5	-
OME ₆	4.0	-
D-OME ₃	1.8	-
OME ₇	1.4	-

Remaining 2.9% are unidentified impurities

Table A.3: Solvent Miscibility of OME₃₋₅

Solvent	δ_D	δ_P	δ_H	Miscible?
acetone	15.5	10.4	7.0	Y
acetonitrile	15.3	18.0	6.1	Y
benzyl benzoate	20.0	5.1	5.2	Y
<i>tert</i> -butyl alcohol	15.2	5.1	14.7	Y
carbon tetrachloride	17.8	0.0	0.6	Y
cyclohexanol	17.4	4.1	13.5	Y
dichloromethane (DCM)	15.3	9.9	3.9	Y
diethylamine	14.9	2.3	6.1	Y
diethyl ether	14.5	2.9	4.6	Y
dimethyl formamide (DMF)	17.4	13.7	11.3	Y
dimethyl sulfoxide (DMSO)	18.4	16.4	10.2	Y
1,4-dioxane	17.5	1.8	9.0	Y
dipropylamine	15.3	1.4	4.1	Y
ethanol	15.8	8.8	19.4	Y
ethanolamine	17.0	15.5	21.0	N
ethyl acetate	15.8	5.3	7.2	Y
ethyl lactate	16.0	7.6	12.5	Y
ethylene carbonate	18.0	21.7	5.1	Y
ethylene glycol	17.0	11.0	26.0	N
formic acid	14.6	10.0	14.0	Y
heptane	15.3	0.0	0.0	Y
<i>N</i> -methyl-2-pyrrolidone (NMP)	18.0	12.3	7.2	Y
1-propanol	16.0	6.8	17.4	Y
propylene carbonate	20.0	18.0	4.1	Y
propylene glycol	16.8	10.4	21.3	Y
tetrahydrofurfuryl alcohol	17.8	8.2	12.9	Y
toluene	18.0	1.4	2.0	Y
water	15.5	16.0	42.3	N

Table A.4: Suzuki Couplings in OME₃₋₅

Biphenyl Coupling Reaction						
	Yield (%)					
	BP	Std Dev				
1,4-dioxane	98.8	1.6				
CPME	97.0	2.6				
OME	98.0	1.7				

Diphenylmethane Coupling Reaction						
	DPM		BP		DB	
	Yield (%)	Std Dev	Yield (%)	Std Dev	Yield (%)	Std Dev
1,4-dioxane	83.7	1.6	4.3	0.9	11.9	0.9
CPME	85.5	1.2	2.3	0.4	12.2	1.2
OME	82.0	1.2	2.4	0.5	15.6	1.2

BP = biphenyl, DPM = diphenylmethane, DB = dibenzyl. Percentage yield was measured with GC-FID following calibration for each product. Results are reported as average with standard deviation (Std Dev) of three independent trials.

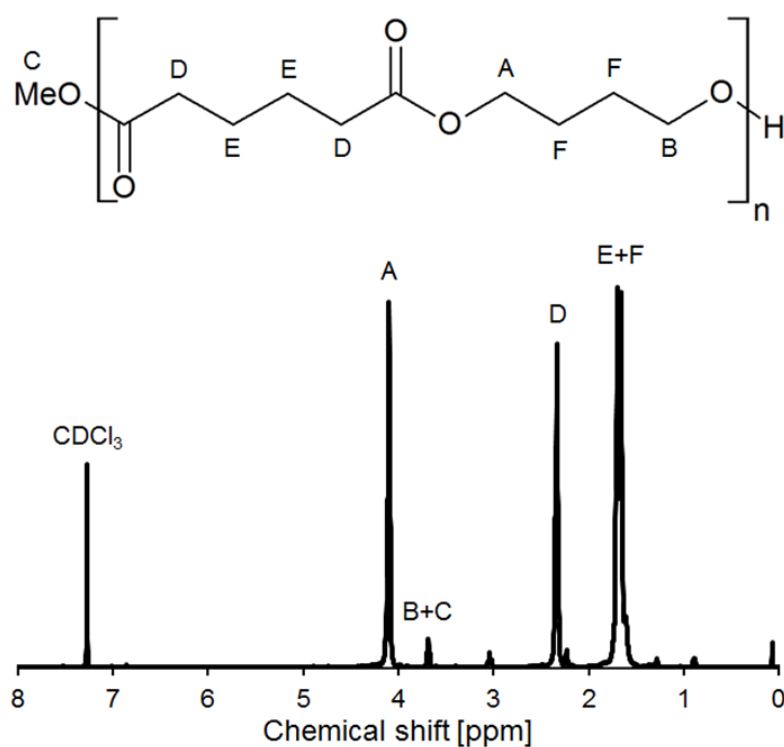


Figure A.11: ¹H-NMR spectrum of poly(1,4-butylene adipate) produced from the reaction of dimethyl adipate (DMA) and 1,4-butanediol (BDO) in OME₃₋₅ solvent, using *Candida antarctica* lipase B as catalyst.

ABBREVIATIONS

- α hydrogen bond donating ability
 β hydrogen bond accepting ability
 ϵ_r relative permittivity
 π^* dipolarity/polarisability
2-MeTHF 2-methyltetrahydrofuran
4-NA 4-nitroaniline
ATR FT-IR attenuated total reflection Fourier transform infrared
BP boiling point
CaLB *Candida antarctica* lipase B
CP cyclopentanone
CPME cyclopentyl methyl ether
DCM dichloromethane
DEN *N,N*-diethyl-4-nitroaniline
DMAc dimethylacetamide
DMF dimethylformamide
DMS dimethyl sulfide
DMSO dimethylsulfoxide
DP degree of polymerisation
DPE diphenyl ether
DSC differential scanning calorimetry
EI electrospray ionisation
ESP electrostatic potential energy
ETBE ethyl-*tert*-butyl ether
EU European Union
eV electron volts
FP flash point
FT-IR Fourier transform infrared
G' shear storage modulus
G'' shear loss modulus
GBL γ -butyrolactone
GC-MS gas chromatography-mass spectrometry

GHB γ -hydroxybutyrate
GHS Globally Harmonized System of Classification and Labelling of Chemicals
GPC gel permeation chromatography
GVL γ -valerolactone
HSP Hansen Solubility Parameters
HSPiP Hansen Solubility Parameters in Practice
IL ionic liquid
IR infrared
IUPAC International Union of Pure and Applied Chemistry
KAT Kamlet-Abboud-Taft
kDa kilodaltons
LCA life cycle assessment
LiCl lithium chloride
MeTHF 2-methyltetrahydrofuran
MGC minimum gelator concentration
MI mass intensity
M_n number-averaged molecular weight
MOF metal-organic framework
MP melting point
M_w weight-averaged molecular weight
MW molecular weight
NIPS non-solvent induced phase inversion
NMMO *N*-methylnmorpholine-*N*-oxide
NMP *N*-methyl-2-pyrrolidinone
NMR nuclear magnetic resonance
OECD Organisation for Economic Cooperation and Development
OME poly(oxymethylene) dimethyl ether, or oxymethylene ether
PAI polyamide-imide
PES polyethersulfone
PI polyimide
PP polypropylene
PS polystyrene
PSU polysulfone

PVDF polyvinylidene difluoride
PVP polyvinylpyrrolidone
 R_0 HSP sphere radius
 R_a HSP distance
REACH Registration, Evaluation, Authorisation and Restriction of Chemicals
RED relative energy difference
RME reaction mass efficiency
SEM scanning electron microscopy
SMILES simplified molecular-input line-entry system
SO_x sulfur oxides
TAME *tert*-amyl methyl ether
TBAC tetrabutylammonium chloride
TBAF tetrabutylammonium fluoride
THF tetrahydrofuran
TIPS thermally induced phase separation
TMO tetramethyloxylane
UV-Vis ultraviolet-visible
VOC volatile organic compounds
XRD X-ray diffraction
Y-MB Yamamoto-Molecular Break

REFERENCES

- (1) D. van der Hoeven, *Circular Bioeconomy: An Uneasy Marriage of Concepts, so Far*, 2018, <https://www.biobasedpress.eu/2018/03/circular-bioeconomy-an-uneasy-marriage-concepts-so-far/> (visited on 05/06/2019).
- (2) M. Cuff, *Understanding the Policy Principles for a 'Just Transition'*, 2019, <https://www.businessgreen.com/bg/analysis/3070087/the-policy-principles-for-a-just-transition> (visited on 05/06/2019).
- (3) M. Carus and L. Dammer, *Food or Non-Food: Which Agricultural Feedstocks Are Best for Industrial Uses?*, 2013.
- (4) L. Friedman, N. Popovich and H. Fountain, *The New York Times, Climate*, 2019.
- (5) J. Kennedy, *Aeon*, 2016.
- (6) M. Lorch, *The Guardian, Science*, 2014.
- (7) M. Godoy, *Is The Food Babe A Fearmonger? Scientists Are Speaking Out*, 2014, <https://www.npr.org/sections/thesalt/2014/12/04/364745790/food-babe-or-fear-babe-as-activist-s-profile-grows-so-do-her-critics> (visited on 05/06/2019).
- (8) P. A. Offit, *New England Journal of Medicine*, 2007, **357**, 1278–1279.
- (9) J. Kennedy, *On the \$\$\$ Fuelling Chemophobia – Part 3*, 2016, <https://jameskennedymonash.wordpress.com/2016/02/12/on-the-irrationality-of-chemophobia-part-3/> (visited on 05/06/2019).
- (10) G. Pyrgiotakis, J. McDevitt, A. Bordini, E. Diaz, R. Molina, C. Watson, G. De-loid, S. Lenard, N. Fix, Y. Mizuyama, T. Yamauchi, J. Brain and P. Demokritou, *Environmental Science: Nano*, 2014, **1**, 15–26.
- (11) G.-h. Moon, H.-i. Kim, Y. Shin and W. Choi, *RSC Advances*, 2012, **2**, 2205–2207.
- (12) European Commission, *Impacts of REACH and Corresponding Legislation Governing the Conditions for Marketing and Use of Chemicals in Different Countries/Regions on International Competitiveness of EU Industry*, 2016.
- (13) GC3, *Member Companies — Green Chemistry & Commerce Council (GC3)*, 2019, <https://greenchemistryandcommerce.org/membership/current-members/> (visited on 05/07/2019).
- (14) Trucost, *Making the Business and Economic Case for Safer Chemistry*, 2015, p. 40.
- (15) P. T. Anastas and J. C. Warner, *Green Chemistry: Theory and Practice*, Oxford University Press, New York, 1998.

- (16) V. Zuin and L. Mammìno, *Worldwide Trends in Green Chemistry Education*, 2015, 329 pp.
- (17) D. J. C. Constable, A. D. Curzons and V. L. Cunningham, *Green Chemistry*, 2002, **4**, 521–527.
- (18) C. R. McElroy, A. Constantinou, L. C. Jones, L. Summerton and J. H. Clark, *Green Chemistry*, 2015, **17**, 3111–3121.
- (19) F. G. Calvo-Flores, *ChemSusChem*, 2009, **2**, 905–919.
- (20) A. M. Voutchkova-Kostal, J. Kostal, K. A. Connors, B. W. Brooks, P. T. Anastas and J. B. Zimmerman, *Green Chemistry*, 2012, **14**, 1001–1008.
- (21) J. Kostal, A. Voutchkova-Kostal, P. T. Anastas and J. B. Zimmerman, *Proceedings of the National Academy of Sciences*, 2015, **112**, 6289–6294.
- (22) N. D. Austin, N. V. Sahinidis and D. W. Trahan, *Chemical Engineering Research and Design*, 2016, **116**, 2–26.
- (23) B. E. Dale, *Journal of Chemical Technology & Biotechnology*, 2003, **78**, 1093–1103.
- (24) R. A. Sheldon, *Green Chemistry*, 2014, **16**, 950–963.
- (25) L. Filiciotto and R. Luque, *Current Green Chemistry*, 2018, **5**, 47–59.
- (26) W. McDonough and M. Braungart, *Cradle to Cradle: Remaking the Way We Make Things*, San Val, 2002, 193 pp.
- (27) R. Mülhaupt, *Macromolecular Chemistry and Physics*, 2013, **214**, 159–174.
- (28) R. A. Sheldon, *ACS Sustainable Chemistry & Engineering*, 2018, **6**, 32–48.
- (29) S. Wenda, S. Illner, A. Mell and U. Kragl, *Green Chemistry*, 2011, **13**, 3007–3047.
- (30) Z. Chen and C. Wan, *Renewable and Sustainable Energy Reviews*, 2017, **73**, 610–621.
- (31) Y. Lu and S. Ozcan, *Nano Today*, 2015, **10**, 417–420.
- (32) N. E. Leadbeater, *Microwave Heating as a Tool for Sustainable Chemistry*, CRC Press, Boca Raton, FL, 2010, 107 pp.
- (33) S. L. James, C. J. Adams, C. Bolm, D. Braga, P. Collier, T. Friščić, F. Grepioni, K. D. M. Harris, G. Hyett, W. Jones, A. Krebs, J. Mack, L. Maini, A. Guy Orpen, I. P. Parkin, W. C. Shearouse, J. W. Steed and D. C. Waddell, *Chemical Society Reviews*, 2012, **41**, 413–447.
- (34) R. A. Sheldon, *Green Chemistry*, 2017, **19**, 18–43.

- (35) J. Andraos, *Organic Process Research & Development*, 2005, **9**, 149–163.
- (36) K. Van Aken, L. Streckowski and L. Patiny, *Beilstein Journal of Organic Chemistry*, 2006, **2**, 3.
- (37) C. Capello, U. Fischer and K. Hungerbühler, *Green Chemistry*, 2007, **9**, 927–934.
- (38) F. P. Byrne, S. Jin, G. Paggiola, T. H. M. Petchey, J. H. Clark, T. J. Farmer, A. J. Hunt, C. Robert McElroy and J. Sherwood, *Sustainable Chemical Processes*, 2016, **4**, 7.
- (39) D. Prat, J. Hayler and A. Wells, *Green Chemistry*, 2014, **16**, 4546–4551.
- (40) L. J. Diorazio, D. R. J. Hose and N. K. Adlington, *Organic Process Research & Development*, 2016, **20**, 760–773.
- (41) D. Prat, A. Wells, J. Hayler, H. Sneddon, C. R. McElroy, S. Abou-Shehada and P. J. Dunn, *Green Chemistry*, 2016, **18**, 288–296.
- (42) M. D. Tabone, J. J. Cregg, E. J. Beckman and A. E. Landis, *Environmental Science & Technology*, 2010, **44**, 8264–8269.
- (43) C. Jiménez-González, D. J. C. Constable and C. S. Ponder, *Chemical Society Reviews*, 2012, **41**, 1485–1498.
- (44) G. J. Ruiz-Mercado, R. L. Smith and M. A. Gonzalez, *Industrial & Engineering Chemistry Research*, 2012, **51**, 2309–2328.
- (45) F.-J. Santos Arévalo, I. Gómez Martínez, L. Agulló García, M.-T. Reina Maldonado and M. García León, *Nuclear Instruments and Methods in Physics Research Section B: Beam Interactions with Materials and Atoms*, 2015, **361**, 354–357.
- (46) S. Gartiser, K. Schneider, M. A. Schwarz and T. Junker, *Assessment of Environmental Persistence: Regulatory Requirements and Practical Possibilities – Available Test Systems, Identification of Technical Constraints and Indication of Possible Solutions*, (UBA-FB) 002326, Umweltbundesamt, 2017.
- (47) A. McNaught and A. Wilkinson, *IUPAC Compendium of Chemical Terminology*, Blackwell Scientific Publications, Oxford, 2nd, 1997.
- (48) E. V. Anslyn and D. A. Dougherty, *Modern Physical Organic Chemistry*, University Science Books, Sausalito, California, 2006, 1146 pp.
- (49) B. Averill and P. Eldredge, *General Chemistry: Principles, Patterns, and Applications*, Saylor Foundation, 2011.
- (50) C. M. Hansen, *Hansen Solubility Parameters: A User's Handbook, Second Edition*, CRC Press, 2nd, 2007, 544 pp.
- (51) S. Abbott, *Solubility Science: Principles and Practice*, 1.0.1.2, 2018, 194 pp.

- (52) C. Reichardt, *Angewandte Chemie International Edition in English*, 1979, **18**, 98–110.
- (53) M. J. Kamlet, J. L. M. Abboud, M. H. Abraham and R. W. Taft, *The Journal of Organic Chemistry*, 1983, **48**, 2877–2887.
- (54) P. G. Jessop, D. A. Jessop, D. Fu and L. Phan, *Green Chemistry*, 2012, **14**, 1245–1259.
- (55) J. M. Hughes, D. Aherne and J. N. Coleman, *Journal of Applied Polymer Science*, 2013, **127**, 4483–4491.
- (56) M. J. Louwse, A. Maldonado, S. Rousseau, C. Moreau-Masselon, B. Roux and G. Rothenberg, *Chemphyschem*, 2017, **18**, 2999–3006.
- (57) A. Klamt, *The Journal of Physical Chemistry*, 1995, **99**, 2224–2235.
- (58) C. Loschen and A. Klamt, *Industrial & Engineering Chemistry Research*, 2014, **53**, 11478–11487.
- (59) S. Abbott, C. M. Hansen and H. Yamamoto, *Hansen Solubility Parameters in Practice*, Hansen-Solubility.com, 4th, 2008, 242 pp.
- (60) B. García, S. Aparicio, R. Alcalde, R. Ruiz, M. J. Dávila and J. M. Leal, *The Journal of Physical Chemistry B*, 2004, **108**, 3024–3029.
- (61) A. Duereh, Y. Sato, R. L. Smith and H. Inomata, *The Journal of Physical Chemistry B*, 2016, **120**, 4467–4481.
- (62) C. Reichardt, *Chemical Reviews*, 1994, **94**, 2319–2358.
- (63) M. J. Kamlet and R. W. Taft, *Journal of the American Chemical Society*, 1976, **98**, 377–383.
- (64) R. W. Taft and M. J. Kamlet, *Journal of the American Chemical Society*, 1976, **98**, 2886–2894.
- (65) T. Yokoyama, R. W. Taft and M. J. Kamlet, *Journal of the American Chemical Society*, 1976, **98**, 3233–3237.
- (66) P. Anastas and N. Eghbali, *Chemical Society Reviews*, 2010, **39**, 301–312.
- (67) P. G. Jessop, *Green Chemistry*, 2011, **13**, 1391–1398.
- (68) L. Bergkamp and N. Herbatschek, *Review of European, Comparative & International Environmental Law*, 2014, **23**, 221–245.
- (69) J. H. Clark, T. J. Farmer, A. J. Hunt and J. Sherwood, *International Journal of Molecular Sciences*, 2015, **16**, 17101–17159.
- (70) UK, *The Solvent Emissions (England and Wales) Regulations 2004*, 2004.

- (71) UK, *The Pollution Prevention and Control (England and Wales) Regulations 2000*, 2000.
- (72) J. Clark, T. J. Farmer, L. Herrero-Davila and J. Sherwood, *Green Chemistry*, 2016, **18**, 3914–3934.
- (73) A. Kienzler, S. K. Bopp, S. van der Linden, E. Berggren and A. Worth, *Regulatory Toxicology and Pharmacology*, 2016, **80**, 321–334.
- (74) H. Ravikumar, S. S. Rao and C. Karigar, *Indian Journal of Science and Technology*, 2012, **5**, 1977–1987.
- (75) R. Wool and X. S. Sun, *Bio-Based Polymers and Composites*, Elsevier, 2011, 641 pp.
- (76) S. D. Williams and W. H. Schmitt, *Chemistry and Technology of the Cosmetics and Toiletries Industry*, Springer Science & Business Media, 2012, 412 pp.
- (77) A. Uner and F. Yilmaz, *Journal of Surfactants and Detergents*, 2015, **18**, 213–224.
- (78) B. A. Miller-Chou and J. L. Koenig, *Progress in Polymer Science*, 2003, **28**, 1223–1270.
- (79) K. Holmberg, B. Jönsson, B. Kronberg and B. Lindman, *Surfactants and Polymers in Aqueous Solution*, Wiley, Chichester, 2 edition, 2002, 562 pp.
- (80) B. Lindman, G. Karlström and L. Stigsson, *Journal of Molecular Liquids*, 2010, **156**, 76–81.
- (81) G. M. Geise, H.-S. Lee, D. J. Miller, B. D. Freeman, J. E. McGrath and D. R. Paul, *Journal of Polymer Science Part B: Polymer Physics*, 2010, **48**, 1685–1718.
- (82) D.-M. Wang and J.-Y. Lai, *Current Opinion in Chemical Engineering*, 2013, **2**, 229–237.
- (83) G.-d. Kang and Y.-m. Cao, *Journal of Membrane Science*, 2014, **463**, 145–165.
- (84) A. Figoli, T. Marino, S. Simone, E. D. Nicolò, X.-M. Li, T. He, S. Tornaghi and E. Drioli, *Green Chemistry*, 2014, **16**, 4034–4059.
- (85) J. T. Jung, J. F. Kim, H. H. Wang, E. di Nicolo, E. Drioli and Y. M. Lee, *Journal of Membrane Science*, 2016, **514**, 250–263.
- (86) A. Bottino, G. Camera-Roda, G. Capannelli and S. Munari, *Journal of Membrane Science*, 1991, **57**, 1–20.
- (87) G. R. Guillen, Y. Pan, M. Li and E. M. V. Hoek, *Industrial & Engineering Chemistry Research*, 2011, **50**, 3798–3817.
- (88) F. Liu, N. A. Hashim, Y. Liu, M. R. M. Abed and K. Li, *Journal of Membrane Science*, 2011, **375**, 1–27.

- (89) C. A. Smolders, A. J. Reuvers, R. M. Boom and I. M. Wienk, *Journal of Membrane Science*, 1992, **73**, 259–275.
- (90) S. A. McKelvey and W. J. Koros, *Journal of Membrane Science*, 1996, **112**, 29–39.
- (91) P. van de Witte, P. J. Dijkstra, J. W. A. van den Berg and J. Feijen, *Journal of Membrane Science*, 1996, **117**, 1–31.
- (92) T.-H. Young, L.-P. Cheng, D.-J. Lin, L. Fane and W.-Y. Chuang, *Polymer*, 1999, **40**, 5315–5323.
- (93) M. L. Yeow, Y. T. Liu and K. Li, *Journal of Applied Polymer Science*, 2004, **92**, 1782–1789.
- (94) S. S. Madaeni and A. Rahimpour, *Polymers for Advanced Technologies*, 2005, **16**, 717–724.
- (95) M. Gu, J. Zhang, X. Wang, H. Tao and L. Ge, *Desalination*, 2006, **192**, 160–167.
- (96) I. Soroko, Y. Bhole and A. Guy Livingston, *Green Chemistry*, 2011, **13**, 162–168.
- (97) N. T. Hassankiadeh, Z. Cui, J. H. Kim, D. W. Shin, A. Sanguineti, V. Arcella, Y. M. Lee and E. Drioli, *Journal of Membrane Science*, 2014, **471**, 237–246.
- (98) J. E. Camp, *ChemSusChem*, 2018, **11**, 3048–3055.
- (99) Circa, *Press Release: Circa Group's Commercial Demonstration Plant Comes Online and Produces First Batch of 99% Pure Cyrene®*, 2019, <https://www.sustainabilityconsult.com/news/373-press-release-circa-group-s-commercial-demonstration-plant-comes-online-and-produces-first-batch-of-99-pure-cyrene> (visited on 05/09/2019).
- (100) J. Sherwood, M. D. Bruyn, A. Constantinou, L. Moity, C. R. McElroy, T. J. Farmer, T. Duncan, W. Raverty, A. J. Hunt and J. H. Clark, *Chemical Communications*, 2014, **50**, 9650–9652.
- (101) D. E. Richardson and W. D. Raverty, *Appita*, 2016, **69**, 344–351.
- (102) Circa, *Press Release: Circa Receives Green Light to Sell Non-Toxic, Bio-Based and Biodegradable Solvent in EU*, 2018, <https://www.sustainabilityconsult.com/news/361-press-release-circa-receives-green-light-to-sell-non-toxic-bio-based-and-biodegradable-solvent-in-eu> (visited on 05/09/2019).
- (103) Sigma-Aldrich, *SDS 807796 - Cyrene*, 2018.
- (104) K. L. Wilson, A. R. Kennedy, J. Murray, B. Greatrex, C. Jamieson and A. J. B. Watson, *Beilstein Journal of Organic Chemistry*, 2016, **12**, 2005–2011.

- (105) J. Zhang, G. B. White, M. D. Ryan, A. J. Hunt and M. J. Katz, *ACS Sustainable Chemistry & Engineering*, 2016, **4**, 7186–7192.
- (106) L. Mistry, K. Mapesa, T. W. Bousfield and J. E. Camp, *Green Chemistry*, 2017, **19**, 2123–2128.
- (107) K. L. Wilson, J. Murray, C. Jamieson and A. J. B. Watson, *Organic & Biomolecular Chemistry*, 2018, **16**, 2851–2854.
- (108) K. L. Wilson, J. Murray, C. Jamieson and A. J. B. Watson, *Synlett*, 2018, **14**, 650–654.
- (109) A. Alves Costa Pacheco, J. Sherwood, A. Zhenova, C. R. McElroy, A. J. Hunt, H. L. Parker, T. J. Farmer, A. Constantinou, M. De bruyn, A. C. Whitwood, W. Raverty and J. H. Clark, *ChemSusChem*, 2016, **9**, 3503–3512.
- (110) H. J. Salavagione, J. Sherwood, M. D. Bruyn, V. L. Budarin, G. J. Ellis, J. H. Clark and P. S. Shuttleworth, *Green Chemistry*, 2017, **19**, 2550–2560.
- (111) D. H. Gharib, S. Gietman, F. Malherbe and S. E. Moulton, *Carbon*, 2017, **123**, 695–707.
- (112) S. Lawrenson, M. North, F. Peigneguy and A. Routledge, *Green Chemistry*, 2017, **19**, 952–962.
- (113) L. Gaines, *Sustainable Materials and Technologies*, 2014, **1-2**, 2–7.
- (114) D. Larcher and J.-M. Tarascon, *Nature Chemistry*, 2015, **7**, 19–29.
- (115) X. Zeng, J. Li and N. Singh, *Critical Reviews in Environmental Science and Technology*, 2014, **44**, 1129–1165.
- (116) T. Georgi-Maschler, B. Friedrich, R. Weyhe, H. Heegn and M. Rutz, *Journal of Power Sources*, 2012, **207**, 173–182.
- (117) I. Tsiropoulos, D. Tarvydas and N. Lebedeva, *Li-Ion Batteries for Mobility and Stationary Storage Applications – Scenarios for Costs and Market Growth*, Website EUR 29440 EN, Publications Office of the European Union, Luxembourg, 2018.
- (118) C. Daniel, *The Bridge*, 2015, **45**, 21–24.
- (119) M. Contestabile, S. Panero and B. Scrosati, *Journal of Power Sources*, 2001, **92**, 65–69.
- (120) European Chemicals Agency, *1-Methyl-2-Pyrrolidone - Substance Information - ECHA*, 2019, <https://echa.europa.eu/substance-information/-/substanceinfo/100.011.662> (visited on 05/04/2019).
- (121) J.-Y. Sanchez, F. Alloin and J. Saunier, in *Fluorinated Materials for Energy Conversion*, ed. T. Nakajima and H. Groult, Elsevier Science, Amsterdam, 2005, pp. 305–333.

- (122) Z. Wang, Y. Tang and B. Li, *RSC Advances*, 2018, **8**, 25159–25167.
- (123) Q. Zhou, Z. Wang, H. Shen, Z. Zhu, L. Liu, L. Yang and L. Cheng, *Journal of Chemical Technology & Biotechnology*, 2016, **91**, 1697–1708.
- (124) Y. Tang, Y. Lin, W. Ma, Y. Tian, J. Yang and X. Wang, *Journal of Applied Polymer Science*, 2010, **118**, 3518–3523.
- (125) Z. Song, W. Yang, J. Zhang, Y. Li and S. Yuan, *Journal of Polymer Engineering*, 2015, **35**, 709–717.
- (126) Q. Li, Z.-L. Xu and L.-Y. Yu, *Journal of Applied Polymer Science*, 2010, **115**, 2277–2287.
- (127) H. Wang, G. Gurau and R. D. Rogers, *Chemical Society Reviews*, 2012, **41**, 1519–1537.
- (128) M.-m. Tao, F. Liu, B.-r. Ma and L.-x. Xue, *Desalination*, 2013, **316**, 137–145.
- (129) J. Yang, X.-L. Wang, Y. Tian, Y. Lin and F. Tian, *Journal of Polymer Science Part B: Polymer Physics*, 2010, **48**, 2468–2475.
- (130) Y. J. Park, Y. S. Kang and C. Park, *European Polymer Journal*, 2005, **41**, 1002–1012.
- (131) T. Boccaccio, A. Bottino, G. Capannelli and P. Piaggio, *Journal of Membrane Science*, 2002, **210**, 315–329.
- (132) T. Marino, F. Galiano, A. Molino and A. Figoli, *Journal of Membrane Science*, 2019, **580**, 224–234.
- (133) Solvay, *Solef® PVDF for Li-Ion Batteries*, 2019, <https://www.solvay.com/en/solutions-market/electrical-electronics/solef-pvdf-li-ion-batteries> (visited on 05/03/2019).
- (134) F. Machui, S. Langner, X. Zhu, S. Abbott and C. J. Brabec, *Solar Energy Materials and Solar Cells*, 2012, **100**, 138–146.
- (135) A. Bottino, G. Capannelli, S. Munari and A. Turturro, *Journal of Polymer Science Part B: Polymer Physics*, 1988, **26**, 785–794.
- (136) L. Moity, M. Durand, A. Benazzouz, C. Pierlot, V. Molinier and J.-M. Aubry, *Green Chemistry*, 2012, **14**, 1132–1145.
- (137) Inkemia Green Chemicals, *Inkemia Green Solvents Catalogue*, 2018, <https://shop.inkemiagreenchemicals.com/collections/index> (visited on 04/11/2019).
- (138) M. A. Rasool and I. F. J. Vankelecom, *Green Chemistry*, 2019, **21**, 1054–1064.
- (139) *CRC Handbook of Chemistry and Physics*, ed. D. R. Lide, CRC Press, Boca Raton, FL, 85th edn., 2004.

- (140) Sigma-Aldrich, *SDS W391018 - Cyclopentanone*, 2016.
- (141) K.-M. Roy, in *Ullmann's Encyclopedia of Industrial Chemistry*, American Cancer Society, 2000.
- (142) M. E. Cisney and J. D. Wethern, *US Pat.*, 2816832A, James River Corp of Nevada, 1957.
- (143) M. E. Lane, *International Journal of Pharmaceutics*, 2013, **447**, 12–21.
- (144) D. Prat, O. Pardigon, H.-W. Flemming, S. Letestu, V. Ducandas, P. Isnard, E. Guntrum, T. Senac, S. Ruisseau, P. Cruciani and P. Hosek, *Organic Process Research & Development*, 2013, **17**, 1517–1525.
- (145) D. Glindemann, J. Novak and J. Witherspoon, *Environmental Science & Technology*, 2006, **40**, 202–207.
- (146) I. T. Horváth, H. Mehdi, V. Fábos, L. Boda and L. T. Mika, *Green Chemistry*, 2008, **10**, 238–242.
- (147) D. M. Alonso, S. G. Wettstein and J. A. Dumesic, *Green Chemistry*, 2013, **15**, 584–595.
- (148) WHO Secretariat, *Gamma-Butyrolactone Critical Review Report*, World Health Organization, 2014, p. 28.
- (149) M. Hronec and K. Fulajtarová, *Catalysis Communications*, 2012, **24**, 100–104.
- (150) Y. Yang, Z. Du, Y. Huang, F. Lu, F. Wang, J. Gao and J. Xu, *Green Chemistry*, 2013, **15**, 1932–1940.
- (151) European Chemicals Agency, *Cyclopentanone - Registration Dossier - ECHA*, 2019, <https://echa.europa.eu/registration-dossier/-/registered-dossier/13920/4/9> (visited on 05/06/2019).
- (152) C. M. Alder, J. D. Hayler, R. K. Henderson, A. M. Redman, L. Shukla, L. E. Shuster and H. F. Sneddon, *Green Chemistry*, 2016, **18**, 3879–3890.
- (153) M. Caillon-Caravanier, B. Claude-Montigny, D. Lemordant and G. Bossier, *Journal of Power Sources*, 2002, **107**, 125–132.
- (154) A. Munch Elmér and P. Jannasch, *Polymer*, 2005, **46**, 7896–7908.
- (155) M. Palazzo and E. S. Takeuchi, *US Pat.*, 6759164B2, Greatbatch Ltd, 2004.
- (156) W. P. Kosar, *US Pat.*, 20180056247A1, Arkema Inc, 2018.

- (157) R. Hackworth, J. R. Moriera, R. Maxwell, R. Kotha and A. A. Ayon, 2011 Symposium on Design, Test, Integration Packaging of MEMS/MOEMS (DTIP), 2011, pp. 138–141.
- (158) D. Thuau, K. Kallitsis, F. D. D. Santos and G. Hadziioannou, *Journal of Materials Chemistry C*, 2017, **5**, 9963–9966.
- (159) M. A. Navarra, S. Materazzi, S. Panero and B. Scrosati, *Journal of The Electrochemical Society*, 2003, **150**, A1528–A1532.
- (160) A. Martinelli, M. A. Navarra, A. Matic, S. Panero, P. Jacobsson, L. Börjesson and B. Scrosati, *Electrochimica Acta*, 2005, **50**, 3992–3997.
- (161) K. S. Nanjundaswamy, H. D. Friend, C. O. Kelly, D. J. Standlee and R. L. Higgins, IECCEC-97 Proceedings of the Thirty-Second Intersociety Energy Conversion Engineering Conference (Cat. No.97CH6203), 1997, vol. 1, 42–45 vol.1.
- (162) F. Fei, H. A. Le Phuong, C. F. Blanford and G. Szekely, *ACS Applied Polymer Materials*, 2019, **1**, 452–460.
- (163) Q. Wang, Z. Wang and Z. Wu, *Desalination*, 2012, **297**, 79–86.
- (164) D.-J. Lin, C.-L. Chang, C.-K. Lee and L.-P. Cheng, *European Polymer Journal*, 2006, **42**, 2407–2418.
- (165) T. Otsuka and Y. Chujo, *Polymer*, 2009, **50**, 3174–3181.
- (166) M. Tazaki, R. Wada, M. O. Abe and T. Homma, *Journal of Applied Polymer Science*, 1997, **65**, 1517–1524.
- (167) M. Okabe, R. Wada, M. Tazaki and T. Homma, *Polymer Journal*, 2003, **35**, 798–803.
- (168) S. Mal and A. K. Nandi, *Langmuir*, 1998, **14**, 2238–2244.
- (169) Y. Osada, J. P. Gong and Y. Tanaka, *Journal of Macromolecular Science, Part C*, 2004, **44**, 87–112.
- (170) R. Bansil and M. K. Gupta, *Ferroelectrics*, 1980, **30**, 63–71.
- (171) B. J. Sobieski, L. Gong, S. R. Aubuchon, I. Noda, D. B. Chase and J. F. Rabolt, *Polymer*, 2017, **131**, 217–223.
- (172) H. Shimizu, Y. Arioka, M. Ogawa, R. Wada and M. Okabe, *Polymer Journal*, 2011, **43**, 540–544.
- (173) S. B. Ross-Murphy, *Journal of Texture Studies*, 1995, **26**, 391–400.
- (174) A. C. Sun, W. Kosar, Y. Zhang and X. Feng, *Desalination*, 2013, **309**, 156–164.

- (175) R. Gregorio, Jr. and M. Cestari, *Journal of Polymer Science Part B: Polymer Physics*, 1994, **32**, 859–870.
- (176) D.-J. Lin, K. Beltsios, T.-H. Young, Y.-S. Jeng and L.-P. Cheng, *Journal of Membrane Science*, 2006, **274**, 64–72.
- (177) P. Sukitpaneemit and T.-S. Chung, *Journal of Membrane Science*, 2009, **340**, 192–205.
- (178) Y. Su, C. Chen, Y. Li and J. Li, *Journal of Macromolecular Science, Part A*, 2007, **44**, 305–313.
- (179) J. W. Cho, H. Y. Song and S. Y. Kim, *Polymer*, 1993, **34**, 1024–1027.
- (180) J. W. Cho and G. W. Lee, *Journal of Polymer Science Part B: Polymer Physics*, 1996, **34**, 1605–1611.
- (181) Eastman Chemical Company, *N-Methyl-2-Pyrrolidone (NMP) Technical Data Sheet*, 2019, [https://productcatalog.eastman.com/tds/ProdDatasheet.aspx?product=71103627&pn=N-Methyl-2-Pyrrolidone+\(NMP\)](https://productcatalog.eastman.com/tds/ProdDatasheet.aspx?product=71103627&pn=N-Methyl-2-Pyrrolidone+(NMP)) (visited on 05/06/2019).
- (182) Gaylord Chemical Company, *Dimethyl Sulfoxide Solubility Data*, 2014.
- (183) S. Wang, A. Lu and L. Zhang, *Progress in Polymer Science*, 2016, **53**, 169–206.
- (184) A. P. Abbott, T. J. Bell, S. Handa and B. Stoddart, *Green Chemistry*, 2006, **8**, 784–786.
- (185) European Chemicals Agency, *4-Methylmorpholine 4-Oxide - Brief Profile - ECHA*, 2019, <https://echa.europa.eu/substance-information/-/substanceinfo/100.028.538> (visited on 05/11/2019).
- (186) K. M. Gupta and J. Jiang, *Chemical Engineering Science*, 2015, **121**, 180–189.
- (187) C. Choi, *Science Magazine*, 2013.
- (188) T. Huber, J. Müssig, O. Curnow, S. Pang, S. Bickerton and M. P. Staiger, *Journal of Materials Science*, 2012, **47**, 1171–1186.
- (189) D. Klemm, B. Heublein, H.-P. Fink and A. Bohn, *Angewandte Chemie International Edition*, 2005, **44**, 3358–3393.
- (190) J. B. Binder and R. T. Raines, *Journal of the American Chemical Society*, 2009, **131**, 1979–1985.
- (191) A. Pinkert, K. N. Marsh and S. Pang, *Industrial & Engineering Chemistry Research*, 2010, **49**, 11121–11130.
- (192) N. Bywater, *Lenzinger Berichte*, 2011, 22–29.
- (193) D. S. Hall and L. A. Losee, *Process Safety Progress*, 1997, **16**, 251–254.

- (194) O. Aaserud, O. J. Hommeren, B. Tvedt, P. Nakstad, G. Mowé, J. Efskind, D. Russell, E. B. Jörgensen, R. Nyberg-Hansen, K. Rootwelt and L. Gjerstad, *American Journal of Industrial Medicine*, 1990, **18**, 25–37.
- (195) European Chemicals Agency, *Carbon Disulphide- Substance Information - ECHA*, 2018, <https://echa.europa.eu/substance-information/-/substanceinfo/100.000.767> (visited on 05/12/2019).
- (196) H.-P. Fink, J. Ganster and A. Lehmann, *Cellulose*, 2014, **21**, 31–51.
- (197) T. Rosenau, A. Potthast, H. Sixta and P. Kosma, *Progress in Polymer Science*, 2001, **26**, 1763–1837.
- (198) S. Righi, A. Morfino, P. Galletti, C. Samorì, A. Tugnoli and C. Stramigioli, *Green Chemistry*, 2011, **13**, 367–375.
- (199) H.-P. Fink, P. Weigel, H. J. Purz and J. Ganster, *Progress in Polymer Science*, 2001, **26**, 1473–1524.
- (200) A. F. Turbak, A. El-Kafrawy, J. Snyder and A. B. Auerbach, *pat.*, 4 302 252, International Telephone and Telegraph Corp., 1981.
- (201) C. L. McCormick, P. A. Callais and B. H. Hutchinson, *Macromolecules*, 1985, **18**, 2394–2401.
- (202) A.-L. Dupont, *Polymer*, 2003, **44**, 4117–4126.
- (203) SDS 72336 - Dimethylacetamide, 2016.
- (204) T. C. Wanger, *Conservation Letters*, 2011, **4**, 202–206.
- (205) T. Heinze, R. Dicke, A. Koschella, A. H. Kull, E.-A. Klohr and W. Koch, *Macromolecular Chemistry and Physics*, 2000, **201**, 627–631.
- (206) R. Rinaldi, *Chemical Communications*, 2010, **47**, 511–513.
- (207) E. Gale, R. H. Wirawan, R. L. Silveira, C. S. Pereira, M. A. Johns, M. S. Skaf and J. L. Scott, *ACS Sustainable Chemistry & Engineering*, 2016, **4**, 6200–6207.
- (208) C. Yuan, W. Shi, P. Chen, H. Chen, L. Zhang, G. Hu, L. Jin, H. Xie, Q. Zheng and S. Lu, *New Journal of Chemistry*, 2019, **43**, 330–337.
- (209) M. Kostag, T. Liebert, O. A. E. Seoud and T. Heinze, *Macromolecular Rapid Communications*, 2013, **34**, 1580–1584.
- (210) B. Medronho and B. Lindman, *Current Opinion in Colloid & Interface Science*, 2014, **19**, 32–40.
- (211) C. Cuissinat and P. Navard, *Macromolecular Symposia*, 2006, **244**, 1–18.

- (212) H. Ono, T. Matsui and I. Miyamoto, *US Pat.*, 6541627B1, Asahi Kasei Corp, 2003.
- (213) L. Belloni, *Journal of Physics: Condensed Matter*, 2000, **12**, R549–R587.
- (214) B. Medronho, A. Romano, M. G. Miguel, L. Stigsson and B. Lindman, *Cellulose*, 2012, **19**, 581–587.
- (215) M. Ghasemi, M. Tsianou and P. Alexandridis, *Bioresource Technology*, 2017, **228**, 330–338.
- (216) M. Ghasemi, M. Tsianou and P. Alexandridis, *Agricultural Research & Technology: Open Access Journal*, 2018, **16**.
- (217) J. Cai, L. Zhang, S. Liu, Y. Liu, X. Xu, X. Chen, B. Chu, X. Guo, J. Xu, H. Cheng, C. C. Han and S. Kuga, *Macromolecules*, 2008, **41**, 9345–9351.
- (218) W. G. Glasser, R. H. Atalla, J. Blackwell, R. Malcolm Brown, W. Burchard, A. D. French, D. O. Klemm and Y. Nishiyama, *Cellulose*, 2012, **19**, 589–598.
- (219) M. De bruyn, V. L. Budarin, A. Misefari, S. Shimizu, H. Fish, M. Cockett, A. J. Hunt, H. Hofstetter, B. M. Weckhuysen, J. H. Clark and D. J. Macquarrie, *ACS Sustainable Chemistry & Engineering*, 2019, **7**, 7878–7883.
- (220) T. Röder, B. Morgenstern, N. Schelosky and O. Glatter, *Polymer*, 2001, **42**, 6765–6773.
- (221) M. Kihlman, B. F. Medronho, A. L. Romano, U. Germgård and B. Lindman, *Journal of the Brazilian Chemical Society*, 2013, **24**, 295–303.
- (222) M. Sharma, C. Mukesh, D. Mondal and K. Prasad, *RSC Advances*, 2013, **3**, 18149–18155.
- (223) J. Cai and L. Zhang, *Macromolecular Bioscience*, 2005, **5**, 539–548.
- (224) M. Mazza, D.-A. Catana, C. Vaca-Garcia and C. Cecutti, *Cellulose*, 2009, **16**, 207–215.
- (225) C. M. Lee, A. Mittal, A. L. Barnette, K. Kafle, Y. B. Park, H. Shin, D. K. Johnson, S. Park and S. H. Kim, *Cellulose*, 2013, **20**, 991–1000.
- (226) H. J. Marrinan and J. Mann, *Journal of Polymer Science*, 1956, **21**, 301–311.
- (227) N.-J. Cao, Q. Xu, C.-S. Chen, C. S. Gong and L. F. Chen, *Applied Biochemistry and Biotechnology*, 1994, **45**, 521–530.
- (228) Q. Xu and L.-F. Chen, *Journal of Applied Polymer Science*, 1999, **71**, 1441–1446.
- (229) A. Naderi, *Cellulose*, 2017, **24**, 1933–1945.

- (230) Y.-B. Huang, P.-P. Xin, J.-X. Li, Y.-Y. Shao, C.-B. Huang and H. Pan, *ACS Sustainable Chemistry & Engineering*, 2016, **4**, 2286–2294.
- (231) A. J. Sayyed, L. V. Mohite, N. A. Deshmukh and D. V. Pinjari, *Ultrasonics Sonochemistry*, 2018, **49**, 161–168.
- (232) M. Ashokkumar, J. Lee, S. Kentish and F. Grieser, *Ultrasonics Sonochemistry*, 2007, **14**, 470–475.
- (233) H. Jadhav, E. Taarning, C. M. Pedersen and M. Bols, *Tetrahedron Letters*, 2012, **53**, 983–985.
- (234) N. Isobe, K. Noguchi, Y. Nishiyama, S. Kimura, M. Wada and S. Kuga, *Cellulose*, 2013, **20**, 97–103.
- (235) H. Dogan and N. D. Hilmioglu, *Carbohydrate Polymers*, 2009, **75**, 90–94.
- (236) R. J. Sengwa, V. Khatri and S. Sankhla, *Journal of Molecular Liquids*, 2009, **144**, 89–96.
- (237) L. Wu, J. Sun and Q. Wang, *Journal of Membrane Science*, 2006, **285**, 290–298.
- (238) J. H. Kim, B. R. Min, J. Won, H. C. Park and Y. S. Kang, *Journal of Membrane Science*, 2001, **187**, 47–55.
- (239) H. Strathmann and K. Kock, *Desalination*, 1977, **21**, 241–255.
- (240) M. A. Frommer and R. M. Messalem, *Product R&D*, 1973, **12**, 328–333.
- (241) Sigma-Aldrich, *SDS 309966 - Diethyl Ether*, 2018.
- (242) X. Meng, P. Zheng, J. Wu and Z. Liu, *Fluid Phase Equilibria*, 2008, **271**, 1–5.
- (243) *Surface Tension of Diethyl Ether from Dortmund Data Bank*, 2015, http://www.ddbst.com/en/EED/PCP/SFT_C12.php (visited on 08/03/2019).
- (244) Sigma-Aldrich, *SDS 401757 - Tetrahydrofuran*, 2018.
- (245) D. H. S. Ramkumar and A. P. Kudchadker, *Journal of Chemical & Engineering Data*, 1989, **34**, 463–465.
- (246) Sigma-Aldrich, *SDS 296309 - 1,4-Dioxane*, 2018.
- (247) T. R. Kubendran, *Journal of Chemical & Engineering Data*, 2004, **49**, 421–425.
- (248) Sigma-Aldrich, *SDS 240834 - Diphenyl Ether*, 2014.
- (249) *Diphenyl Ether*, 2015, <https://toxnet.nlm.nih.gov/cgi-bin/sis/search2/r?dbs+hsdb:@term+@rn+@rel+101-84-8> (visited on 08/03/2019).

- (250) Sigma-Aldrich, *SDS 296295 - Anisole*, 2017.
- (251) S. Viswanathan, M. Anand Rao and D. H. L. Prasad, *Journal of Chemical & Engineering Data*, 2000, **45**, 764–770.
- (252) *Anisole*, 1996, <https://toxnet.nlm.nih.gov/cgi-bin/sis/search2/f?./temp/~LKVSsa:1> (visited on 08/03/2019).
- (253) *2-Methoxy-2-Methylbutane - Brief Profile*, 2019, <https://echa.europa.eu/brief-profile/-/briefprofile/100.012.374> (visited on 08/03/2019).
- (254) Sigma-Aldrich, *SDS 283096 - Tert-Amyl Methyl Ether*, 2012.
- (255) W. Ahmad, A. Vakilinejad, Z. M. Aman and G. R. Vakili-Nezhaad, *Journal of Chemical & Engineering Data*, 2019, **64**, 459–470.
- (256) Sigma-Aldrich, *SDS 791962 - Cyclopentyl Methyl Ether*, 2017.
- (257) K. Watanabe, N. Yamagiwa and Y. Torisawa, *Organic Process Research & Development*, 2007, **11**, 251–258.
- (258) Sigma-Aldrich, *SDS 253898 - Tert-Butyl Ethyl Ether*, 2019.
- (259) A. Ćwiklińska, C. M. Kinart, W. J. Kinart and D. Chęcińska-Majak, *Physics and Chemistry of Liquids*, 2008, **46**, 27–33.
- (260) Sigma-Aldrich, *SDS 673277 - 2-Methyltetrahydrofuran*, 2018.
- (261) A. Villares, L. Sanz, B. Giner, C. Lafuente and M. C. López, *Journal of Chemical & Engineering Data*, 2005, **50**, 1334–1337.
- (262) Y. Gu and F. Jérôme, *Chemical Society Reviews*, 2013, **42**, 9550–9570.
- (263) B. Niethammer, S. Wodarz, M. Betz, P. Haltenort, D. Oestreich, K. Hackbarth, U. Arnold, T. Otto and J. Sauer, *Chemie Ingenieur Technik*, 2018, **90**, 99–112.
- (264) M. Härtl, K. Gaukel, D. Pélerin and G. Wachtmeister, *MTZ Worldwide*, 2017, **78**, 52–59.
- (265) X. Zhang, A. Kumar, U. Arnold and J. Sauer, *Energy Procedia*, 2014, **61**, 1921–1924.
- (266) J. Burger, M. Siegert, E. Ströfer and H. Hasse, *Fuel*, 2010, **89**, 3315–3319.
- (267) M. Schappals, T. Breug-Nissen, K. Langenbach, J. Burger and H. Hasse, *Journal of Chemical & Engineering Data*, 2017, **62**, 4027–4031.
- (268) Q. Liu, X. Zhang and B. Ma, *Journal of Chemical & Engineering Data*, 2016, **61**, 3254–3265.

- (269) European Chemicals Agency, *Dimethoxymethane - Substance Information - ECHA*, 2019, <https://echa.europa.eu/substance-information/-/substanceinfo/100.003.378> (visited on 04/19/2019).
- (270) L. Lautenschütz, D. Oestreich, P. Seidenspinner, U. Arnold, E. Dinjus and J. Sauer, *Fuel*, 2016, **173**, 129–137.
- (271) D. Deutsch, D. Oestreich, L. Lautenschütz, P. Haltenort, U. Arnold and J. Sauer, *Chemie Ingenieur Technik*, 2017, **89**, 486–489.
- (272) M.-R. Kang, H.-Y. Song, F.-X. Jin and J. Chen, *Journal of Fuel Chemistry and Technology*, 2017, **45**, 837–845.
- (273) E. Jacob and W. Maus, Wiener Motorensymposium, Vienna, 2014, vol. 35, pp. 325–347.
- (274) N. Schmitz, F. Homberg, J. Berje, J. Burger and H. Hasse, *Industrial & Engineering Chemistry Research*, 2015, **54**, 6409–6417.
- (275) M. Ouda, G. Yarce, R. J. White, M. Hadrlich, D. Himmel, A. Schaadt, H. Klein, E. Jacob and I. Krossing, *Reaction Chemistry & Engineering*, 2017, **2**, 50–59.
- (276) A. Peter, S. M. Fehr, V. Dybbert, D. Himmel, I. Lindner, E. Jacob, M. Ouda, A. Schaadt, R. J. White, H. Scherer and I. Krossing, *Angewandte Chemie International Edition*, 2018, **57**, 9461–9464.
- (277) M. Held, Y. Tönges, D. Pélerin, M. Härtl, G. Wachtmeister and J. Burger, *Energy & Environmental Science*, 2019, **12**, 1019–1034.
- (278) Q. Wu, M. Wang, Y. Hao, H. Li, Y. Zhao and Q. Jiao, *Industrial & Engineering Chemistry Research*, 2014, **53**, 16254–16260.
- (279) C. J. Baranowski, A. M. Bahmanpour and O. Kröcher, *Applied Catalysis B: Environmental*, 2017, **217**, 407–420.
- (280) Y. Zheng, F. Liu, L. Guo, T. Wang and J. Wang, *RSC Advances*, 2016, **6**, 77116–77125.
- (281) M. Ouda, F. Mantei, K. Hesterwerth, E. Bargiacchi, H. Klein and R. J. White, *Reaction Chemistry & Engineering*, 2018, **3**, 676–695.
- (282) Independent Chemical Information Services, *ICIS Chemical Market Reporter*, 2006.
- (283) F. Byrne, B. Forier, G. Bossaert, C. Hoebbers, T. J. Farmer, J. H. Clark and A. J. Hunt, *Green Chemistry*, 2017, **19**, 3671–3678.
- (284) J. D. Evanseck, *Journal of the American Chemical Society*, 2011, **133**, 642–642.
- (285) V. Gutmann, *Coordination Chemistry Reviews*, 1976, **18**, 225–255.

- (286) D. J. C. Constable, C. Jimenez-Gonzalez and R. K. Henderson, *Organic Process Research & Development*, 2007, **11**, 133–137.
- (287) K. Alfonsi, J. Colberg, P. J. Dunn, T. Fevig, S. Jennings, T. A. Johnson, H. P. Kleine, C. Knight, M. A. Nagy, D. A. Perry and M. Stefaniak, *Green Chemistry*, 2008, **10**, 31–36.
- (288) D. S. MacMillan, J. Murray, H. F. Sneddon, C. Jamieson and A. J. B. Watson, *Green Chemistry*, 2013, **15**, 596–600.
- (289) F. I. McGonagle, D. S. MacMillan, J. Murray, H. F. Sneddon, C. Jamieson and A. J. B. Watson, *Green Chemistry*, 2013, **15**, 1159–1165.
- (290) G. A. Molander and M. D. Elia, *The Journal of Organic Chemistry*, 2006, **71**, 9198–9202.
- (291) W. Schutyser, S. V. den Bosch, T. Renders, T. D. Boe, S.-F. Koelewijn, A. Dewaele, T. Ennaert, O. Verkinderen, B. Goderis, C. M. Courtin and B. F. Sels, *Green Chemistry*, 2015, **17**, 5035–5045.
- (292) A. Douka, S. Vouyiouka, L.-M. Papaspyridi and C. D. Papaspyrides, *Progress in Polymer Science*, 2018, **79**, 1–25.
- (293) G. Paggiola, A. J. Hunt, C. R. McElroy, J. Sherwood and J. H. Clark, *Green Chemistry*, 2014, **16**, 2107–2110.
- (294) A. Iemhoff, J. Sherwood, C. R. McElroy and A. J. Hunt, *Green Chemistry*, 2018, **20**, 136–140.
- (295) H. Uyama and S. Kobayashi, in *Enzyme-Catalyzed Synthesis of Polymers*, ed. S. Kobayashi, H. Ritter and D. Kaplan, Springer Berlin Heidelberg, Berlin, Heidelberg, 2006, pp. 133–158.
- (296) Y. Jiang, A. J. J. Woortman, G. O. R. A. van Ekenstein and K. Loos, *Polymer Chemistry*, 2015, **6**, 5198–5211.
- (297) A. Pellis, J. W. Comerford, A. J. Maneffa, M. H. Sipponen, J. H. Clark and T. J. Farmer, *European Polymer Journal*, 2018, **106**, 79–84.
- (298) S. Weinberger, A. Pellis, J. W. Comerford, T. J. Farmer and G. M. Guebitz, *Catalysts*, 2018, **8**, 369.
- (299) A. Pellis, M. Vastano, F. Quartinello, E. H. Acero and G. M. Guebitz, *Biotechnology Journal*, 2017, **12**, 1700322.
- (300) A. Pellis, V. Ferrario, M. Cespugli, L. Corici, A. Guarneri, B. Zartl, E. H. Acero, C. Ebert, G. M. Guebitz and L. Gardossi, *Green Chemistry*, 2017, **19**, 490–502.

- (301) T. Erdmenger, C. Guerrero-Sanchez, J. Vitz, R. Hoogenboom and U. S. Schubert, *Chemical Society Reviews*, 2010, **39**, 3317–3333.
- (302) M. Levitt and M. F. Perutz, *Journal of Molecular Biology*, 1988, **201**, 751–754.
- (303) M. T. García, I. Gracia, G. Duque, A. de Lucas and J. F. Rodríguez, *Waste Management*, 2009, **29**, 1814–1818.
- (304) P. Sanmartín, F. Cappitelli and R. Mitchell, *Construction and Building Materials*, 2014, **71**, 363–374.
- (305) European Commission, *Regulation (EC) No 1907/2006 of the European Parliament and of the Council of 18 December 2006 Concerning the Registration, Evaluation, Authorisation and Restriction of Chemicals (REACH)*, 2006.
- (306) E. Bastiaensen, *OME Safety Data*, E-mail, ChemCom Industries B.V., Netherlands, 2019.
- (307) OECD, *Test No. 473: In Vitro Mammalian Chromosome Aberration Test*, 1997.
- (308) OECD, *Test No. 471: Bacterial Reverse Mutation Test*, 1997.
- (309) OECD, *Test No. 474: Mammalian Erythrocyte Micronucleus Test*, 2014.
- (310) European Commission, *Regulation (EC) No 1272/2008 of the European Parliament and of the Council of 16 December 2008 on Classification, Labelling, and Packaging of Substances and Mixtures (CLP)*, 2008.
- (311) R. J. Kelly, *Chemical Health & Safety*, 1996, 28–36.
- (312) H. Wang and J. Shen, *Catalysis Today*, 2017, **298**, 263–268.
- (313) BBI Consortium, *ReSolve | BBI Public-Private Partnership*, 2017, <https://www.bbi-europe.eu/projects/resolve> (visited on 05/24/2019).
- (314) R. H. Ahrens, *Germany Launches Sustainable Chemistry Centre*, 2017, <https://chemicalwatch.com/57820/germany-launches-sustainable-chemistry-centre> (visited on 05/07/2019).